CERN-THESIS-2008-236

Search for Second Generation Leptoquarks with ATLAS at the LHC

Dissertation der Fakultät für Physik
der
Ludwig-Maximilians-Universität München

vorgelegt von
Gernot Krobath
geboren in Heidelberg

München, den 18. Juli 2008

1. Gutachter: Prof. Dr. Dorothee Schaile
2. Gutachter: Prof. Dr. Wolfgang Dünnweber

Tag der mündlichen Prüfung: 24.09.2008

Abstract

The Large Hadron Collider will collide protons with protons at a center-of-mass energy of up to 14 TeV. New physics phenomena and new particles are predicted to be detectable with the ATLAS detector at the Large Hadron Collider. One of these predicted new particles beyond the Standard Model are leptoquarks.

This thesis deals with the search for scalar second generation leptoquarks produced in pairs. Second generation leptoquarks decay into a muon-type lepton and a quark. In this thesis the decay of both second generation leptoquarks into a muon and a quark is considered. Since pair production is studied the final state consists of two high-energetic muons and two high-energetic jets.
This thesis studies second generation leptoquarks with masses of $m_{LQ} = 300$ GeV, $m_{LQ} = 400$ GeV, $m_{LQ} = 600$ GeV and $m_{LQ} = 800$ GeV. The best cut variables for the discrimination between the signal and the main Standard Model backgrounds $t\bar{t}$ and Z/γ^* found in this analysis are the p_T of the muons, S_T (the scalar sum of the transverse momenta of the two selected muons and the transverse energies of the two selected jets), the mass of the selected dimuon system and the reconstructed leptoquark mass.
The latter three cut variables have been optimized for a discovery with a 5σ significance including the systematic uncertainties and trigger efficiencies.

Second generation leptoquarks have been excluded up to the mass of ∼300 GeV with a 95% confidence level at present experiments. The expected integrated luminosities needed for a 5σ discovery of the tested second generation leptoquark masses with the ATLAS detector have been calculated. This thesis shows that for a disocvery with 5σ significance of a second generation leptoquark with $m_{LQ} = 300$ GeV and $m_{LQ} = 400$ GeV an expected integrated luminosity of 1.51 pb^{-1} and 7.42 pb^{-1} is needed respectively; this corresponds to a very early phase, i.e. the first few months, of the Large Hadron Collider run. For the discovery with a 5σ significance of second generation leptoquarks with masses of $m_{LQ} = 600$ GeV and $m_{LQ} = 800$ GeV an expected integrated luminosity of 103.3 pb^{-1} and 663 pb^{-1} is needed respectively; this corresponds to several months and about half a year to a year of the Large Hadron Collider run respectively.

Zusammenfassung

Der Large Hadron Collider wird Protonen mit Protonen bei einer Schwerpunktsenergie von bis zu 14 TeV kollidieren lassen. Neue Physikphänomene und neue Teilchen werden voraussichtlich mit dem ATLAS Detektor am Large Hadron Collider entdeckbar sein. Eines dieser vorhergesagten neuen Teilchen jenseits des Standardmodells sind Leptoquarks.

Diese Doktorarbeit beschäftigt sich mit der Suche nach skalaren Leptoquarks der zweiten Generation, die paarweise produziert werden. Leptoquarks der zweiten Generation zerfallen in ein Myon-artiges Lepton und ein Quark. In dieser Doktorarbeit wird der Zerfall von beiden Leptoquarks der zweiten Generation in ein Myon und ein Quark betrachtet; da Paarproduktion untersucht wird, besteht der Endzustand aus zwei hochenergetischen Myonen und zwei hochenergetischen Jets.
In dieser Doktorarbeit wurden Leptoquarks der zweiten Generation mit Massen von $m_{LQ} = 300$ GeV, $m_{LQ} = 400$ GeV, $m_{LQ} = 600$ GeV und $m_{LQ} = 800$ GeV untersucht. Die besten Schnittvariablen zur Unterscheidung zwischen Signal und Haupt-Standardmodelluntergründen $t\bar{t}$ und Z/γ^*, die in dieser Analyse gefunden wurden, sind: p_T der Myonen, S_T (die skalare Summe der transversalen Impulse der beiden selektierten Myonen und der transversalen Energien der beiden selektierten Jets), die Masse des selektierten Zwei-Myon-Systems und die rekonstruierte Leptoquarkmasse.
Die letzteren drei Schnittvariablen wurden für eine Entdeckung mit einer Signifikanz von 5σ optimiert, wobei die systematischen Unsicherheiten und die Triggereffizienzen berücksichtigt wurden.

Leptoquarks der zweiten Generation wurden bis zu einer Masse von ∼300 GeV bei einem Vertrauensniveau von 95% an bisherigen Experimenten ausgeschlossen. Die erwarteten integrierten Luminositäten, die für eine 5σ Entdeckung von Leptoquarks der zweiten Generation mit den getesteten Massen mit dem ATLAS Detektor benötigt werden, wurden berechnet. Diese Doktorarbeit zeigt, daß für eine Entdeckung mit einer Signifikanz von 5σ von Leptoquarks der zweiten Generation für $m_{LQ} = 300$ GeV eine integrierte Luminosität von 1.51 pb^{-1} und für $m_{LQ} = 400$ GeV eine integrierte Luminosität von 7.42 pb^{-1} benötigt wird. Dies entspricht einer sehr frühen Phase, d.h. den ersten Monaten, des Betriebs des Large Hadron Collider. Für die Entdeckung mit einer Signifikanz von 5σ von Leptoquarks der zweiten Generation wird für $m_{LQ} = 600$ GeV eine integrierte Luminosität von 103.3 pb^{-1} und für $m_{LQ} = 800$ GeV eine integrierte Luminosität von 663 pb^{-1} benötigt. Dies entspricht jeweils einigen Monaten bis zu ungefähr einem halben bis ganzen Jahr des Betriebs des Large Hadron Collider.

Contents

Chapter 1

Introduction

Symmetry in nature has always been considered as an ideal. From ancient times on men tried to find symmetry in nature and were quite successful explaining nature and its laws by it. In physics symmetry is closely connected to conservation laws according to Noether's theorem. One important success while trying to find symmetry in physics is the Standard Model of particle physics, which explains the particles of matter and their interactions by means of exchange particles. There are fermions, coming in 3 families (or generations) of leptons, consisting of charged particles (e,μ,τ) and their uncharged associated neutrinos, and in three families of quarks (up, down; charm, strange; top, bottom). Each fermion has an associated anti-particle, which has the exact same charges just with opposite sign. Also there are 4 types of interaction particles ($W^{\pm}$, Z, γ, gluon) in the Standard Model [1].

The Standard Model (SM) has been a great success over the decades, explaining many phenomena even though it has been challenged many times. Only one of nature's interactions, gravity, is not included in the SM.

The surprising symmetry between the fermion and the quark sector, which is essential in achieving an exact cancellation of chiral (triangular) anomalies, lead to a basket of unsolved questions and motivates the existence of particles called leptoquarks (LQs) which would connect these two so far mostly unrelated regimes. LQs are bosons carrying both lepton and baryon quantum numbers and fractional electric charge. LQs could theoretically decay in a mix of quarks and leptons of all generations, but experimental results on lepton number violation, on flavor changing neutral currents and on proton decay lead to the assumption that there are 3 different generations of leptoquarks, each coupling to just one lepton family and one quark family [2].

In 1997 the H1 collaboration at HERA reported an excess of events at very high momentum transfers Q^2 [3]. These events were e + p $\rightarrow$ e + jet + X with

a reconstructed electron+jet mass of $\simeq$ 200 GeV[1]. The number of these events could not be explained by the Standard Model. The ZEUS experiment reported also an excess of events around the same time [4], even though their excess was smaller than the one of H1. One possible explanation would have been the involvement of leptoquarks in this process: e + p $\rightarrow$ LQ + X $\rightarrow$ e + j + X. These results triggered an avalanche of experimental efforts to search for leptoquarks as well as many new models and ideas on leptoquarks from the theoretical side. Later analyses showed that both excesses were due to mere statistical fluctuations [5, 6, 7].

While ep-collider experiments, like ZEUS and H1 at HERA, are almost only sensitive to first generation leptoquarks, hadron collider experiments are sensitive to all 3 generations of leptoquarks.

This thesis is divided in 8 chapters. Chapter 2 gives an overview and an introduction to the theoretical model of leptoquarks and to the open questions of the Standard Model. Furthermore it presents some theoretical extensions of the Standard Model comprising leptoquarks which could solve (some of) these problems. Also the production of scalar leptoquarks at the Large Hadron Collider is discussed. In Chapter 3 the Large Hadron Collider and the ATLAS experiment are described. Also the ATLAS computing model is explained. Chapter 4 discusses the search strategy for second generation leptoquarks in μ + jet + μ + jet events. It describes the main backgrounds, cut variables and selection cuts among other things. In Chapter 5 the triggers which can be used for the search for second generation leptoquarks in μ + jet + μ + jet events are analyzed. Also the efficiencies of the various triggers in the different trigger levels are given. Chapter 6 discusses the various sources of systematic uncertainties and their effects on the number of signal and background events. In Chapter 7 the sensitivity of this analysis for different second generation leptoquark masses is discussed. In Chapter 8 the results of the analysis are summarized and discussed. In Appendix A the plots for the tested second generation leptoquark masses m_{LQ} = 300 GeV and m_{LQ} = 600 GeV can be found. The calculation of the 5σ significance with the S_{cP} program is described in Appendix B. In Appendix C the Monte Carlo datasets used for signal and background and the PYTHIA parameters for the signal samples are listed and described. In Appendix D the GRID and the ATLAS software installation is described.

[1]The Heaviside-Lorentz system is used throughout this thesis, i.e. c = 1 and $\hbar$ = 1.

Chapter 2

Leptoquarks

Leptoquarks are chiral color triplet scalar or vector bosons, which carry fractional electric charge and both lepton and baryon numbers. They exist in many extensions of the Standard Model: Grand Unified Theories (GUTs), E_6-inspired models, Technicolor models etc. Most searches at collider experiments have been carried out in the context of effective models (see Section 2.4).

2.1 The Standard Model

The Standard Model (SM) describes the interactions of matter as a gauge theory based on the $SU(3)_C \otimes SU(2)_L \otimes U(1)_Y$ symmetry group. Only the gravitational force is neglected in the SM; it is very weak far below the Planck scale (the energy scale at which quantum effects of gravity become strong) compared to the other 3 known forces. All fundamental particles belong to one of two groups: fermions (half-integer spin) or bosons (integer spin). All particles which matter is built of are fermions while the forces between the fermions are mediated by bosons.

The SM has been a great success over many decades withstanding all its challenges and precise to a few per mill compared with experimental results but it is unlikely to be the final theory, even if we do not consider gravity. A new theory including gravity is also needed for energies higher than the Planck scale where gravity becomes too big to be neglected in particle physics. But even far below the Planck scale there are many unsolved questions:

- Why are there exactly 3 families of quarks and exactly 3 families of leptons?
- Why are the local SM gauge interactions the $SU(3)_C \otimes SU(2)_L \otimes U(1)_Y$ with 3 independent local SM gauge couplings?
- What determines the quark and lepton masses and how do they acquire mass? Why is there an apparent hierarchy of family masses and mixing angles?

- Why is charge quantized? Why are there no fractionally charged hadrons?
- What is the origin of dark energy and dark matter?

There are other experimental phenomena which cannot be explained by the SM, like the asymmetry between matter and anti-matter, which is too large to have its origin only in the complex phase of the Cabibbo-Kobayashi-Maskawa (CKM) matrix. Also there are 19 arbitrary parameters in the SM, which are chosen to match the SM with experimental data: 3 gauge couplings, 9 charged fermion masses, 3 quark-mixing angles and 1 phase in the complex CKM matrix, the Z^0 (or $W^{\pm}$) and the Higgs mass, and the QCD vacuum angle θ [1].
Furthermore the discovered oscillation of neutrinos [1], which implies a non-zero neutrino mass, adds 10 additional arbitrary parameters necessary for the neutrino masses.

To conclude, the SM has too many arbitrary parameters, so the SM is probably not the final and complete theory of particle physics. There are many new theories beyond the SM addressing (some of) these problems. In the next sections a few of these new theories are presented, in which leptoquarks appear as a natural consequence.

2.2 Leptoquarks in Grand Unified Theories

The aim of Grand Unified Theories (GUTs) is to find a gauge group with a single coupling constant which describes all known SM interactions. Most GUTs imply the existence of leptoquarks which would explain the strong similarities between leptons and quarks.
One of the GUTs is the SO(10) GUT model with its maximal breaking pattern $SO(10) \rightarrow SU(4)_C \otimes SU(2)_L \otimes SU(2)_R$, which leads to the Pati-Salam GUT model [8]. The leptonic sector is treated as a fourth color in this model.
Another interesting model is the superstring-inspired E_6 model [9]. E_6 is one of the five so-called exceptional Lie algebras and has rank 6. Its fundamental representation is **27**. The superstring-inspired E_6 model contains many particles in addition to the particles in the SM: super-partners of the SM fermions and gauge bosons, extended gauge and Higgs bosons, new "exotic" quarks and leptons and scalar di- or leptoquarks.

2.3 Leptoquark-like Couplings in R-Parity Violating Supersymmetry

Supersymmetric (SUSY) models predict so-called super-partners of each fermion and each boson of the SM. The masses of theses super-partners are assumed to

be in the TeV scale or above, so they have escaped experimental observation so far. The super-partners of the SM particles are written as the letter of the SM particle with a tilde; so the super-partner of an up-quark the up-squark is written as $\tilde{u}$. A general review of SUSY models can be found in [10].
SUSY models can be divided into two kinds of models, R-parity violating and R-parity conserving models. SM particles carry $R = +1$ while $R = -1$ is assigned to super-partners of the SM particles. R is defined as

$$R = (-1)^{3B+L+2S},$$

where L and B are the lepton and baryon numbers respectively. S denotes the spin of the particle. In R-parity conserving models SUSY particles can be created only in pairs. This also means that the lightest SUSY particle must be stable. In R-parity violating models SUSY particles can be created singly. Searches for leptoquarks can have implications on the search for SUSY particles [11] because squarks in R-parity violating SUSY models might have leptoquark-like decays through Yukawa couplings in addition to their normal decay modes through gauge couplings. For example the $\tilde{u}_L$ squark (the superpartner of the left-handed u-quark) may couple to an e^++d pair via a Yukawa coupling λ'_{111} similar to the coupling of the first generation $\tilde{S}_{1/2,L}$ leptoquark with the electric charge $\frac{2}{3}$. Via the same coupling the $\tilde{d}_L$-like squark (the superpartner of the left-handed d-quark) couples to e^-+u or ν_e+d pairs like the first generation $S_{0,L}$ with the electric charge $\frac{1}{3}$.

2.4 The Effective Leptoquark Model

This introduction of the effective leptoquark model closely follows [11] and [12]. The most general effective Lagrangian for leptoquark interactions with SM fermion pairs which fulfills all of the following conditions was proposed by Buchmüller, Rückl and Wyler [2]. It assumes that LQs

I) have renormizable interactions

II) have interactions invariant under the SM gauge groups $SU(3)_C \otimes SU(2)_L \otimes U(1)_Y$

III) couple only to SM fermions, gauge bosons and the Higgs boson

One further assumption to avoid contradictions with measurements of the minimum lifetime of the proton amongst others is, that LQs

IV) are required to conserve the lepton number L_l and the baryon number B_q separately.

Such leptoquarks carry the fermion number

$$F = 3B_q + L_l \tag{2.1}$$

of either $|F| = 0$ or $|F| = 2$ and have interactions described by the Lagrangian

$$\mathscr{L} = \mathscr{L}_{|F|=2} + \mathscr{L}_{|F|=0} \tag{2.2}$$

with

$$\begin{aligned}
\mathscr{L}_{|F|=2} &= (g_{1L}\bar{q}_L^c i\tau_2 l_L + g_{1R}\bar{u}_R^c i e_R^-)S_0 + \hat{g}_{1R}\bar{d}_R^c e_R^- \hat{S}_0 + g_{3L}\bar{q}_L^c i\tau_2 \tau l_L S_1 \\
&\quad + (g_{2L}\bar{d}_R^c \gamma^\mu l_L + g_{2R}\bar{q}_L^c \gamma^\mu e_R^-)V_{1/2\mu} + \hat{g}_{2L}\bar{u}_R^c \gamma^\mu l_L \hat{V}_{1/2\mu} + h.c. \\
\mathscr{L}_{|F|=0} &= (h_{1L}\bar{q}_L \gamma^\mu l_L + h_{1R}\bar{d}_R \gamma^\mu e_R^-)V_{0\mu} + \hat{h}_{1R}\bar{u}_R \gamma^\mu e_R^- \hat{V}_{0\mu} + h_{3L}\bar{q}_L \tau \gamma^\mu l_L V_{1\mu} \\
&\quad + (h_{2L}\bar{u}_R l_L + h_{2R}\bar{q}_L i\tau_2 e_R^-)S_{1/2} + \hat{h}_{2L}\bar{d}_R l_L \hat{S}_{1/2} + h.c.
\end{aligned}$$

Herein q_L and l_L are the $\mathrm{SU}(2)_L$ left-handed quark and lepton doublets while e_R, d_R and u_R are the corresponding right-handed singlets for leptons, d-type and u-type quarks. The Ψ^c are the charge conjugate of the corresponding fermion field: $\Psi^c \equiv \mathrm{C}\ \bar{\Psi}^T$. The indices L and R appended to the coupling constants indicate the chirality of the fermion involved. The indices for the color and the 3 generations have been dropped for simplicity. S_T and V_T denote the scalar and vector leptoquarks respectively, their index $\mathrm{T} = 0$, $\frac{1}{2}$ or 1 refers to the weak isospin. g_i, $\hat{g}_i$, h_i and $\hat{h}_i$ are the various leptoquark couplings to quarks and leptons. Two more restrictions are imposed to cope with the existing low-energy constraints:

V) each LQ couples to only a single quark-lepton generation, i.e. there are 3 LQ generations

VI) each LQ has pure chiral couplings to SM fermions

The LQ model which fulfills all these restrictions will be henceforward called the "minimum-Buchmüller-Rückl-Wyler effective model" (mBRW). With these restrictions it is sufficient to use the generic symbol λ for the different Yukawa couplings g_i, $\hat{g}_i$, h_i and $\hat{h}_i$. The restriction V) on intra-generational interactions avoids flavor-changing neutral currents as well as flavor-universality violations at tree-level. The last restriction avoids direct contributions to chirally suppressed

$\lvert F\rvert = 2$ Leptoquarks				$\lvert F\rvert = 0$ Leptoquarks			
LQ	Q_{em}	T_3	Decay	LQ	Q_{em}	T_3	Decay
$S_{0,L}$	$-1/3$	0	$e_L^- u_L$ or $\nu_L d_L$	$V_{0,L}$	$-2/3$	0	$e_L^- \bar{d}_R$ or $\nu_L \bar{u}_R$
$S_{0,R}$			$e_R^- u_R$	$V_{0,R}$			$e_R^- \bar{d}_L$
$\hat{S}_{0,R}$	$-4/3$	0	$e_R^- d_R$	$\hat{V}_{0,R}$	$-5/3$	0	$e_R^- \bar{u}_L$
$S_{1,L}$	$-4/3$	-1	$e_L^- d_L$	$V_{1,L}$	$-5/3$	-1	$e_L^- \bar{u}_R$
	$-1/3$	0	$e_L^- u_L$ or $\nu_L d_L$		$-2/3$	0	$e_L^- \bar{d}_R$ or $\nu_L \bar{u}_R$
	$+2/3$	$+1$	$\nu_L u_L$		$+1/3$	$+1$	$\nu_L \bar{d}_R$
$V_{1/2,L}$	$-4/3$	$-1/2$	$e_L^- d_R$	$S_{1/2,L}$	$-5/3$	$-1/2$	$e_L^- \bar{u}_L$
$V_{1/2,R}$	$-4/3$		$e_R^- d_L$	$S_{1/2,R}$	$-5/3$		$e_R^- \bar{u}_R$
	$-1/3$	$+1/2$	$e_R^- u_L$		$-2/3$	$+1/2$	$e_R^- \bar{d}_R$
$\hat{V}_{1/2,L}$	$-1/3$	$-1/2$	$e_L^- u_R$	$\hat{S}_{1/2,L}$	$-2/3$	$-1/2$	$e_L^- \bar{d}_L$
	$+2/3$	$+1/2$	$\nu_L u_R$		$+1/3$	$+1/2$	$\nu_L \bar{d}_L$

Table 2.1: Scalar (S) and vector (V) leptoquarks incorporated in the mBRW model, grouped with respect to the weak isospin and the absolute value of the fermion number F (see Equation 2.1). Q_{em} is the electric charge of the leptoquark (LQ) while T_3 is the third component of the weak isospin. The third row shows the possible decay products of the various leptoquarks.

meson decays such as $\pi \to e\nu$ as well as virtual-loop contributions to the $g-2$ of the muon. The leptoquarks incorporated in the mBRW-model are summarized in Table 2.1.

The same symbol represents LQs of various electric charges within an isospin family for reasons of simplicity. For example the $S_{1/2,R}$ denotes both the leptoquarks $S_{1/2}$ state of the electric charge of -2/3 as well as the state of -5/3, both coupling to a right-handed lepton. Thus one distinguishes 14 types of leptoquarks: 7 scalars with either $|F| = 0$ ($S_{1/2,L}$, $S_{1/2,R}$, $\tilde{S}_{1/2,L}$) or $|F| = 2$ ($S_{0,L}$, $S_{0,R}$, $\tilde{S}_{0,R}$, $S_{1,L}$) and 7 vectors with either $|F| = 0$ ($V_{0,L}$, $V_{0,R}$, $\tilde{V}_{0,R}$, $V_{1,L}$) or $|F| = 2$ ($V_{1/2,L}$, $V_{1/2,R}$, $\tilde{V}_{1/2,L}$). By construction of the model the decay branching ratios $\beta(LQ \to l^{\pm} q)$ are fixed to 0, $\frac{1}{2}$ or 1. A specific underlying theory usually predicts only a subset of the mBRW-leptoquark states. The leptoquark in superstring-inspired E_6 models corresponds to the $S_{0,L}$ of Table 2.1. In a model that tries to reconcile SU(5) GUT theories with the existing data of the proton lifetime and of the Weinberg angle $\sin^2\theta_W$ a light scalar iso-doublet of leptoquarks has been proposed [13] corresponding to the $S_{0,L}$ of Table 2.1. In such models light color-exotic scalars appear to be a generic feature [14]. A weak-isospin singlet vector leptoquark of hypercharge $\frac{2}{3}$ corresponding to the V_0 appears in the Pati-Salam GUT model [15]. All 14 states listed in Table 2.1 appear in a GUT based on the SU(15) gauge group [16, 17, 18].
It is assumed that the decay width of the leptoquarks, which depends on the

unknown quark-lepton-leptoquark coupling, is small compared to the detector resolution.

2.5 Production of Leptoquarks

Leptoquarks can be produced singly or in pairs. The main production at the Large Hadron Collider (LHC) will be pair production via gg-fusion with a minor contribution via $q\bar{q}$ annihilation, unless the Yukawa couplings are rather large (e.g. of the order of the electromagnetic strength or stronger) [19]. The cross-section of scalar pair production only depends on the leptoquark spin and on the fact that it is a color-triplet field while the cross-section of single leptoquark production (Figure 2.1) depends on the unknown Yukawa coupling λ_{lq}, which is model dependent. The lowest-order Feynman diagrams for leptoquark pair-production and decay are shown in Figure 2.2. At the LHC, like at all hadron-hadron colliders, LQs of all three generations can be produced while ep colliders like HERA were mainly sensitive to first-generation leptoquarks.

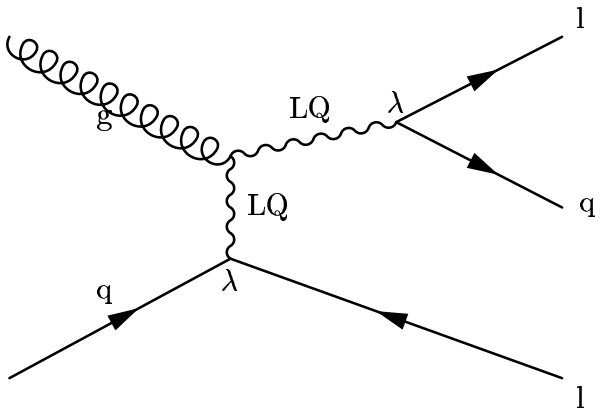

Figure 2.1: Example of leptoquark single production. This process depends on the unknown Yukawa coupling λ

M. Krämer et al. calculated the cross-sections of pair production of scalar leptoquarks for different masses at the LHC [20]. The calculated cross-sections depending on the mass of the scalar leptoquark can be seen in Table 2.2; with increasing scalar leptoquark mass the corresponding cross-section decreases very rapidly. The Feynman-graphs shown in Figure 2.2 were included in their calculations. The systematic errors given in Table 2.2 have been calculated by adding quadratically the errors resulting from the variation of the renormalization and factorization scale by a factor of 2 and the error resulting in the variation of the parton distribution function (PDF). The PDF error has been calculated by using the 40 PDF tables provided by the CTEQ group [21] for the calculation

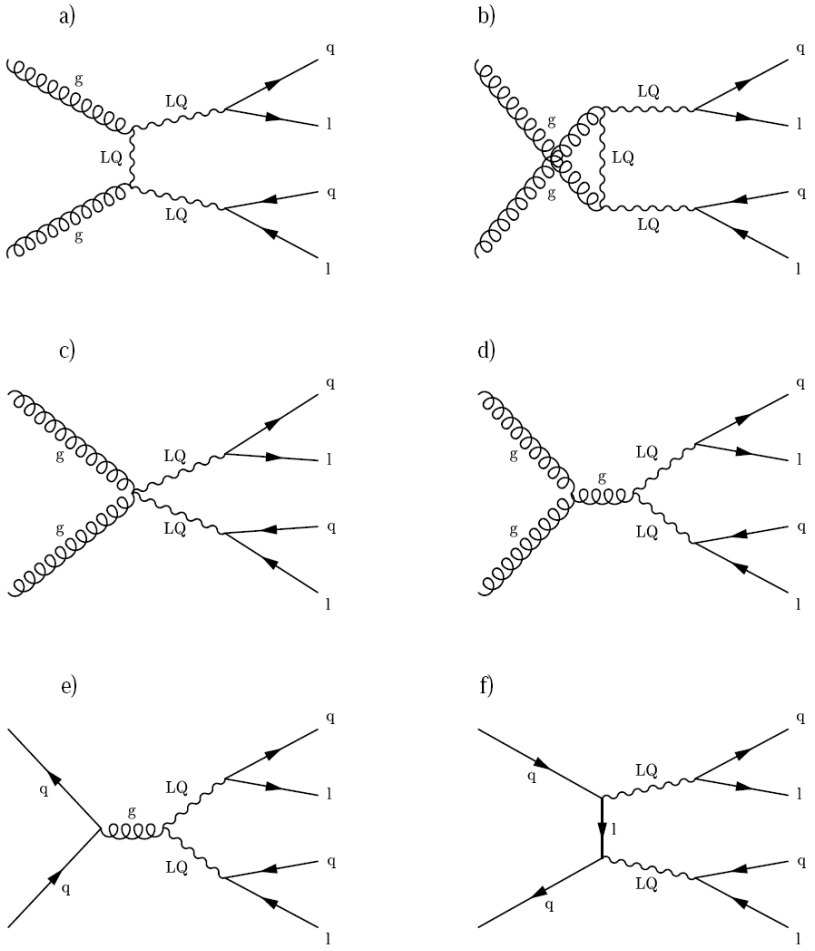

Figure 2.2: Feynman graphs for the LQ pair production.

Scalar Leptoquark m_{LQ} [GeV]	cross-section (NLO) [pb]
300	10.1 ± 1.5
400	2.24 ± 0.36
600	0.225 ± 0.048
800	0.0378 ± 0.0105
1000	0.00836 ± 0.00214
1200	0.00221 ± 0.00095
1400	0.000655 ± 0.000346
1600	0.000210 ± 0.000134
1800	0.0000714 ± 0.0000294

Table 2.2: Cross-sections of scalar leptoquarks depending on their mass for a center-of-mass energy of 14 TeV [20]

of CTEQ6M PDF errors. The CTEQ6M PDF has been used by M. Krämer et al. for their calculation. The error of the CTEQ6M PDF is parametrized in 20 dimensions/variables; so each of the 20 variables has been varied in two directions resulting in 40 PDF tables. The largest difference between the calculated reference cross-section and the 2 cross-sections calculated with the 2 PDF tables, where one variable has been varied in one and the other direction, has been taken. These 20 numbers were added quadratically and the result was taken as PDF error.

As mentioned earlier LQs could decay into a mix of quarks or leptons of different generations. But experimental constraints require LQs to appear in 3 different generations, each decaying into a quark of its generation and a lepton of its generation. Further constraints of the mBRW-model even require the branching ratio of the LQ decaying into a charged lepton and a quark to be 0, 0.5 or 1. This thesis only deals with leptoquarks of the second generation decaying into a (anti-)muon and a charm quark. The branching ratio (BR) β of this decay is assumed to be 1 unless otherwise stated.

2.6 Summary of Experimental Results

This section summarizes the experimental results from searches for second generation leptoquarks and indirect measurements. A good overview of experimental results in leptoquark searches of all generations up to the year 2002 can be found in [11]. The best source for exclusion limits for second generation leptoquarks is Tevatron. For $\beta = 1$ the 95% CL exclusion limit of the DØ [22] and CDF [23] experiments are $m_{LQ} < 300$ GeV and $m_{LQ} < 226$ GeV respectively; these values were obtained with an integrated luminosity of 1 fb^{-1} and 200 pb^{-1} respectively.

The Tevatron exclusion limits are expected to reach up to 300 GeV – 350 GeV in the near future. The DELPHI experiment [24] at LEP1 searched also for single production of second generation leptoquarks and excluded masses up to 73 GeV at 95% confidence level assuming the Yukawa coupling $\lambda = \alpha_{em}$.

Chapter 3

ATLAS and the Large Hadron Collider

The Large Hadron Collider (LHC) is the particle accelerator with the highest center-of-mass energy worldwide up to this date. It opens up exciting new possibilities to probe the laws of nature.

3.1 The Large Hadron Collider

The LHC (Figure 3.1) which will start running in 2008 has been built from 2002-2008 into the LEP tunnel at CERN[1], which is located close to Geneva. The LHC is a proton-proton collider with a center-of-mass energy of up to $\sqrt{s} = 14$ TeV; 7 TeV per beam, which circulate in opposite directions in the beam pipes. A profile of the cryodipoles including the beam pipes can be seen in Figure 3.2. The LHC has a circumference of 26.7 km and its magnets are cooled down to supraconductivity at 4.5 K. One remarkable characteristic of the LHC is its high instantaneous luminosity of up to 10^{34} cm^{-2} s^{-1}.

3.1.1 The CERN Accelerator Complex

The protons are accelerated to an energy of 450 GeV before they are injected into the LHC. At the beginning protons are accelerated in the linear accelerator LINAC2 (Figure 3.3) to an energy of 50 MeV. Afterwards they are injected into the Proton Synchrotron (PS) Booster where they reach an energy of 1.4 GeV. From the PS Booster they enter the PS ring. In the PS ring they are accelerated to 26 GeV. From the PS ring they are guided into the Super Proton Synchrotron (SPS) ring where they are once again accelerated to reach an energy of 450 GeV.

[1] Organisation Européenne pour la Recherche Nucléaire, originally: **C**onseil **E**uropéen pour la **R**echerche **N**ucléaire

Figure 3.1: An aerial view of the location of the LHC and SPS ring [25]

Figure 3.2: Profile of one of the 15m long cryodipoles of the LHC [25]

After this step they are injected into the LHC where they reach their maximum energy of up to 7 TeV.

3.2 The ATLAS Detector

ATLAS[2] is one of the four main experiments at the LHC which can be seen in Figure 3.4. The ATLAS detector (Figure 3.5) weighs over 7000 t, is 44 m long and has a diameter of 22 m [26]. It has a 4π onion layout consisting of a series of concentric cylinders increasing in diameter around the beam pipe. The detector can be divided into 3 main parts: the Inner Detector (white), the calorimeters (green and orange) and the muon spectrometers (blue). Each part is composed of multiple layers.

3.2.1 The Inner Detector

The Inner Detector begins a few centimeters away from the beam pipe and has a radius of 1.2 m, stretching over a length of 7 m along the beam pipe. It covers a pseudorapidity range of $|\eta| < 2.5$; the pseudorapidity is defined as $\eta \equiv -\ln(\tan\frac{\theta}{2})$, where θ is the polar angle. $\eta = 0$ corresponds to the direction perpendicular to the beams. The Inner Detector consists of the Pixel Detector, the Semiconductor Tracker (SCT) and the Transition Radiation Tracker (TRT). The Pixel Detector, which is the innermost part, consists of 3 barrels with average radii of 4 cm, 10 cm and 13 cm and of 3 disks on each endcap. There are 1456 barrel and 288 disk modules, each measuring 2 cm $\times$ 6 cm. Each module has about 46,080 pixels, where each pixel has the size of 50 μm $\times$ 400 μm. All together the Pixel Detector has about 80 million readout channels, which corresponds to half of all readout channels of the ATLAS detector. The pixels allow a precise measurement of the particles close to the interaction point.

The SCT is very similar to the Pixel Detector but has long narrow strips instead of pixels. Each strip measures 80 μm $\times$ 12 cm. The SCT consists of 2 double layers of silicon and contributes 6.2 million readout channels.

The TRT is a Transition Radiation Detector with straw trackers. The barrel part contains about 52,000 axial straws of about 150 cm length covering the radial range from 56 cm to 107 cm. The endcaps have about 245,000 radial straws covering the radial range from 64 cm to 103 cm. There are about 420,000 channels, each providing a drift time measurement and 2 independent thresholds. Tracking hits will pass the lower threshold while transition radiation hits will pass the higher one. The TRT has a good performance even at high occupancy.

[2] **A** **T**oroidal **L**HC **A**pparatu**S**

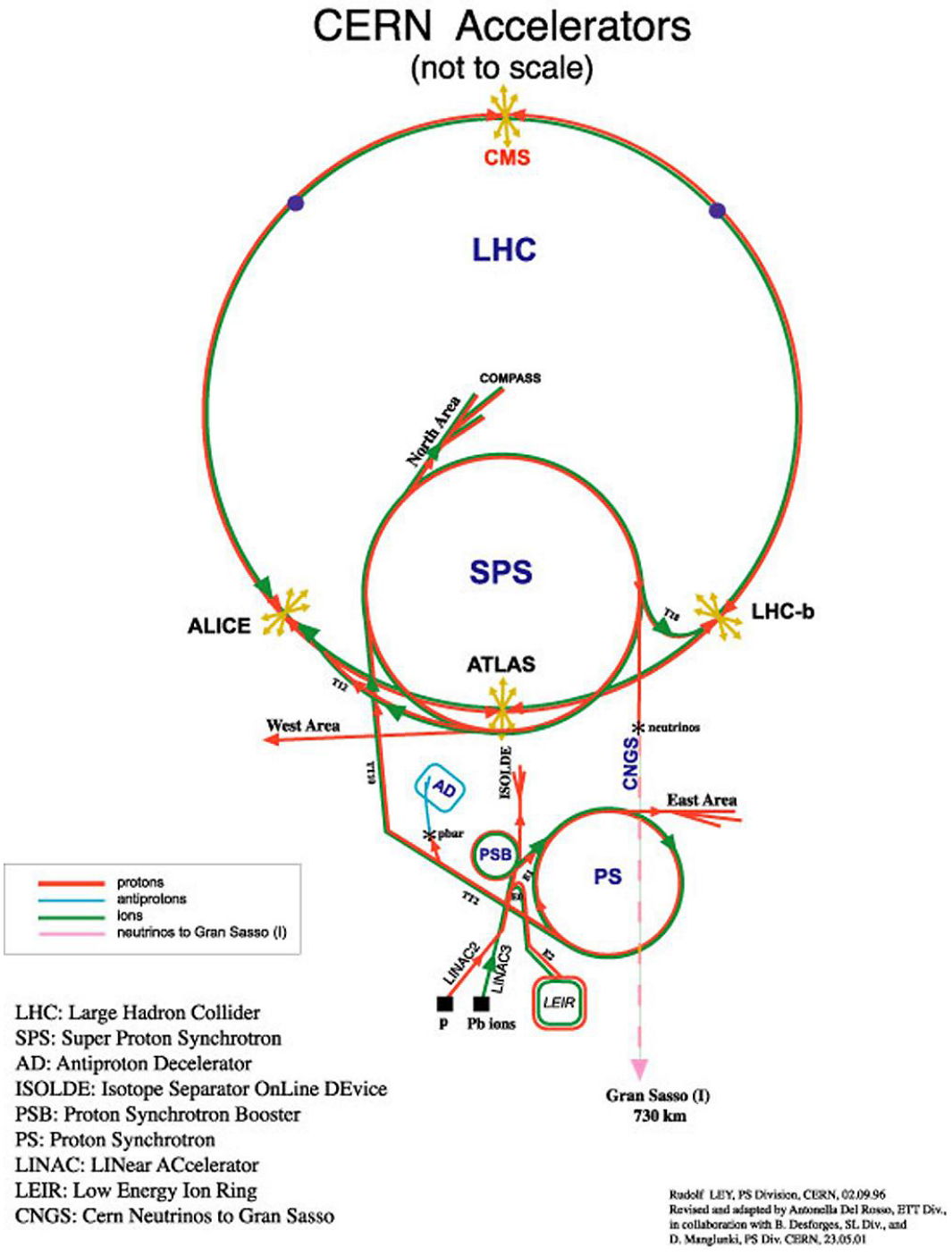

Figure 3.3: The CERN accelerator complex [25]

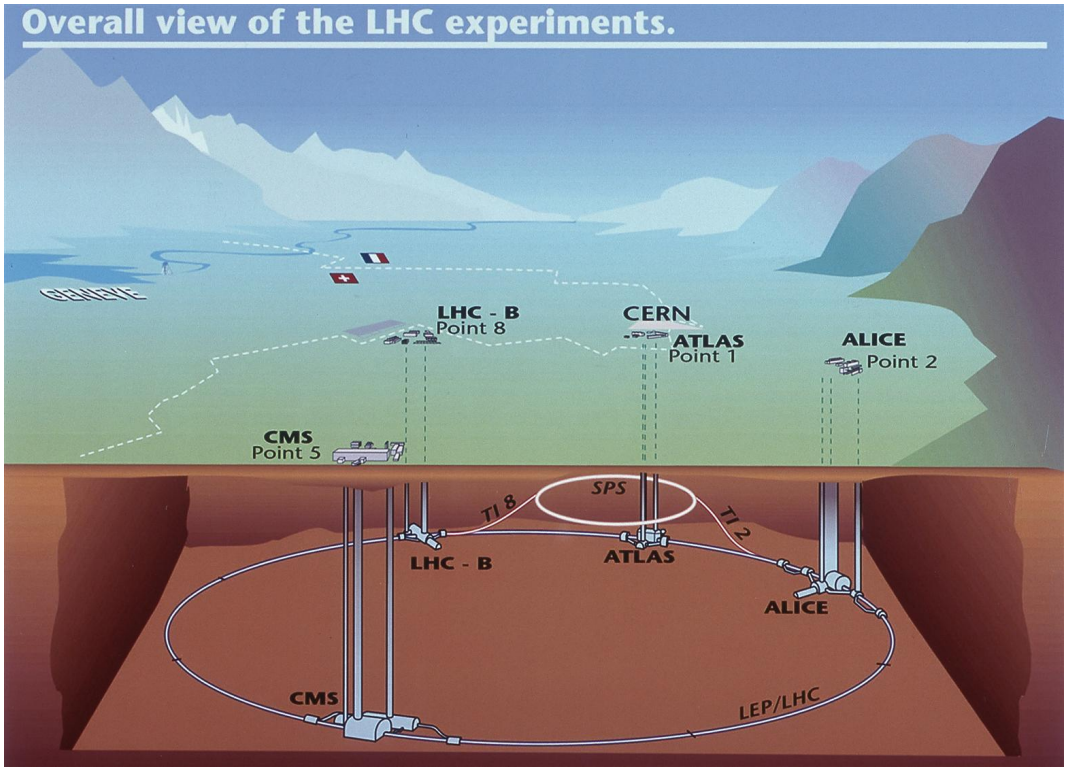

Figure 3.4: Overall view of the location of the LHC experiments [25]

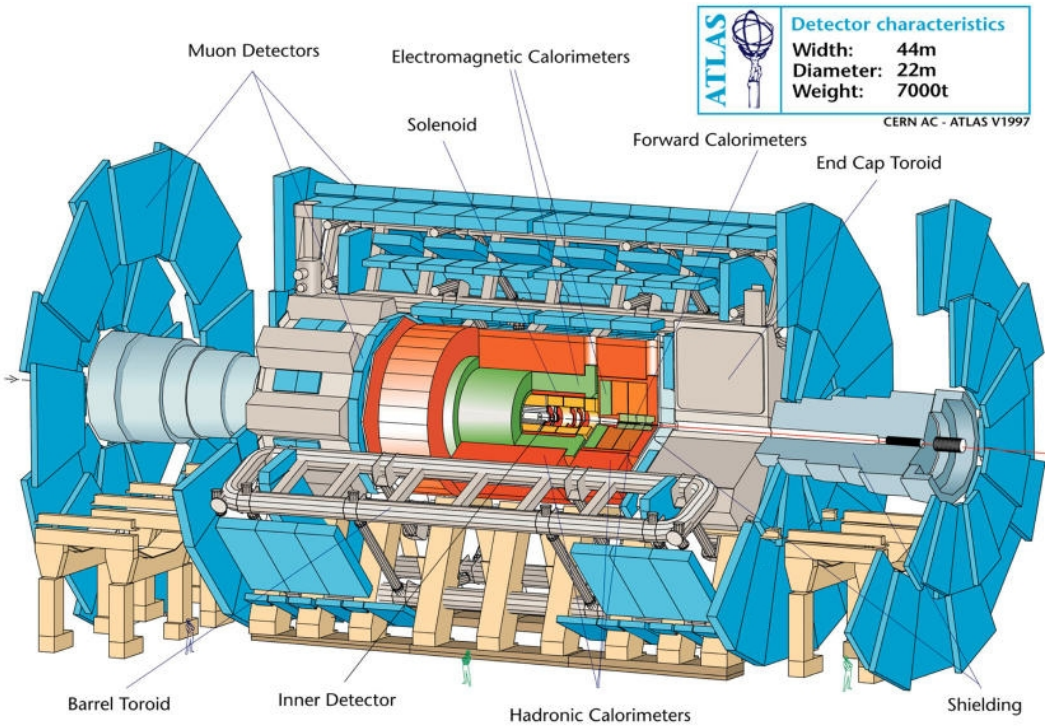

Figure 3.5: 3-dimensional view of the ATLAS detector [25]

3.2.2 The Calorimeters

The ATLAS calorimeters consist of an inner electromagnetic calorimeter covering the region $|\eta| < 3.2$ and an outer hadronic calorimeter covering the region $|\eta| < 4.9$ all together. Both are sampling calorimeters, i.e. they are sandwiches consisting of alternating slides of energy absorbing metal and detector material. The electromagnetic calorimeter is a detector with an accordion geometry in the barrel-part to prevent cracks in the azimuthal angle ϕ, i.e. to cover the full ϕ-range. It consists of lead and stainless steel as sampling material and liquid argon as detector (LAr) and mainly detects photons and electrons; it also detects a part of the hadron shower. A cryostat is installed around the calorimeter to keep the argon in a liquid phase. The ATLAS hadronic calorimeter is a sandwich of iron and plastic scintillators covering a region of $|\eta| < 1.7$. Over the range $\sim 1.5 < |\eta| < 4.9$ LAr calorimeters were chosen. The diameter of the hadronic calorimeter is 8 m and it covers 12 m along the beam pipe. The far-forward sections of the hadronic calorimeter are contained in the electromagnetic calorimeter's cryostat and uses liquid argon, too, because a higher radiation resistance is needed.

3.2.3 The Muon System

The outermost part is the muon system (see Figure 3.6), since muons with a momentum of at least 6 GeV are the only SM particles (besides neutrinos) to reach this point of the detector. The muon system consists of several subdetectors with the muon drift tubes (MDTs) as their main part. An MDT chamber (see Figure 3.7) consists of 6 to 8 drift tube layers which are arranged in 2 so-called multi-layers. The tubes are composed of aluminum and are filled with a mixture of argon and CO_2. In the center of the tube is a wire; the wire is at a positive potential of about 3 kV to the tube. A muon which passes the tube ionizes the gas and the created free electrons drift to the wire in the center while the positive ions drift to the tube wall. The drift time of these electrons is calculated using the triggers mentioned below and the distance between the muon that passed and the wire is calculated, which gives one drift circle per tube. Since the muon passed (in most cases) three tubes per multi-layer one can do a tangential fit to these six drift circles which gives the approximate track of the passed muon.
The track of the muons is measured at three different distances from the interaction point and their momentum is calculated from their curvature [27]. The muon system covers a region of $|\eta| < 2.7$. In the far-forward region Cathode Strip Chambers (CSCs) are used instead of the MDTs because they can resist higher radiation. The CSCs are multiwire proportional chambers (MWPCs). As a trigger system Resistive Plate Chambers (RPCs) are used in the barrel region and Thin Gap Chambers (TGCs) are used in the endcap region. The RPCs are gaseous detectors without any wires in them. The basic RPC unit consists of two

parallel resistive bakelite plates, separated by 2 mm of insulating spacers, and such forming a narrow gas gap. They are read out by metal strips on both sides of the detector. The RPCs allow a very precise time resolution. The TGCs are similar to MWPCs but the distance between the anode wires is larger than the cathode-anode distance, in contrast to normal MWPCs.

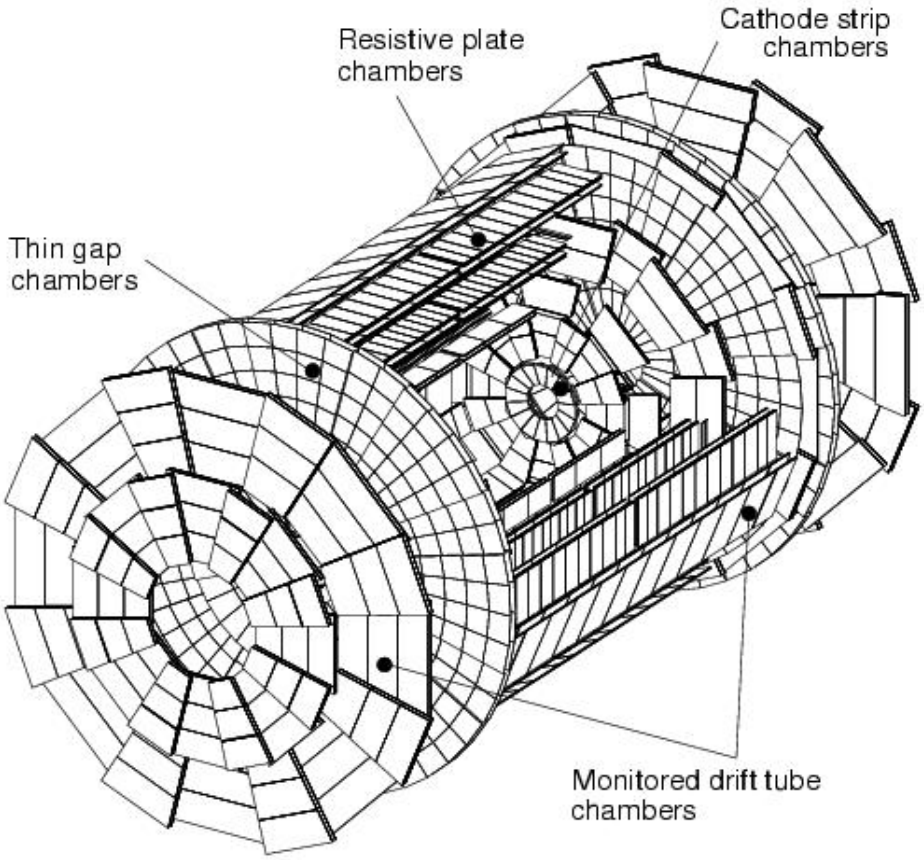

Figure 3.6: The ATLAS Muon Spectrometer [25]

3.2.4 The Magnet System

In the ATLAS detector there are 2 kinds of magnets. A supraconducting solenoid cooled down to 4.5 K is located between the inner detector and the calorimeter and creates an almost uniform magnetic field with a strength of up to 2 T. The

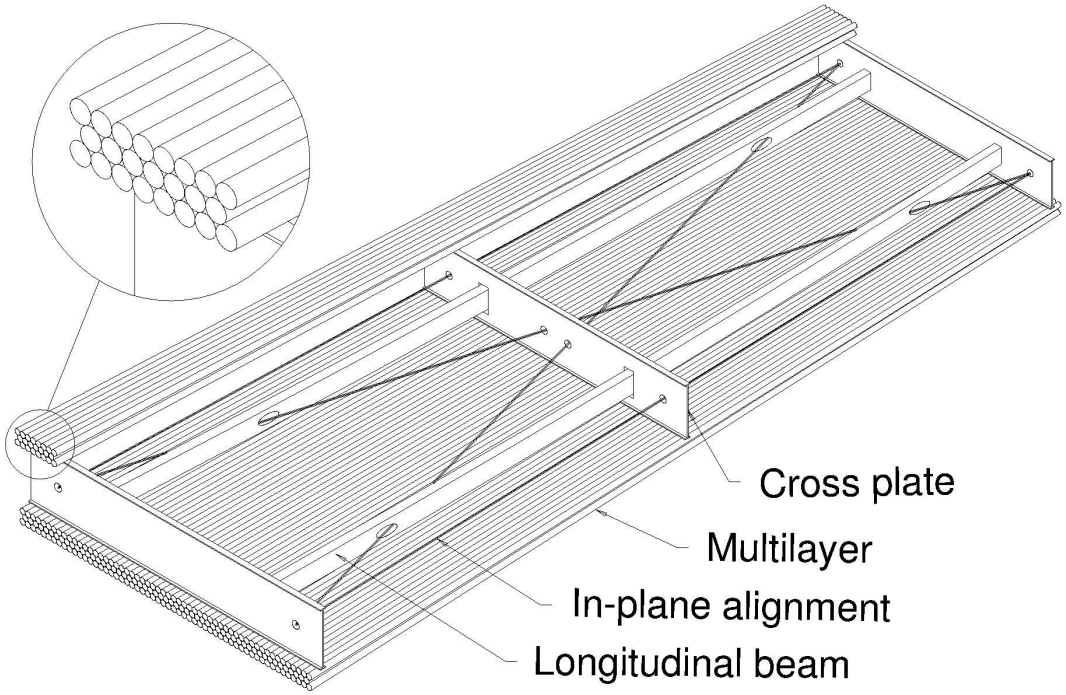

Figure 3.7: Sketch of a MDT, six layers of tubes in 2 multi-layers

solenoid is 5.3 m long and has a diameter of 2.5 m.
A toroidal magnetic field is created by 8 large supraconducting air-core coils in the barrel region plus 8 coils in each of the two endcaps. They are located outside of the calorimeters and create the magnetic field for the muon detectors. The magnetic field created by the air-cores is up to 4 T and is non-uniform; it covers an η-range of up to 2.7. The overall dimensions of the magnet system are 26 meters in length and 20 meters in diameter.

3.2.5 Alignment

An optical alignment system is being used to measure the displacement of all chambers within a projective tower relative to their ideal position of up to $\pm$ 30 μm. Displacements up to $\sim$ 1 cm between chambers of different towers can then be corrected in the offline analysis.

3.3 Trigger System

The LHC has a very high bunching rate of up to one bunch every 25 ns. One bunch consists of $1 \cdot 10^{11}$ protons and has a length of 7.5 cm. There will be up to 23 proton-proton interactions per bunch-crossing. So the rate of data produced

is far too high to be recorded. In order to process this enormous amount of data, events have to be divided into interesting and uninteresting events, where only the interesting events will be processed; the uninteresting events will be "thrown away", i.e. not processed or recorded. The system to select the events is the trigger system which has 3 levels in the ATLAS experiment: Level-1, Level-2 and the EventFilter, see Figure 3.8. Each trigger level reduces the rate of events and only events that survive all trigger levels are stored permanently. The Level-1 trigger reduces the rate from 40 MHz to 75 kHz. The Level-2 trigger reduces the rate from 75 kHz to 1 kHz and the EventFilter trigger to the final rate of 200 Hz. Only events that were triggered by the Level-1 trigger reach the Level-2 trigger and only events that were triggered by Level-2 reach the EventFilter trigger. While calculating if the event fulfills the requirements the data from the different detector parts are stored in so-called pipeline memories.

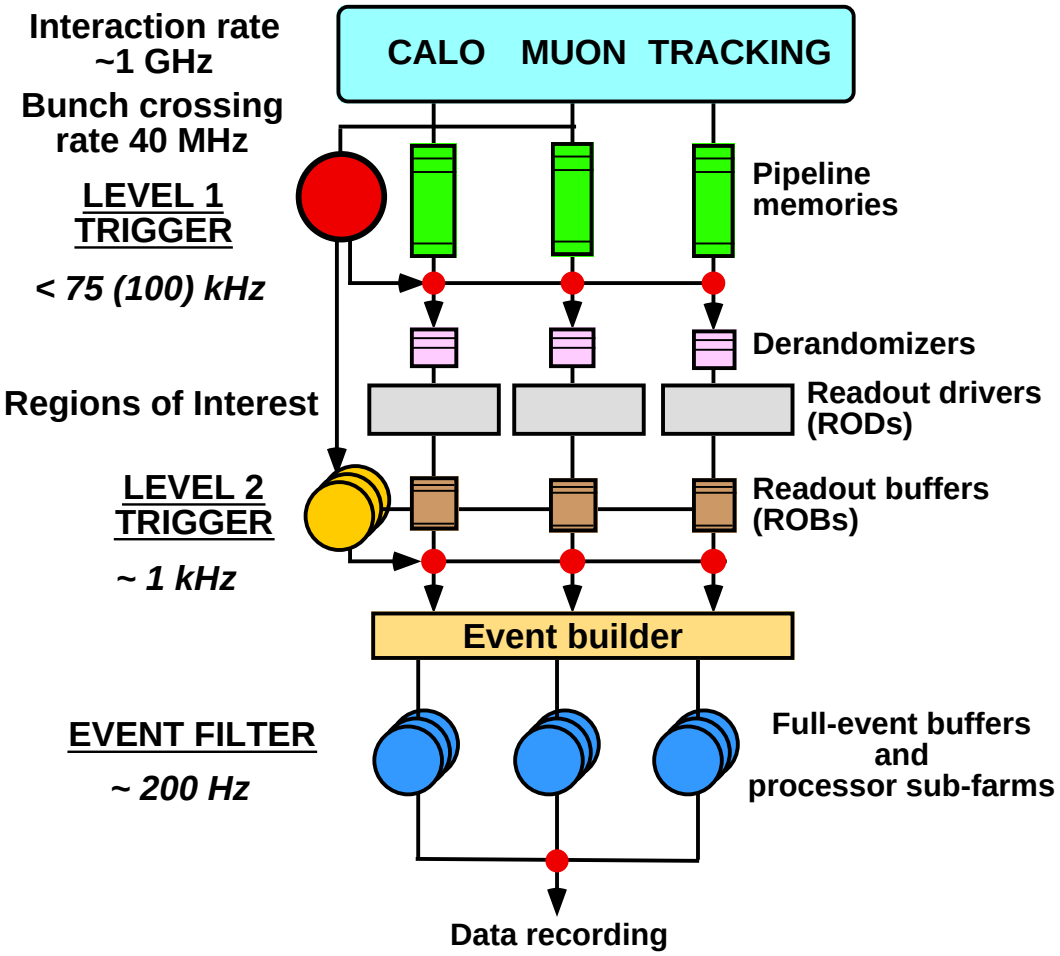

Figure 3.8: Schematic view of the ATLAS trigger system [25]

3.3.1 Level-1 trigger

The Level-1 trigger in the ATLAS experiment consists of two parts: the muon trigger and the calorimeter trigger. Since the Level-1 trigger has only 2.5 μs to decide whether to accept or reject the event the implementation is hardware-based. The Level-1 trigger has only access to certain parts of the detector and uses only a coarse resolution of the calorimeters. The Level-1 trigger defines so-called Regions-of-Interest (ROIs), i.e. regions where interesting particles transverse the detector. The Level-1 trigger passes pointers to events and their ROIs that fulfill one of the triggers onto the Level-2 trigger.

3.3.2 Level-2 trigger

The Level-2 trigger system is software-based since the Level-2 trigger has more time (10 ms) to decide whether to accept or reject the event. The Level-2 trigger has access to all data from all subdetectors within the ROIs defined by the Level-1 trigger. Again events that fulfill one of the Level-2 triggers are passed onto the EventFilter trigger.

3.3.3 EventFilter trigger

The EventFilter trigger is also software-based. The EventFilter trigger has a few seconds to decide whether to store or reject the event. The EventFilter trigger has access to all parts of all the subdetectors. It also has access to the calibration and alignment information. Events that survive the EventFilter trigger are stored permanently on media. Even after this reduction the amount of data to be stored is expected to be around 1 PetaByte per year [28].

3.4 The ATLAS Software Framework ATHENA

The ATLAS software framework called "ATHENA" is based on the Gaudi framework [29] written in C++ and PYTHON. It allows to analyze recorded (or simulated) events and also allows to control the generation of Monte Carlo (MC) events by other programs like PYTHIA [30], Herwig [31] etc. and the simulation of these events by GEANT [32]. Simulated events are needed to do physics analyses like this thesis for physics events, which the ATLAS detector can detect, before the LHC starts its run. Also later simulated events are very important since you have the full (MC) information, i.e. the original energies of the quarks before hadronization etc., and you can compare this information with the measured data. Furthermore simulated events are used for calibration of the detector and estimation of the number of background events in an analysis.
The chain of MC production from the generation over the simulation to the cre-

ation of the so-called Analysis Object Data (AOD) can be seen in Figure 3.9. The full production consists of the following steps:

- Generation: the physics event, i.e. the 4-vectors and vertices of all particles in an event, are generated. This is done by external Monte Carlo generators.
- Simulation: the effect of the generated particles transversing the different parts of the detector, i.e. the interaction between the different particles and the detector material, is calculated. This is done by following the path of a particle in step sizes of 30 μm and less.
- Digitization: the response of the different detector parts on the calculated interactions is calculated. This information has the same format as one would get from real physics data from the detector.
- Reconstruction: using the response of the different detector parts the tracks of the particles in an event are reconstructed.

There is a short-circuit to the full-chain by using ATLFAST which provides a fast simulation of the whole chain by taking the generated events and smearing the tracks of the particles through the detector to produce AODs directly [33]. The disadvantage of the fast simulation is that some physics effects like fake particles cannot be simulated this way and that the resolution of this kind of simulation is quite imprecise so far.
All Monte Carlo samples in ATLAS have been produced centrally. The computing power has been a limiting factor in the number of Monte Carlo events that were fully simulated and produced. Furthermore not all computing power has been available for the production of Monte Carlo samples, but a significant fraction has been used for the validation of new software releases.

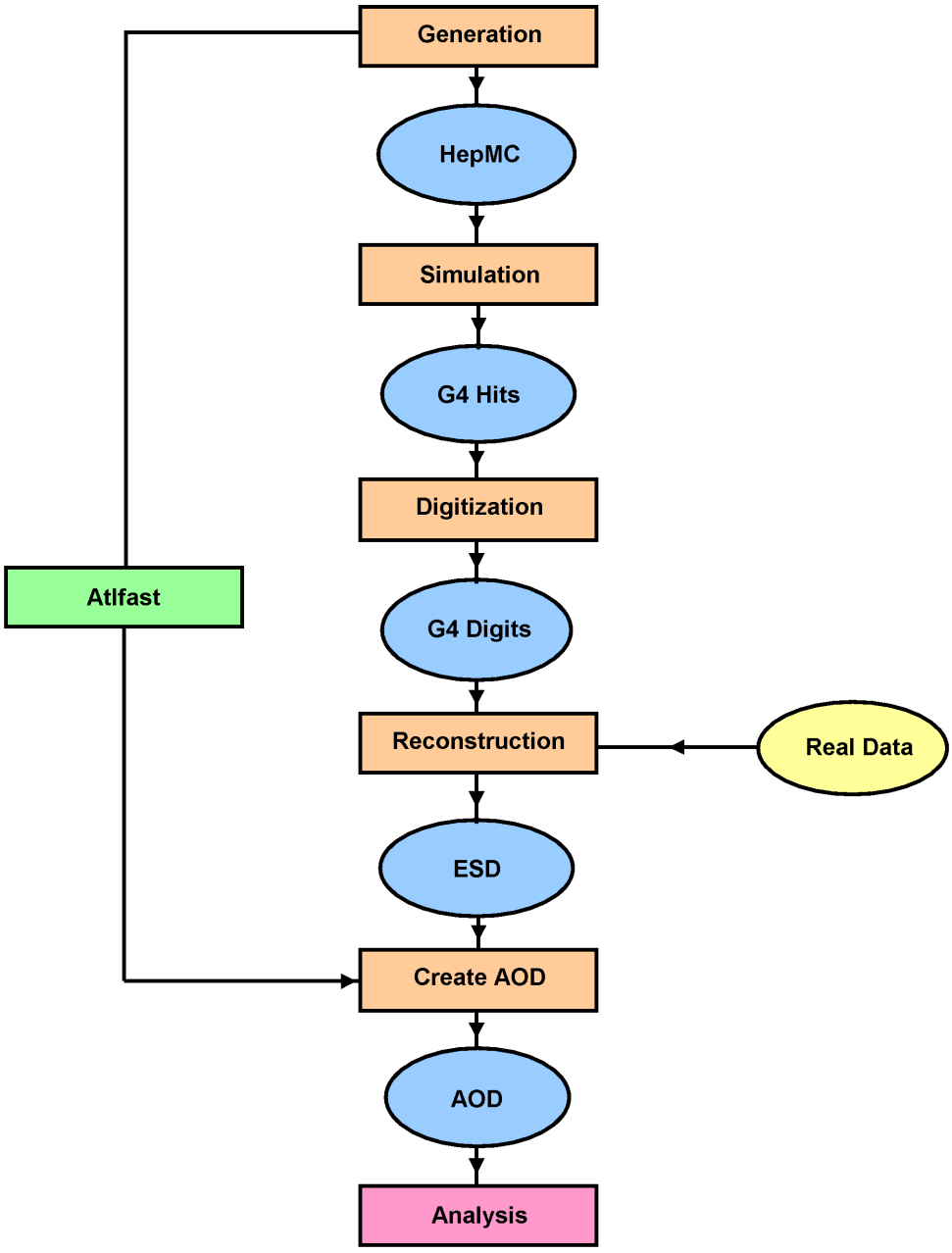

Figure 3.9: The full Monte Carlo chain in ATLAS [33]

Chapter 4

Search for Second Generation Leptoquarks in μ + jet + μ + jet Events

This analysis studies scalar second generation (sec. gen.) leptoquark pair events. Scalar leptoquarks are studied since scalar leptoquarks typically have smaller cross-sections than vector leptoquarks at hadron colliders [34]. It is assumed that 100% of all second generation leptoquarks decay into a muon and a quark (unless otherwise stated). So the final state consists of two muons and two quarks ($\mu + jet + \mu + jet$). The muons and jets have a high energy because of the large mass of the tested second generation leptoquarks.

4.1 Main Standard Model Backgrounds

The main Standard Model (SM) background processes which have the same particles in the final state as the second generation leptoquark events, i.e. two high-energetic muons and two high-energetic jets, are:

- $t\bar{t}$, where each top-quark decays into a b-quark and a W-boson and both W-bosons decay into a muon and a ν_μ
- Z/γ^* decaying into two muons (the initial state radiation mainly produces the two high-energetic jets)
- WW, where both W-bosons decay into a muon and a ν_μ (the initial state radiation mainly produces the two high-energetic jets)
- ZZ, where one Z-boson decays into two muons and the other Z-boson into two jets

process	$\sigma\cdot$ BR in pb	$\int \mathscr{L}$ dt in pb^{-1}
Z/γ^* $m_Z^{MC} > 60$ GeV	2032	249
Z/γ^* $m_Z^{MC} \geq 150$ GeV	9.08	2,175
$t\bar{t}$, decaying not fully hadronically	450	923
WW	40.9	1,222
ZZ	3.94	12,640
ZW	16.4	2,920

Table 4.1: Cross-sections of the main SM backgrounds and the integrated pp luminosities of simulated Monte-Carlo samples, which were available for this analysis [35]

- ZW, where the Z-boson decays into two muons and the W decays hadronically

The cross-sections in pb of these main Standard Model background processes are shown in Table 4.1; the cross-sections were calculated theoretically to next-to-leading-order. The two most important SM backgrounds are $t\bar{t}$, decaying not fully hadronically, and Z/γ^*, decaying into two muons (the latter process will also be referred to as Drell-Yan). The integrated luminosity is the instantaneous luminosity integrated over time. The cross-section of a process multiplied by the integrated luminosity gives the (expected) number of events.

Almost 100% of all top quarks decay into a W-boson and a b-quark. The W-boson can either decay into 2 quarks (hadronically) or into 2 leptons (leptonically). $t\bar{t}$ events where at least one W-bosons decays leptonically are called to be "decaying not fully hadronically".

Two Drell-Yan (DY) Monte-Carlo (MC) samples have been used and combined, since the available DY MC sample with $m_Z^{MC} > 60$ GeV, i.e. a MC value of the Z/γ^* larger than 60 GeV, does not contain a significant amount of events with $m_Z^{MC} \geq 150$ GeV after the basic selection cuts (see below) as can be seen in Figure 4.1; this sample (generated with PYTHIA [30]) has been combined with a DY MC sample with $m_Z^{MC} \geq 150$ GeV (generated with Herwig [31]). So only events with $m_Z^{MC} < 150$ GeV have been used from the DY MC sample with $m_Z^{MC} > 60$ GeV. All DY events with $m_Z^{MC} \geq 150$ GeV have been taken from the DY MC sample with $m_Z^{MC} \geq 150$ GeV. This was done to ensure larger statistics for high DY masses. The cross-sections of the DY $m_Z^{MC} > 60$ GeV has been normalized accordingly. This combination of 2 samples is referred to as "DY sample" or "DY MC sample" in the following.

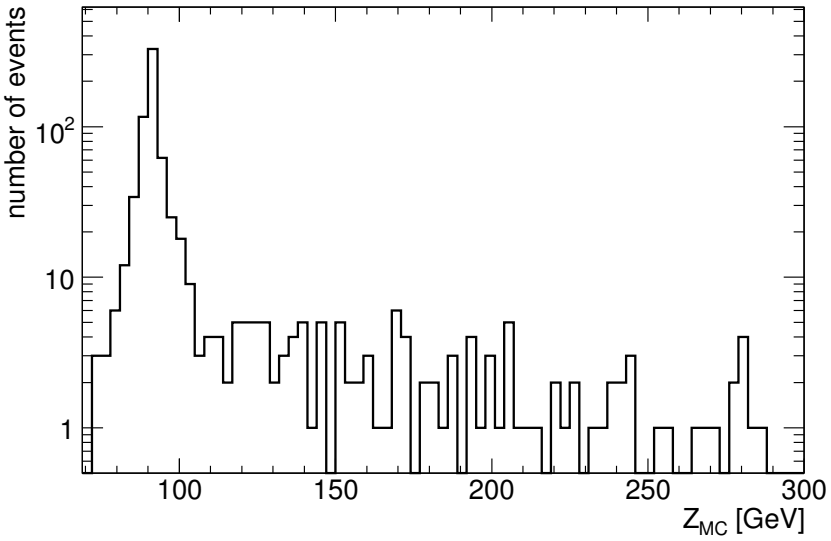

Figure 4.1: m_Z^{MC} of the Drell-Yan sample $m_Z^{MC} > 60$ GeV after basic selection cuts

Also other SM background samples have been studied: QCD di-jet samples, Z-boson with a set number of additional partons, Z-boson decaying into two τ, W + (b-)jets etc. None of the MC events of these samples are left after the analysis cuts. The integrated luminosity of the MC samples has been small for some processes, but for these samples no event was left even after only the basic selection cuts. The details of all signal and background samples which have been studied can be found in Appendix C.

4.2 Preselection of Events and First Analysis Cuts

The following preselection cuts were required in each event:

Muons have to fulfill the following to be considered:

- reconstructed with the so-called STACO algorithm [36]
- tracks in the inner tracking detector whose projections match to tracks in the muon spectrometer [37]
- relative isolation energy requirements $E_T^{iso}/p_T^{\mu} \leq 0.3$, where p_T^{μ} is the muon candidate's transverse momentum and E_T^{iso} is the energy detected in the

calorimeters within a cone of $\Delta\mathrm{R} = \sqrt{(\Delta\eta)^2 + (\Delta\phi)^2} = 0.2$ around the muon candidate's reconstructed trajectory, corrected for the expected energy deposition by the muon

- $p_T \geq 20$ GeV
- $|\eta| \leq 2.5$

Jets are identified as

- energy clusters reconstructed in the calorimeters using a $\Delta\mathrm{R} = 0.4$ cone algorithm [38] with
- $p_T \geq 20$ GeV
- $|\eta| \leq 4.5$
- $\Delta R > 0.1$ between a jet and any electron candidate (as defined below).

Electrons are defined as:

- reconstructed electrons with medium quality [39] with
- $p_T \geq 20$ GeV
- $|\eta| \leq 2.5$

The veto $\Delta R > 0.1$ is imposed to avoid electrons being misidentified as jets. This can happen, since jets as well as electrons are detected in the electromagnetic calorimeter.
Because the DY MC sample starts at $\mathrm{m}_Z^{MC} = 60$ GeV, it is required that the reconstructed dimuon invariant mass is at least 70 GeV.
This set of cuts will be referred to as preselection cuts.

There are 2 more cuts (which are already analysis cuts, but which are part of the so-called basic selection cuts), which have to be fulfilled in each event:

- each muon must have a transverse momentum $p_T \geq 60$ GeV
- each jet must have a transverse energy $E_T \geq 25$ GeV

Since the second generation leptoquark sample contains both single and pair leptoquark events, only events with two generated leptoquarks were selected in the signal samples for this analysis since the cross-section of single leptoquark production is unknown (it could be even zero). 2 muons with opposite electric charge, each fulfilling above requirements, and 2 jets fulfilling above requirements are required in each event.

These set of cuts will be referred to as basic selection cuts from now on.

In Figure 4.2 and in Figure 4.3 the muon distribution of the muon with the highest and lowest p_T of the two selected muons after the preselection can be seen respectively, for second generation leptoquark $m_{LQ} = 400$ GeV and for the SM backgrounds $t\bar{t}$, decaying not fully hadronically, Drell-Yan 60 GeV $< m_Z^{MC} <$ 150 GeV and Drell-Yan $m_Z^{MC} \geq 150$ GeV; the area under each line of this histogram is normalized to 1. The magenta line in the histogram indicates the cut $p_T^{\mu} \geq 60$ GeV. In Figure 4.4 and 4.5 the muon distribution of the muon with the highest and lowest p_T of the two selected muons after the preselection can be seen respectively, for second generation leptoquark $m_{LQ} = 800$ GeV. All histograms for $m_{LQ} = 300$ GeV and $m_{LQ} = 600$ GeV can be found in Appendix A.
The figures show that many of the SM background events, especially $t\bar{t}$, decaying not fully hadronically, and Drell-Yan $m_Z^{MC} > 60$ GeV events, are suppressed by this cut while many of the second generation leptoquark $m_{LQ} = 400$ GeV events remain. For second generation leptoquark $m_{LQ} = 800$ GeV the number of signal events suppressed by this cut is even smaller.

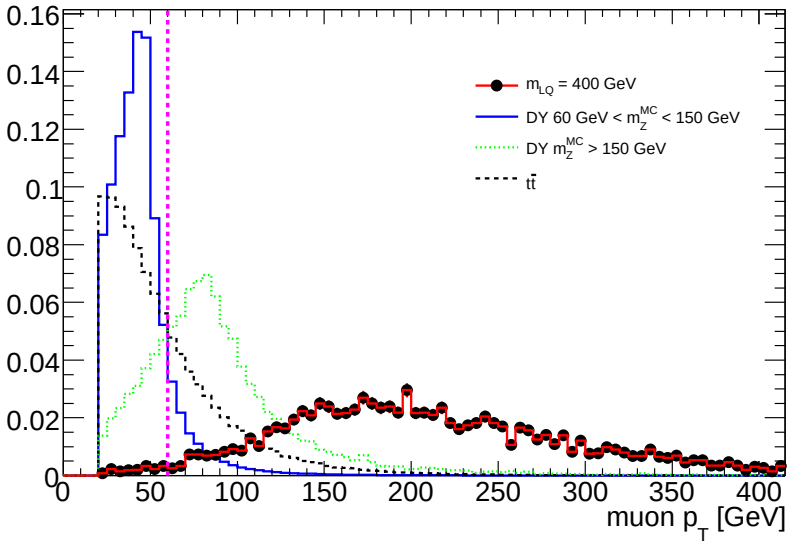

Figure 4.2: p_T distribution of signal and background of the muon of the selected two, which has the highest p_T, after preselection cuts; area under each graph normalized to 1

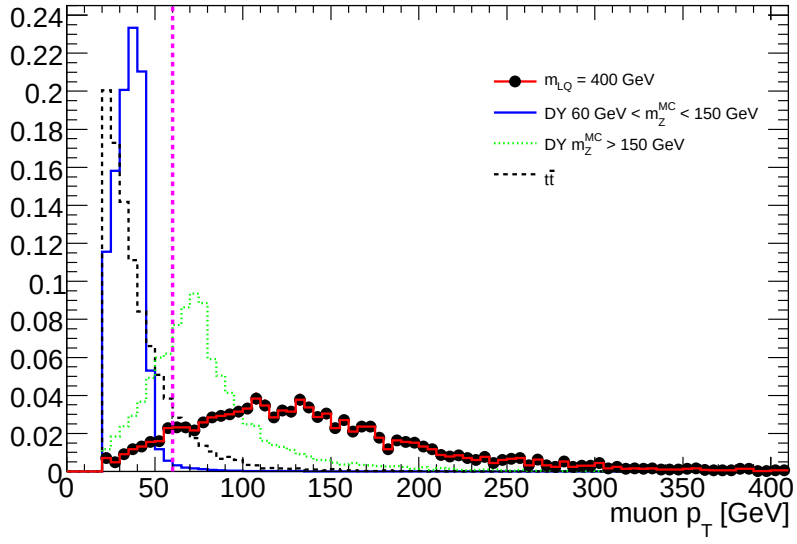

Figure 4.3: p_T distribution of signal and background of the muon of the selected two muons, which has the lowest p_T, after preselection cuts; area under each graph normalized to 1

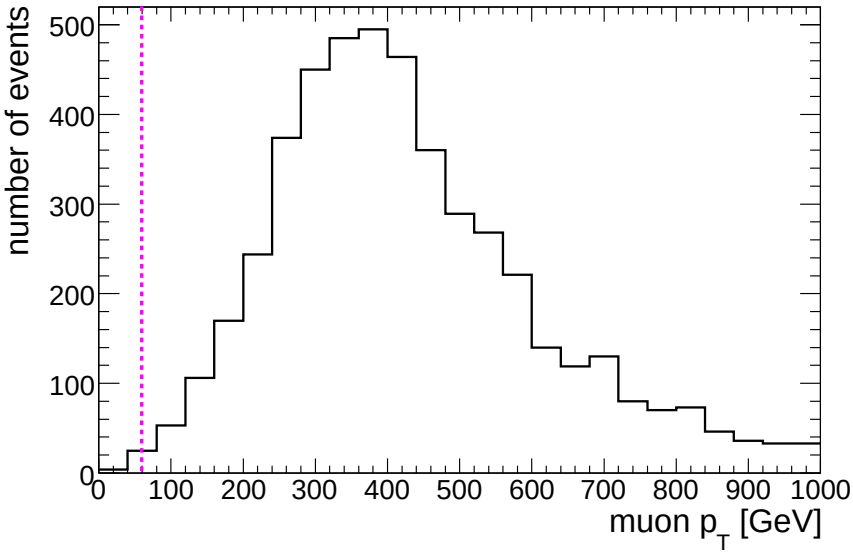

Figure 4.4: p_T distribution of second generation leptoquark m_{LQ}=800 GeV of the muon of the selected two muons, which has the highest p_T, after preselection cuts; not normalized

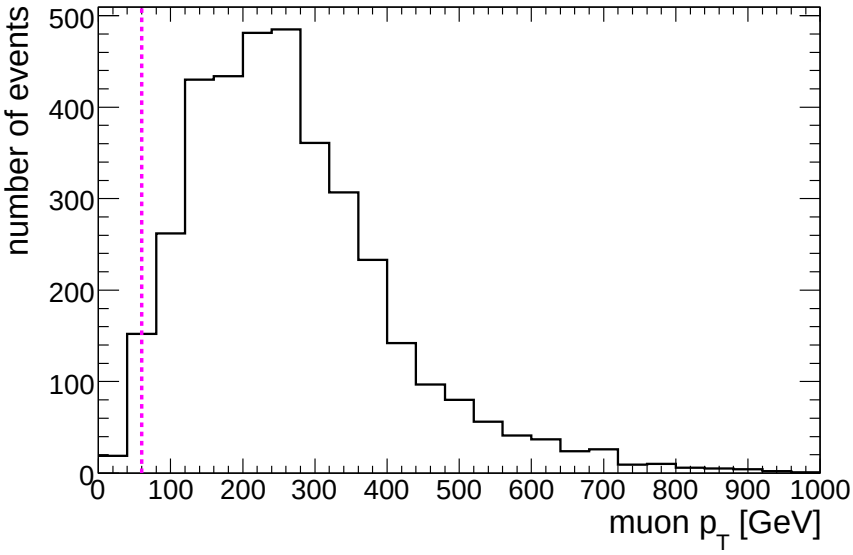

Figure 4.5: p_T distribution of second generation leptoquark m_{LQ}=800 GeV of the muon of the selected two muons, which has the lowest p_T, after preselection cuts; not normalized

4.3 Main Cut Variables

Several variables have been studied to separate the second generation leptoquark signal events from the Standard Model background processes:

- the reconstructed second generation leptoquark mass. Since there are 2 second generation leptoquarks in each event there are 2 muons and 2 jets and there are 2 possibilities to combine one muon with one jet. The reconstructed second generation leptoquark masses are calculated for both combinations and the combination, where the difference between these two reconstructed masses is the smallest, is taken. Henceforth this average is referred to as "reconstructed (rec.) second generation leptoquark mass".

- the mass of the system of the 2 selected muons (dimuon system) (The 4-vectors of the two selected muons are added and the invariant mass of the sum is taken as the mass of the dimuon system.)

- the scalar sum of the p_T of the 2 selected muons and the E_T of the 2 selected jets (= S_T)

- η of the selected dimuon system

- η of the 2 selected jets

- η of the reconstructed second generation leptoquarks
- the angle between the dimuon and the dijet plane, defined by the 2 selected muons and 2 selected jets
- the missing transverse energy of the event
- the invariant mass of the $\mu\mu$ + jet jet system
- the angle between the planes defined by the two "muon + jet" systems which minimize the difference in their reconstructed masses.

The following 6 histograms show the distribution of these variables studied for second generation leptoquark m_{LQ} = 400 GeV, the SM backgrounds $t\bar{t}$, decaying not fully hadronically, Drell-Yan 60 GeV $< m_Z^{MC} <$ 150 GeV and Drell-Yan $m_Z^{MC} \geq$ 150 GeV after the basic selection cuts. The area under each line in these 6 histograms has been normalized to 1.

The η distribution of the selected dimuon system can be seen in Figure 4.6; the η of the selected dimuon system after the basic selection cuts have a Gaussian-like distribution with a mean η of 0. Most SM backgrounds have a similar distribution, so no cut on η of the selected dimuon system has been applied.

The η distribution of the 2 selected jets can be seen in Figure 4.7. The η of the 2 selected jets has a Gaussian distribution with a mean η of 0 and a σ of 1.21. The η of the 2 selected jets of the main SM backgrounds has also a Gaussian distribution around 0 with a σ of 1.83 and 1.47 for DY $m_Z^{MC} \geq$ 150 GeV and $t\bar{t}$, decaying not fully hadronically, respectively. So no analysis cut on η of the selected jets has been used.

The η distribution of the reconstructed second generation leptoquark can be seen in Figure 4.8; the η of the reconstructed second generation leptoquark for second generation leptoquark m_{LQ} = 400 GeV has a Gaussian distribution with a mean of 0 and a σ of 1.55. The η distributions of the SM backgrounds DY $m_Z^{MC} \geq$ 150 GeV and $t\bar{t}$, decaying not fully hadronically, also have a Gaussian distribution with a mean of 0 and a σ of 1.74 and 1.76 respectively. Thus no cut on this value is efficient to suppress background events while keeping most of the signal events.

The angle between the planes defined by the two "muon + jet" systems which minimizes the difference in their reconstructed masses can be seen in Fig. 4.9. The distribution of the signal has a small peak around an angle of 0.8 and 2.8 which is due to detector effects. The distributions of the SM backgrounds DY $m_Z^{MC} \geq$ 150 GeV and $t\bar{t}$, decaying not fully hadronically, have a similar structure with small peaks at the same angles. The SM background DY 60 GeV $< m_Z^{MC} <$ 150 GeV has a different distribution with a significant peak

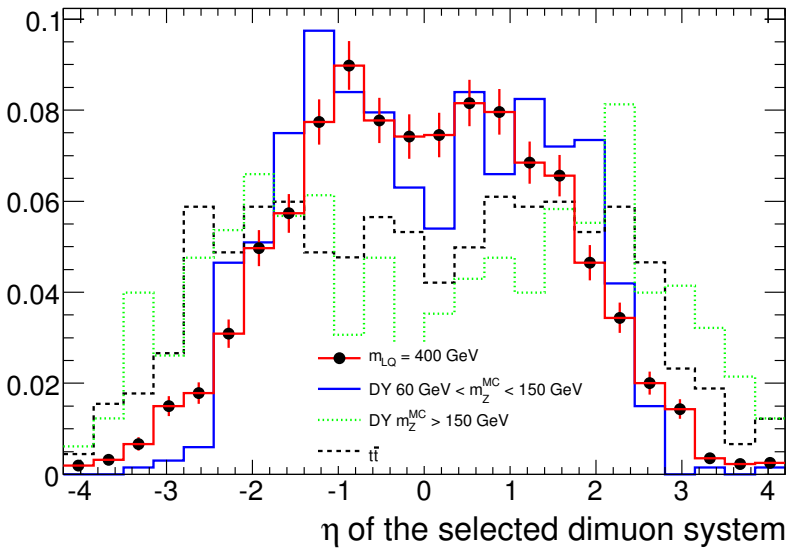

Figure 4.6: η distribution of the selected dimuon system for second generation leptoquark $m_{LQ} = 400$ GeV and for the SM backgrounds $t\bar{t}$, decaying not fully hadronically, Drell-Yan 60 GeV $< m_Z^{MC} <$ 150 GeV and Drell-Yan $m_Z^{MC} \geq 150$ GeV after the basic selection cuts

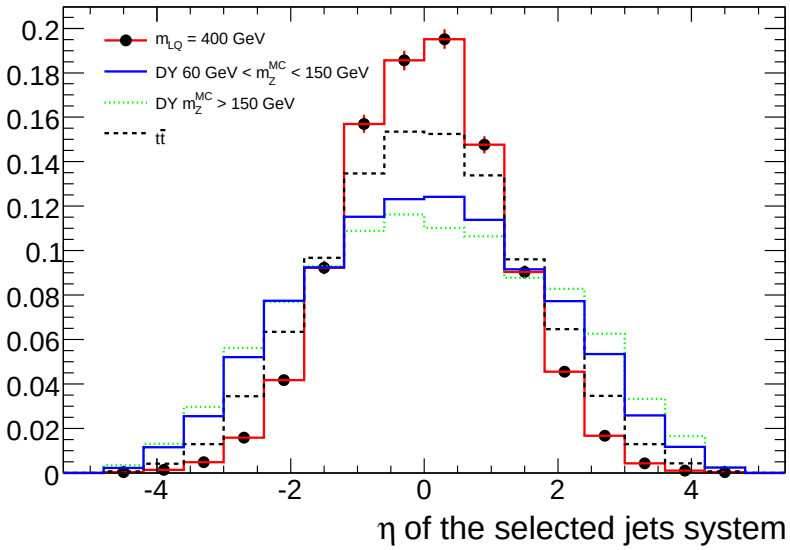

Figure 4.7: η distribution of the 2 selected jets for second generation leptoquarks $m_{LQ} = 400$ GeV and for the SM backgrounds $t\bar{t}$, decaying not fully hadronically, Drell-Yan 60 GeV $< m_Z^{MC} <$ 150 GeV and Drell-Yan $m_Z^{MC} \geq 150$ GeV after the basic selection cuts

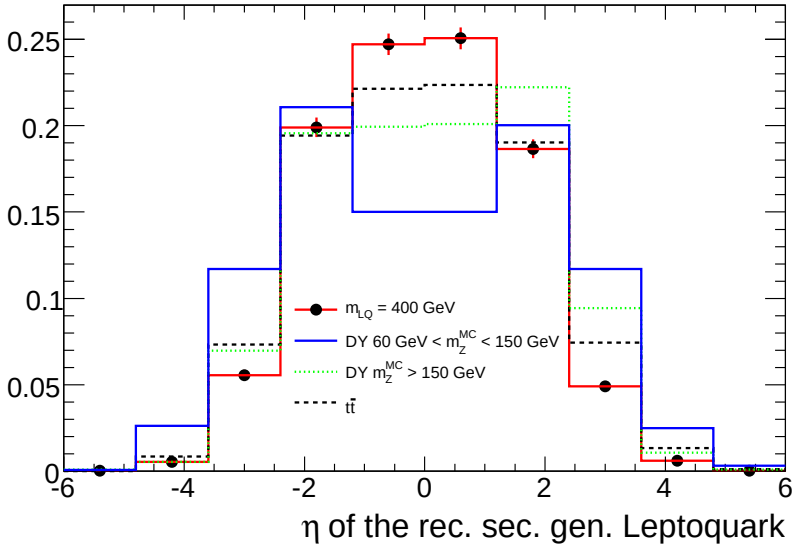

Figure 4.8: η distribution of rec. second generation leptoquarks for second generation leptoquark $m_{LQ} = 400$ GeV and for the SM backgrounds $t\bar{t}$, decaying not fully hadronically, Drell-Yan 60 GeV $< m_Z^{MC} <$ 150 GeV and Drell-Yan $m_Z^{MC} \geq 150$ GeV after the basic selection cuts

at an angle of 0.4, but this SM background is well suppressed by the optimized analysis cuts (see below), so no cut on this value is efficient for suppressing events of backgrounds, which are not already very well suppressed by other cuts, while keeping most of the signal events.

The angle between the dimuon and the dijet plane defined by the 2 selected muons and 2 selected jets can be seen in Figure 4.10. The distribution of the signal and most SM backgrounds are essentially flat. The distribution of the SM background $t\bar{t}$, decaying not fully hadronically, has a small peak at smaller angles, but the SM background $t\bar{t}$, decaying not fully hadronically, is already well suppressed by the used analysis cut. The distribution of the angle between the dimuon and the dijet plane of the remaining $t\bar{t}$ events, decaying not fully hadronically, after all cuts is essentially flat; so no cut on the angle between the dimuon and the dijet plane has been applied.

The distribution of the missing transverse energy ($\not{E}_T$) can be seen in Figure 4.11; $\not{E}_T$ can be used to discriminate second generation leptoquark signal from the SM background $t\bar{t}$, decaying not fully hadronically, because $t\bar{t}$ events already contain $\not{E}_T$ without any detector effects. But since the main focus of this thesis is on the early phase of the LHC run, no cut on $\not{E}_T$ has been used in this thesis, confer Section 4.5.

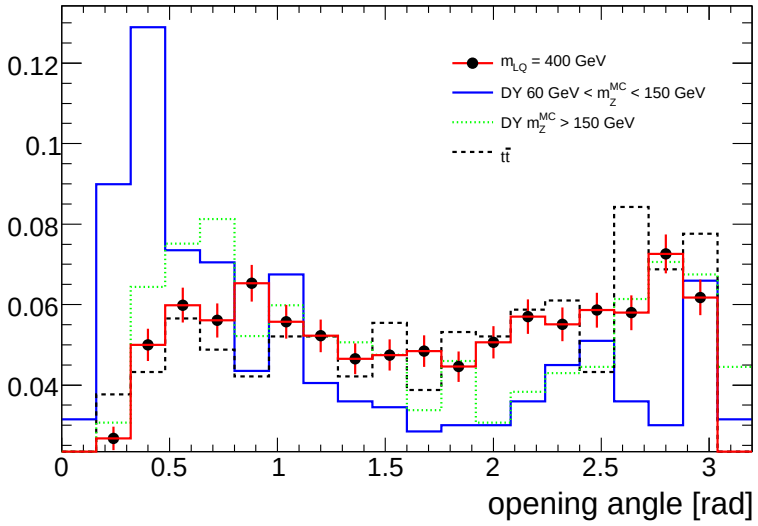

Figure 4.9: Angle between the planes defined by the two "muon + jet" systems which minimize the difference in their reconstructed masses for second generation leptoquark $m_{LQ} = 400$ GeV and for the SM backgrounds $t\bar{t}$, decaying not fully hadronically, Drell-Yan 60 GeV $< m_Z^{MC} <$ 150 GeV and Drell-Yan $m_Z^{MC} \geq 150$ GeV after the basic selection cuts

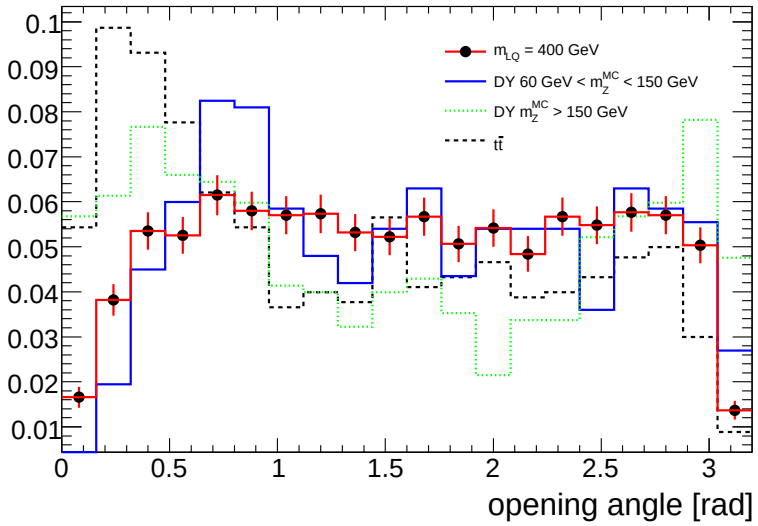

Figure 4.10: Angle between the dimuon and the dijet plane, defined by the 2 selected muons and 2 selected jets for second generation leptoquark $m_{LQ} = 400$ GeV and for the SM backgrounds $t\bar{t}$, decaying not fully hadronically, Drell-Yan 60 GeV $< m_Z^{MC} <$ 150 GeV and Drell-Yan $m_Z^{MC} \geq 150$ GeV after the basic selection cuts

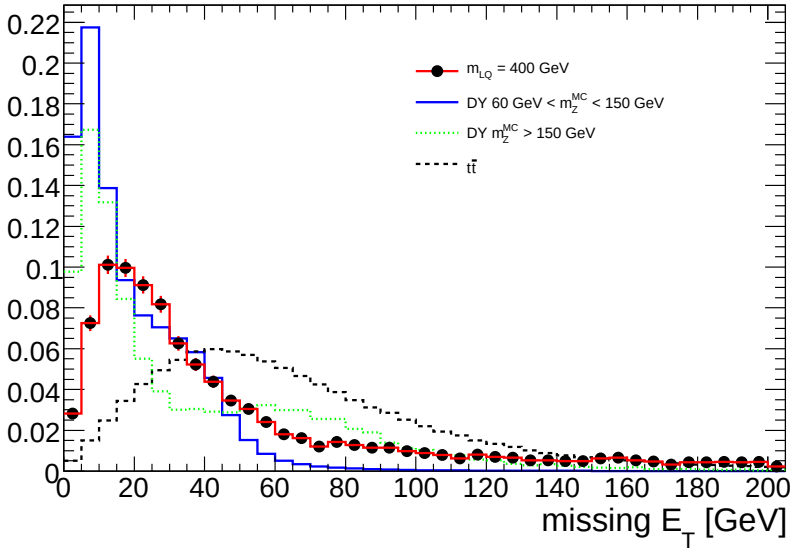

Figure 4.11: $\not{E}_T$ distribution for second generation leptoquark m_{LQ} = 400 GeV and for the SM backgrounds $t\bar{t}$, decaying not fully hadronically, Drell-Yan 60 GeV < m_Z^{MC} < 150 GeV and Drell-Yan $m_Z^{MC} \geq$ 150 GeV after the basic selection cuts

The main variables which differ strongly between the second generation leptoquark signal and the main Standard Model background processes are S_T (the scalar sum of the p_T of the 2 selected muons and the E_T of the 2 selected jets), the dimuon mass (the mass of the selected dimuon system) and the reconstructed second generation leptoquark mass.

The cuts on S_T, dimuon mass and reconstructed second generation leptoquark mass shown in the following have been optimized simultaneously for a 5σ discovery level, calculated with the S_{cP} significance calculator [40] including the systematic uncertainties and the trigger efficiencies (see Appendix B for S_{cP} and Chapter 7 for results). A 5σ significance corresponds to a probability of $5 * 10^{-7}$ that the expected number of background events only fluctuates up to (at least) the number of signal + background events for a set integrated luminosity. The S_T-cut has been varied between 0 GeV and 1000 GeV; the dimuon mass-cut has been varied between 0 GeV and 190 GeV. And the reconstructed second generation leptoquark mass-cut has been varied between a window size of 50 GeV and a window size of 225 GeV around the tested real second generation leptoquark mass (the given window size is the size of the window in one direction, so for a value of 50 GeV the mass window starts at m_{LQ}^{tested} - 50 GeV and ends at m_{LQ}^{tested} + 50 GeV). Each combination of these cuts has been taken and applied on second generation leptoquark signal and on SM backgrounds and the number

of events that fulfilled these cuts has been analyzed. The integrated luminosity to discover the second generation leptoquark signal with a 5σ significance has been calculated. The optimal cut combination for a tested second generation leptoquark mass has been defined as the cut combination where the integrated luminosity for a discovery with 5σ significance is the smallest.

The first main cut variable is S_T. Figure 4.12 shows S_T for a second generation leptoquark with $m_{LQ} = 400$ GeV and the main backgrounds DY, $t\bar{t}$, decaying not fully hadronically, and vector boson (VB) pairs. The magenta line in the figure indicates the optimized S_T-cut: $S_T \geq 600$ GeV for $m_{LQ} = 400$ GeV. This S_T-cut suppresses much of the background events, especially $t\bar{t}$, decaying not fully hadronically, and DY with $m_Z^{MC} > 60$ GeV events, while suppressing only a small part of the signal events.

The next main cut variable is the invariant mass of the selected dimuon system. Figure 4.13 shows the dimuon mass after the S_T-cut for a second generation leptoquark with $m_{LQ} = 400$ GeV and the main backgrounds DY, $t\bar{t}$, decaying not fully hadronically, and VB pairs. Again the magenta line indicates the optimized cut; each event must have a dimuon mass $m_{\mu\mu} \geq 110$ GeV. This dimuon mass-cut suppresses the peak of the Z-boson at 91 GeV very well; only a very small fraction of the signal events is lost due to this cut.

The last main cut variable is the reconstructed leptoquark mass. Figure 4.14 shows the reconstructed second generation leptoquark mass for second generation leptoquark $m_{LQ} = 400$ GeV and the SM backgrounds DY, $t\bar{t}$, decaying not fully hadronically, and VB pairs after all cuts. The two magenta lines indicate the reconstructed second generation leptoquark mass window-cut, i.e. the mass window around the tested second generation leptoquark mass in which the reconstructed leptoquark mass has to be. The optimized mass window size is $\pm$ 75 GeV for a second generation leptoquark of $m_{LQ} = 400$ GeV. Figure 4.15 shows the reconstructed second generation leptoquark mass for second generation leptoquark $m_{LQ} = 400$ GeV after basic selection cuts as a comparison.

In Figure 4.16 the reconstructed second generation leptoquark mass can be seen with a Gaussian function fitted to it. The mean of the fit is at 372 GeV and the width σ is 35 GeV. The result of the fit is just an estimate to describe the reconstructed second generation leptoquark mass distribution.

Most of the signal events are within this optimized mass window, while the remaining background events are further suppressed by this cut. The rec. second generation leptoquark mass distribution has a peak slightly below the real tested second generation leptoquark mass. This is mainly due to final state radiation, so the reconstructed jets have less energy than the quarks which the second generation leptoquark decays into. Even for second generation leptoquark $m_{LQ} = 400$ GeV many events consist of more than 2 jets; a significant number

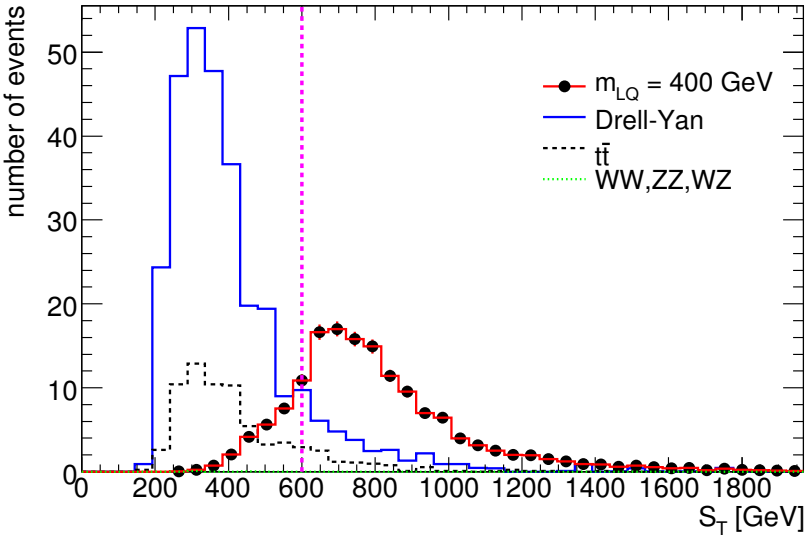

Figure 4.12: S_T distributions for second generation leptoquark (m_{LQ}=400 GeV) signal, SM backgrounds DY, $t\bar{t}$, decaying not fully hadronically, and VB pairs after basic selection cuts normalized to 100 pb^{-1} of integrated pp luminosity. The vertical line indicates the $S_T \geq 600$ GeV requirement

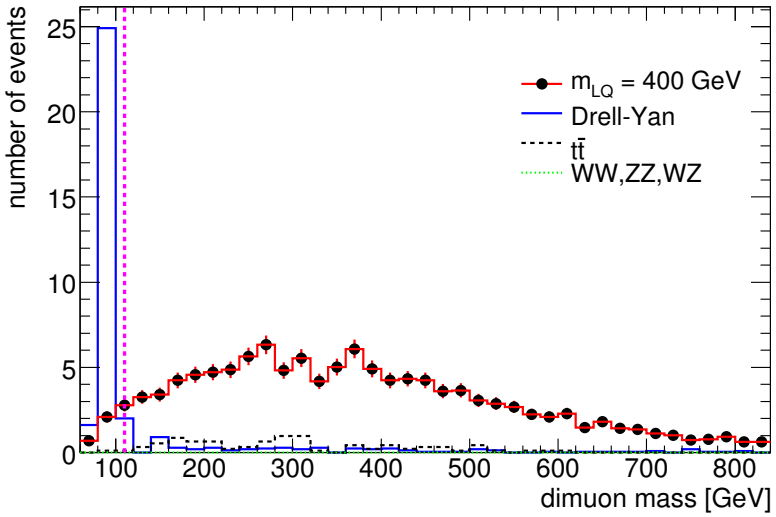

Figure 4.13: Dimuon reconstructed invariant mass distributions for second generation leptoquark (m_{LQ} = 400 GeV) signal, SM backgrounds DY, $t\bar{t}$, decaying not fully hadronically, and VB pairs after the S_T selection cut normalized to 100 pb^{-1} of integrated pp luminosity. The vertical line indicates the $m(\mu\mu) \geq 110$ GeV requirement

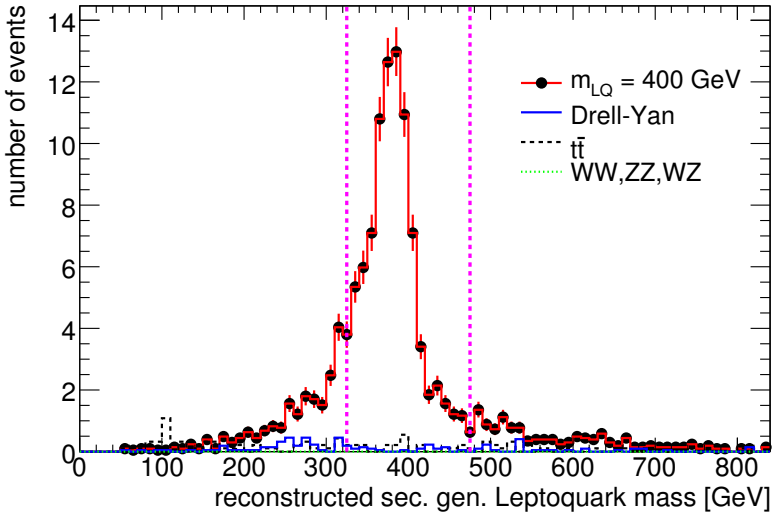

Figure 4.14: Leptoquark reconstructed invariant mass distributions for second generation leptoquark ($m_{LQ} = 400$ GeV) signal, SM backgrounds DY, $t\bar{t}$, decaying not fully hadronically, and VB pairs after applying all but leptoquark mass window selection criteria normalized to 100 pb^{-1} of integrated pp luminosity. The vertical lines indicate the leptoquark signal invariant mass window.

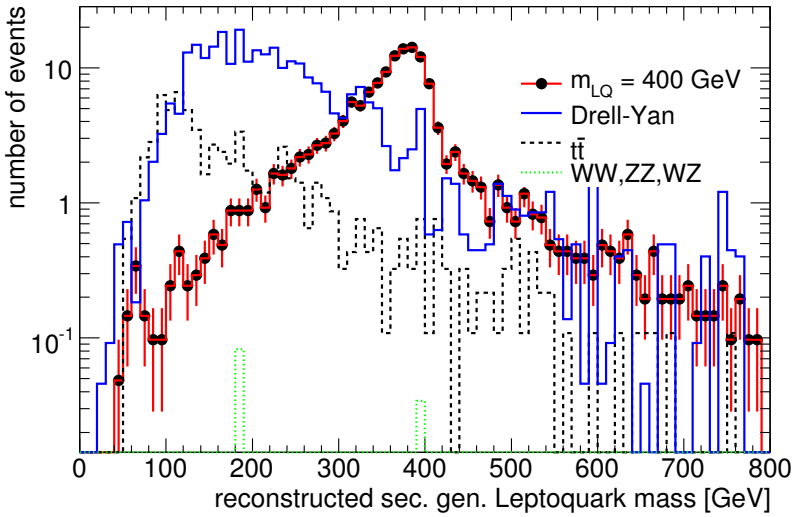

Figure 4.15: Leptoquark reconstructed invariant mass distributions for second generation leptoquark ($m_{LQ} = 400$ GeV) signal, SM backgrounds DY, $t\bar{t}$, decaying not fully hadronically, and VB pairs after basic selection cuts normalized to 100 pb^{-1} of integrated pp luminosity

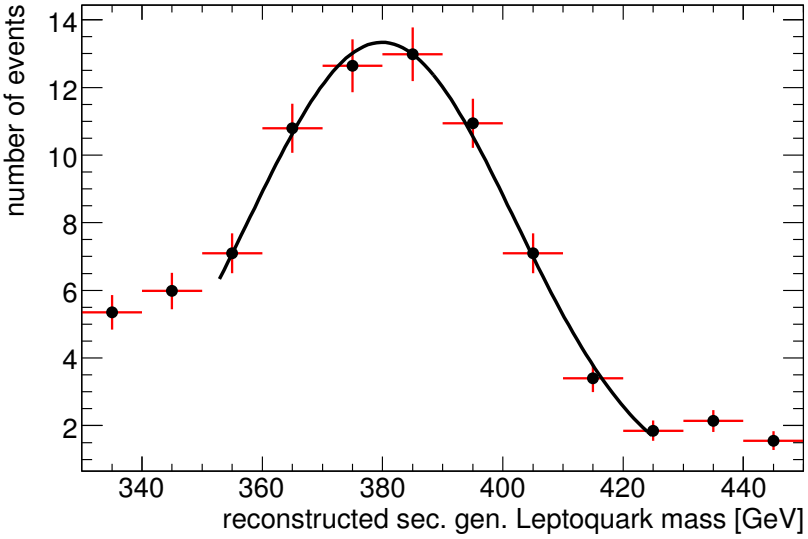

Figure 4.16: Reconstructed second generation leptoquark mass distribution for $m_{LQ} = 400$ GeV with a Gaussian fit after all cuts normalized to 100 pb^{-1} of integrated pp luminosity. The mean of the fit is at 372 GeV and the width σ is 35 GeV.

of events have 3 or more jets, see Figure 4.17.

The S_T-distribution for second generation leptoquark $m_{LQ} = 800$ GeV and the main SM backgrounds can be seen in Figure 4.18. As it is expected, the S_T-distribution of the signal is shifted to higher values. The optimized cut $S_T \geq 900$ GeV, indicated by the magenta line in the figure, suppresses almost all of the background events; only some of the DY with $m_Z^{MC} > 60$ GeV events are left after this cut.

Figure 4.19 shows the dimuon mass distribution for second generation leptoquark $m_{LQ} = 800$ GeV and the main SM backgrounds after the optimized S_T-cut. The peak of the Z-boson at around 91 GeV is clearly visible but not as prominent as for the second generation leptoquark $m_{LQ} = 400$ GeV dimuon mass distribution since the S_T-cut is higher. With the optimized cut at 150 GeV (only events with a dimuon mass ≥ 150 GeV are considered), indicated by the magenta line in the figure, the peak of the Z-boson is suppressed while suppressing only very few second generation leptoquark $m_{LQ} = 800$ GeV signal events.

The reconstructed second generation leptoquark mass distribution for second generation leptoquark $m_{LQ} = 800$ GeV and the main SM backgrounds after the S_T- and dimuon mass-cut can be seen in Figure 4.20. Almost all of the background events are suppressed already. The optimized rec. second generation leptoquark mass window is again indicated by the two magenta lines. The peak of the signal

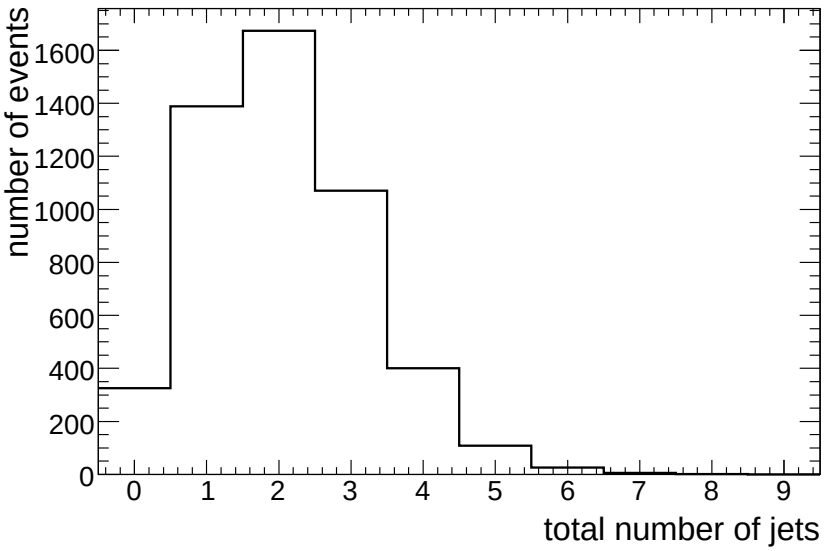

Figure 4.17: Total number of jets in an event for second generation leptoquark $m_{LQ} = 400$ GeV after preselection cuts; not normalized

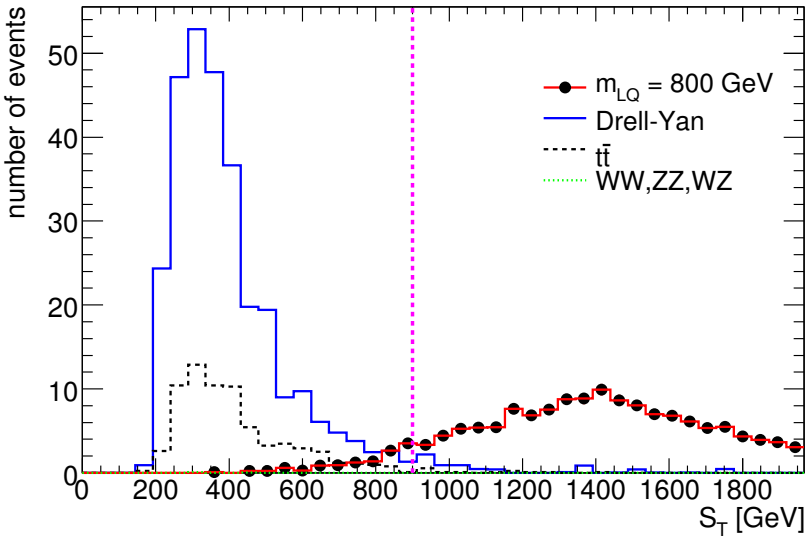

Figure 4.18: S_T distributions for second generation leptoquark (m_{LQ}=800 GeV) signal, DY, $t\bar{t}$, decaying not fully hadronically, and VB pairs after basic selection cuts normalized to 100 pb^{-1} of integrated pp luminosity. The vertical line indicates the $S_T \geq 900$ GeV requirement.

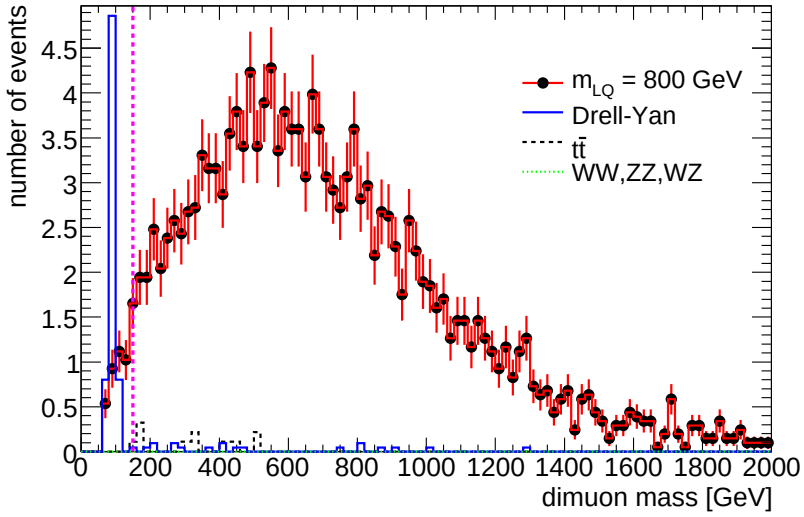

Figure 4.19: Reconstructed invariant dimuon mass distributions for second generation leptoquark (m_{LQ} = 800 GeV) signal, SM backgrounds DY, $t\bar{t}$, decaying not fully hadronically, and VB pairs after the S_T-cut normalized to 100 pb^{-1} of integrated pp luminosity. The vertical line indicates the $M(\mu\mu) \geq 150$ GeV requirement.

distribution lies clearly within the optimized mass window.

Figure 4.21 shows the reconstructed second generation leptoquark mass for second generation leptoquark m_{LQ} = 800 GeV after basic selection cuts as a comparison.

Figure 4.22 shows the rec. second generation leptoquark mass with a Gaussian function fitted to it. The mean of this fit is 757 GeV and the width σ is 45 GeV. Again the result of the fit is just an estimate to describe the reconstructed second generation leptoquark mass distribution. The peak of this mass distribution lies below the real tested second generation leptoquark mass. This is mainly due to final state radiation, which is greater for second generation leptoquark m_{LQ} = 800 GeV events than for m_{LQ} = 400 GeV events, because the second generation leptoquarks have a higher mass and so the resulting jets are more energetic. There are more events for m_{LQ} = 800 GeV which have more than 2 jets than for m_{LQ} = 400 GeV, see Figure 4.23. This is the reason why the difference between the peak of the rec. second generation leptoquark mass distribution and the real tested second generation leptoquark masses becomes greater and greater for higher second generation leptoquark masses. The rec. second generation leptoquark mass distribution becomes also wider for higher second generation leptoquark masses. This is due to the resulting muons being more energetic and the resolution gets worse for higher momenta for muons (since

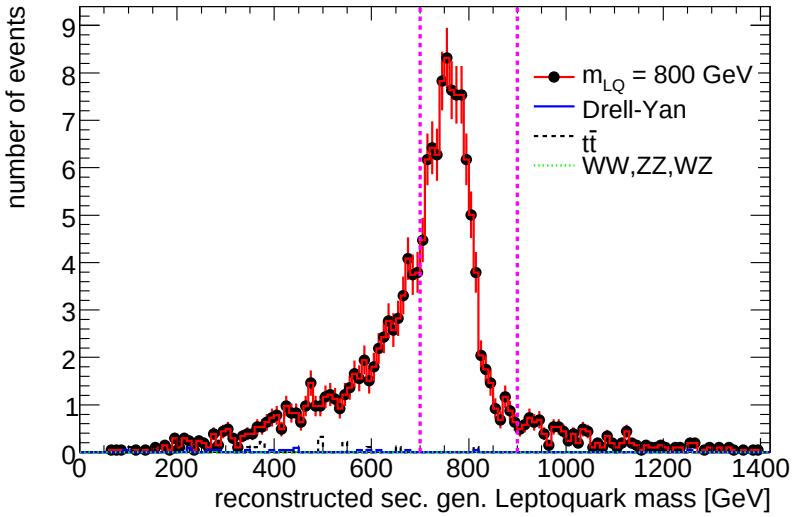

Figure 4.20: Reconstructed invariant leptoquark mass distributions for second generation leptoquark (m_{LQ} = 800 GeV) signal, SM backgrounds DY, $t\bar{t}$, decaying not fully hadronically, and VB pairs after applying all but rec. leptoquark mass window-cut normalized to 100 pb^{-1} of integrated pp luminosity. The vertical lines indicate the rec. leptoquark mass window-cut.

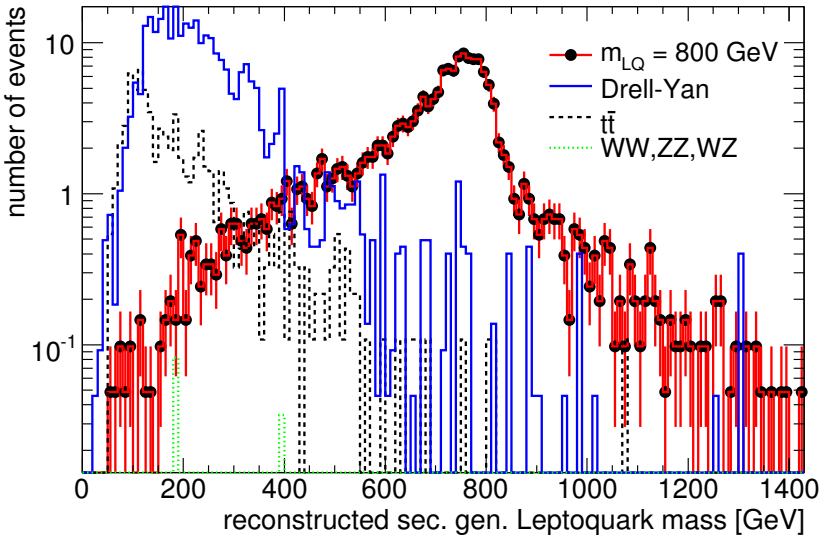

Figure 4.21: Reconstructed invariant leptoquark mass distributions for second generation leptoquark m_{LQ} = 800 GeV, SM backgrounds DY, $t\bar{t}$, decaying not fully hadronically, and VB pairs after basic selection cuts normalized to 100 pb^{-1} of integrated pp luminosity

for higher momenta the tracks of the particles have a smaller curvature in the detector). The value of the real tested second generation leptoquark mass is one sigma of the Gaussian fit above the peak of the Gaussian fit to the rec. second generation leptoquark mass for all tested second generation leptoquark masses. This is understandable when both effects, worse resolution for higher momenta and more final state radiation for jets with higher energy, are considered. The final state radiation shifts the peak of the distribution to lower masses. Since the distribution becomes wider for higher momenta, because of the worse resolution, the difference between the peak of the Gaussian fit of the rec. second generation leptoquark mass and the tested second generation leptoquark mass stays at one sigma of the Gaussian fit.

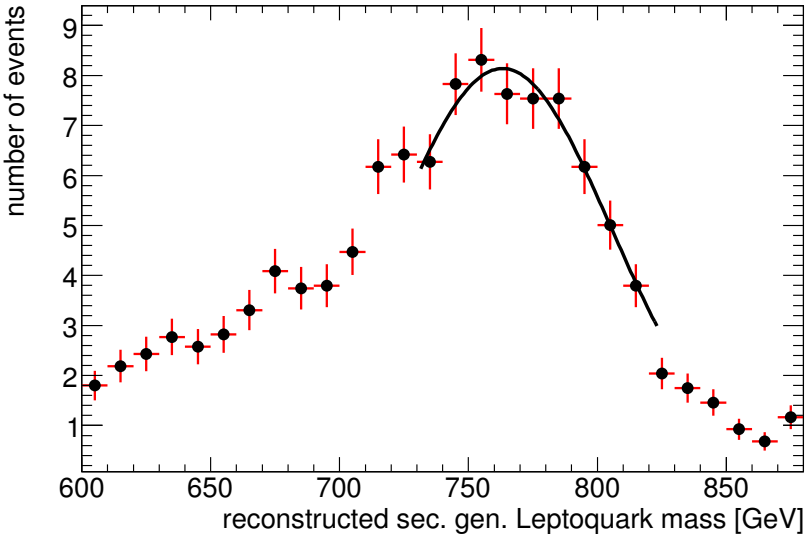

Figure 4.22: Reconstructed second generation leptoquark mass distribution for $m_{LQ} = 800$ GeV with a Gaussian fit after all cuts normalized to 100 pb^{-1} of integrated pp luminosity. The mean of the fit is at 757 GeV and the width σ is 45 GeV.

Optimizing the leptoquark mass window this way slightly underestimates the signal efficiency. For higher second generation leptoquark masses the signal efficiency is underestimated more strongly, since the leptoquark mass window is around the real tested leptoquark mass, while the peak of the rec. second generation leptoquark mass distribution is (for the tested masses) always about one sigma of the Gaussian fit below the real tested second generation leptoquark mass.

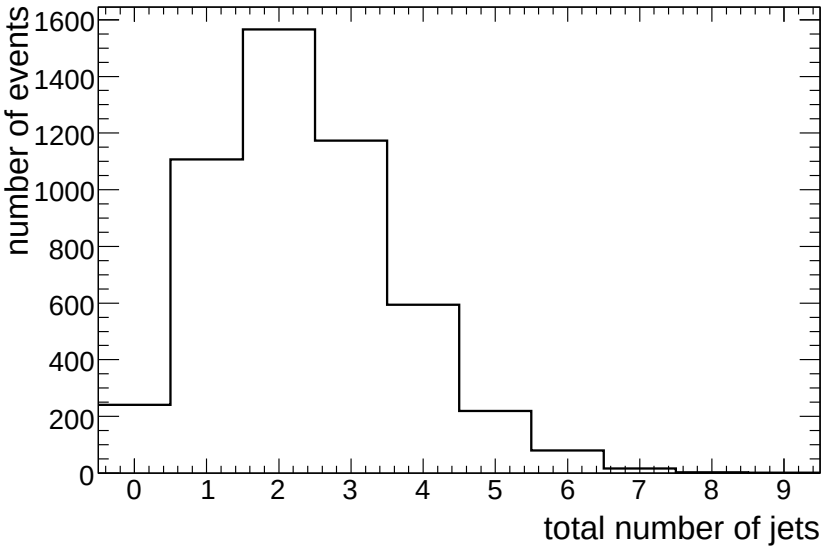

Figure 4.23: Total number of jets in an event for second generation leptoquark $m_{LQ} = 800$ GeV after preselection cuts; not normalized

The figures for second generation leptoquark $m_{LQ} = 300$ GeV and $m_{LQ} = 600$ GeV can be found in Appendix A.

Table 4.2 shows the different signal and background processes with the optimized cuts for different scalar second generation leptoquark masses. Each entry in the table shows the remaining cross-section of the different processes in pb after all cuts including the rec. leptoquark mass window-cut. The background processes are well suppressed while the efficiencies for the signal processes are 37%–44%.

Table 4.3 shows the cut-flow for second generation leptoquark $m_{LQ} = 400$ GeV and the main SM backgrounds in detail. After the preselection the cuts on the transverse momenta of the muons and the transverse energies of the jets discard a large percentage of the background events, especially $t\bar{t}$, decaying not fully hadronically, and DY $m_Z^{MC} \geq 60$ GeV, while keeping most of the leptoquark signal events. Adding the S_T-cut only a small fraction of leptoquark signal events is discarded; the remaining cross-sections of the two main SM backgrounds DY $m_Z^{MC} \geq 60$ GeV and $t\bar{t}$, decaying not fully hadronically, decrease about one order of magnitude each. At this stage the remaining cross-sections of the vector boson pair processes are already negligible. As it is expected the next cut on the dimuon mass suppresses the DY $m_Z^{MC} \geq 60$ GeV, WZ and ZZ background strongly, while the other SM backgrounds and the signal have only a small change.

The last cut on the reconstructed second generation leptoquark mass suppresses about 30% of the remaining signal cross-section left after the previous cuts but it suppresses the SM background events even more: about 82% of the remaining DY $m_Z^{MC} \geq 60$ GeV cross-section and about 77% of the remaining $t\bar{t}$, decaying not fully hadronically, cross-section is discarded by this cut.

process	remaining $\sigma\cdot$ Br(pb) after cuts for m_{LQ} = 300 GeV	remaining $\sigma\cdot$ Br(pb) after cuts for m_{LQ} = 400 GeV	remaining $\sigma\cdot$ Br(pb) after cuts for m_{LQ} = 600 GeV	remaining $\sigma\cdot$ Br(pb) after cuts for m_{LQ} = 800 GeV
second generation leptoquark m_{LQ} = 300 GeV	4.44			
second generation leptoquark m_{LQ} = 400 GeV		0.83		
second generation leptoquark m_{LQ} = 600 GeV			0.057	
second generation leptoquark m_{LQ} = 800 GeV				0.0146
DY (60 GeV $< m_Z^{MC} <$ 150 GeV)	0.020	0	0	0
DY ($m_Z^{MC} \geq$ 150 GeV)	0.084	0.011	0.0018	0.00046
$t\bar{t}$, decaying not fully hadronically	0.111	0.020	0.0033	0
WW	0.003	0	0	0
WZ	0.003	0.001	0.0003	0
ZZ	0.001	0	0	0
S_T-cut in GeV	400	600	1000	900
dimuon mass-cut in GeV	130	110	100	150
rec. leptoquark mass window in GeV	[150 ; 450]	[325 ; 475]	[400 ; 800]	[700 ; 900]

Table 4.2: Remaining cross-sections for second generation leptoquark and main SM backgrounds, and optimized cuts for the tested second generation leptoquark masses

Physics sample	Before selection	Pre-selection	$p_T^{\mu}\geq$60 GeV $E_T^{jet}\geq$25 GeV	$S_T \geq$ 600 GeV	$M(\mu\mu) \geq$ 110 GeV	325 GeV $<$ rec. mass $<$ 475 GeV
m_{LQ}=400 GeV	2.24	1.63	1.47	1.23	1.18	0.829
DY $\geq$ 60 GeV	1808	76.35	2.8083	0.3240	0.0588	0.0106
$t\bar{t}$	450	4.0043	0.6706	0.0780	0.0748	0.0173
WW	40.90	0.393	0.0098	0.000818	0.000818	0.000000
ZZ	3.94	0.3456	0.0176	0.002057	0.000554	0.0002373
WZ	1.64	0.4574	0.0363	0.005136	0.001370	0.0006848

Table 4.3: Remaining cross-sections in pb for second generation leptoquark m_{LQ} = 400 GeV and the SM backgrounds after optimized cuts

4.4 Final State Radiation Correction by Adding a Third Jet

The rec. second generation leptoquark mass distribution is shifted to lower masses mainly due to final state radiation. The higher the tested real second generation leptoquark mass is the more final state radiation is generated and so the shift of the second generation leptoquark mass distribution is larger. One idea to correct for this effect is to select a third jet in an event (the one with the next higher energy after the two selected jets) that fulfills the jet requirements given in section 4.2 and add this jet to the jet with the lowest energy of the 2 selected ones. For lower second generation leptoquark masses like $m_{LQ} = 400$ GeV adding a third jet does not shift the peak of the rec. second generation leptoquark mass distribution significantly but creates a long tail at high masses, see Figure 4.24. For higher tested second generation leptoquark masses like m_{LQ}= 800 GeV adding a third jet shifts the peak of the rec. second generation leptoquark mass distribution closer to the tested real second generation leptoquark mass, but it also creates a long tail at high masses in the distribution, see Figure 4.25. The long tail is created through events, where there is no additional third jet coming from final state radiation, but the third jet is coming from initial state radiation. So adding a third jet this way has not been considered an efficient way to correct the jet energies for final state radiation in this thesis.

One other idea has been to add a third jet to one of the 2 selected jets, such that the difference between the 2 rec. second generation leptoquark masses becomes smaller. Doing this also did not shift the peak of the signal for second generation leptoquark $m_{LQ} = 400$ GeV, but created a long tail at high masses, too. The long tail is also created for second generation leptoquark $m_{LQ} = 800$ GeV when one adds a third jet this way. So this idea has not been studied further. Another idea has been to add a third jet to one of the selected jets if the distance $\Delta R < 1.0$ to one of the 2 selected jets. By doing this no significant change in the rec. second generation leptoquark distribution for second generation leptoquark $m_{LQ} = 400$ GeV and $m_{LQ} = 800$ GeV could be observed, so no third jet has been added for this analysis.

4.5 Missing Transverse Energy

No cut on the missing transverse energy of an event has been applied in this analysis, since the main focus of this thesis is on early ATLAS data, i.e. on ATLAS data which will be recorded in the first few months up to about one year. The missing transverse energy ($\not\!\!E_T$) of an event is calculated by adding up vectorially the transverse energies measured in the calorimeters and correcting for the muons. Since the incoming protons have a transverse energy of almost zero, the difference between the sum and zero is defined as $\not\!\!E_T$. In this early period of data

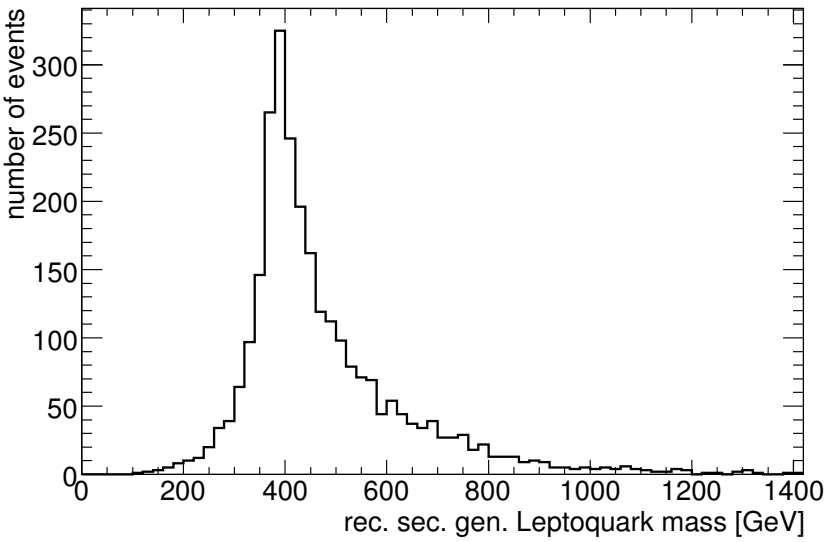

Figure 4.24: Reconstructed second generation leptoquark mass for second generation leptoquark m_{LQ} = 400 GeV after S_T-, dimuon mass- and LQ mass window-cuts; a third jet has been added to the selected jet with the lowest energy if it fulfills the jet criteria; not normalized

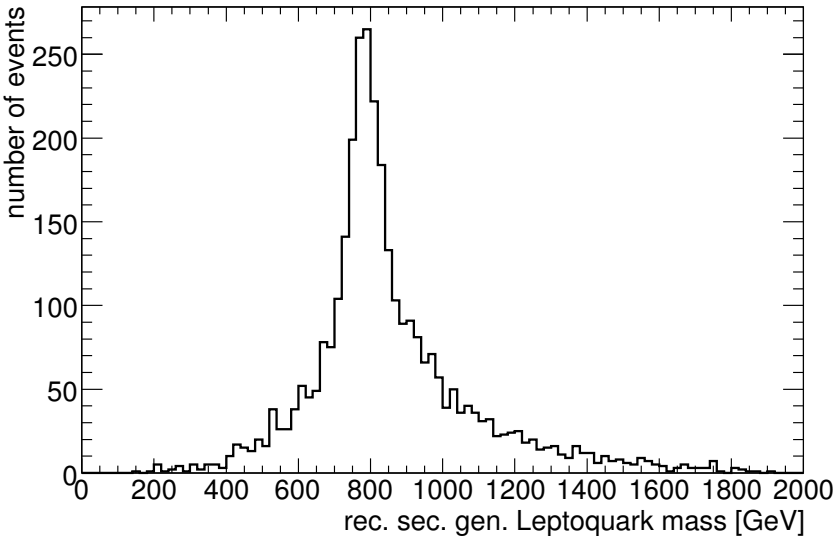

Figure 4.25: Reconstructed second generation leptoquark mass for second generation leptoquark m_{LQ} = 800 GeV after S_T-, dimuon mass- and LQ mass window-cuts, a third jet has been added to the selected jet with the lowest energy if it fulfills the jet criteria

taking the value of $\not\!\!E_T$ won't be very precise, since every time a new detector is activated, it needs several months until all components of the detector have been calibrated and unexpected detector effects are well understood. When the detector is calibrated and understood well enough $\not\!\!E_T$ can be used to discriminate second generation leptoquark events from specific other events, like $t\bar{t}$ events and events from R-parity conserving SUSY models; in these models the supersymmetric particle with the lowest mass is stable and carries no electric charge and hence is undetectable directly in the ATLAS detector. Undetected particles generate $\not\!\!E_T$. Second generation leptoquark events generate no $\not\!\!E_T$ per se (all decay particles are detectable in the ATLAS detector), but since no detector measures all particles perfectly, second generation leptoquark events can contain $\not\!\!E_T$. Figure 4.26 shows the $\not\!\!E_T$ of second generation leptoquark $m_{LQ} = 400$ GeV and of the SM backgrounds DY, $t\bar{t}$, decaying not fully hadronically, and VB pairs after all cuts, i.e. after the S_T-, dimuon mass- and rec. leptoquark mass window-cuts.

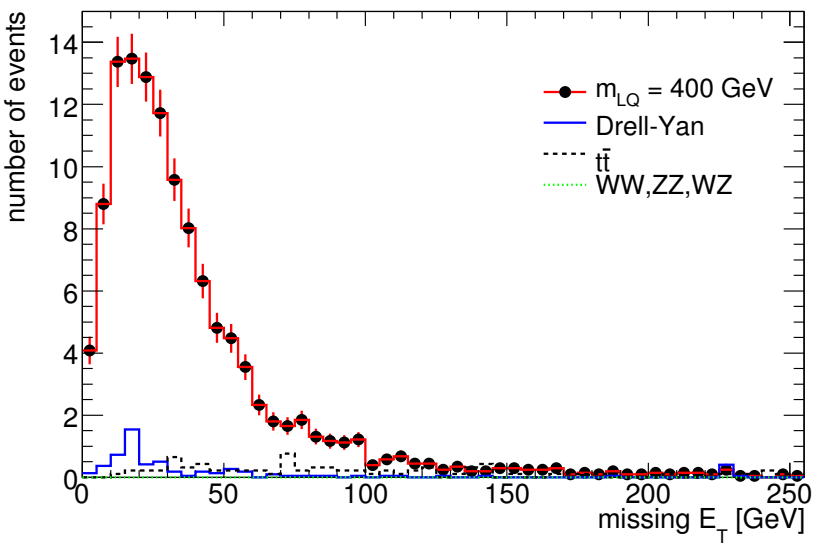

Figure 4.26: $\not\!\!E_T$ of second generation leptoquark $m_{LQ} = 400$ GeV and SM backgrounds DY, $t\bar{t}$, decaying not fully hadronically, and VB pairs after S_T-, dimuon mass- and rec. leptoquark mass window-cuts normalized to 100 pb^{-1} of integrated pp luminosity

Chapter 5

Trigger Efficiencies

As described in Chapter 3.3 a very large percentage of all physics events are discarded because they cannot be recorded as fast as they happen [26]. A variety of different triggers is defined in the ATLAS trigger menu (trigger menu "CSC06" has been used here). Table 5.1 shows the percentage of the number of selected second generation leptoquark events, i.e. the second generation leptoquark events which passed all cuts including the leptoquark mass window-cut, that fulfill the corresponding trigger for the different tested second generation leptoquark masses; the 4 numbers in each table entry of the background samples are the trigger efficiencies for optimized cuts for m_{LQ} = 300 GeV, m_{LQ} = 400 GeV, m_{LQ} = 600 GeV and m_{LQ} = 800 GeV, respectively. "-" in a table entry means that there are no events selected after all cuts, so no trigger efficiency can be calculated. There are 2 muons in each second generation leptoquark event but a single muon trigger is better than a dimuon trigger, since the trigger efficiency of the leptoquark signal is much higher. Only one of the two muons in an event has to fulfill the trigger so that the event is recorded. The trigger called "L1_MU20"[1] requires a muon with a transverse momentum of at least 20 GeV; the first part of the trigger name always refers to the corresponding level of the trigger system (confer Section 3.3): Level 1 (L1), Level 2 (L2) and Level 3 (EventFilter EF). The trigger "L2_MU40" requires a muon with a transverse momentum of at least 40 GeV that fulfilled the "L1_MU40" trigger. The trigger "L2_MU20i" requires also a muon with a transverse momentum of at least 20 GeV that fulfilled the "L1_MU20" or the "L1_MU40" trigger; the "i" in "MU20i" originally stood for an isolation cut but the isolation requirement has been dropped. The trigger "EF_MU20i" requires a muon with a transverse momentum of at least 20 GeV that fulfilled the "L2_MU20i" trigger. The trigger efficiencies given are absolute efficiencies, i.e. all events that fulfill the EventFilter-trigger already fulfilled the corresponding Level-1 and Level-2 triggers.

[1] The Level-1 triggers are exclusive, i.e. a muon with for example a transverse momentum of 65 GeV triggers the "L1_MU40" trigger but not the "L1_MU20" trigger. So the efficiencies of these two triggers have to be added. The Level-2 and EventFilter-triggers are inclusive.

	L1_MU20 or L1_MU40	L2_MU20i	EF_MU20i
second generation leptoquark m_{LQ} = 300 GeV	97.81%	96.64%	96.04%
second generation leptoquark m_{LQ} = 400 GeV	97.75%	96.74%	95.78%
second generation leptoquark m_{LQ} = 600 GeV	97.59%	96.68%	95.35%
second generation leptoquark m_{LQ} = 800 GeV	97.20%	96.35%	95.06%
$t\bar{t}$, decaying not fully hadronically	98%/100%/ -/-	99%/100%/ -/-	97%/100%/ -/-
DY $m_Z^{MC} > 60$ GeV	98%/100%/ 100%/100%	98%/100%/ 100%/100%	97%/100%/ 100%/100%
vector boson pairs	100%/100%/ -/-	100%/100%/ -/-	100%/100%/ -/-

Table 5.1: Trigger efficiencies; percentage of selected events that fulfilled the corresponding trigger; the 4 numbers in each table entry for the background samples are the trigger efficiencies for optimized cuts for m_{LQ} = 300 GeV, m_{LQ} = 400 GeV, m_{LQ} = 600 GeV and m_{LQ} = 800 GeV respectively

The efficiencies of the EventFilter-triggers for the second generation leptoquark signal lie between 95% and 96%. This high efficiency is expected since there are two muons in each second generation leptoquark event but the triggers require only at least one muon to fulfill the requirement. Futhermore the muon is required to have a transverse momentum of at least 60 GeV in the analysis cuts. The trigger efficiency is also very high for the SM backgrounds, i.e. close to 100%. These backgrounds also have 2 muons in each event, otherwise they would not be selected by this analysis. Furthermore the same analysis cuts are used for the backgrounds and so the muons also have a high energy.

Chapter 6

Systematic Uncertainties

There are many different sources of systematic uncertainty which have to be considered for the calculation of discovery and exclusion limits. An overview of the different systematic uncertainty sources, the sizes assumed and the effects on the number of signal and background events for second generation leptoquarks with $m_{LQ} = 400$ GeV can be found in Table 6.1.

The effects on the number of signal and background events for all systematic uncertainties have been calculated separately for each systematic uncertainty. For systematic uncertainties affecting only one background sample (e.g. the DY cross-section) the cross-section fraction of a sample on the total background cross-section has been considered. For example the Drell-Yan sample $m_Z^{MC} > 60$ GeV constitutes about 40% of the background cross-section left after all cuts for $m_{LQ} = 400$ GeV, so the relative error of the Drell-Yan sample has been multiplied by 0.4 to get the share of the Drell-Yan sample of the effective systematic uncertainty of the total background.

The first systematic uncertainty to be considered is the systematic uncertainty on the integrated *pp* luminosity. There are three ways to measure the integrated luminosity. One way is to measure the instantaneous luminosity directly via the beam parameters [41]. One can also calculate the instantaneous luminosity if it is possible to detect elastically scattered protons at small angles. The angle must be in a momentum transfer range sensitive to Coulomb and nuclear interactions and their interference [42]. The measurement of the angular distribution of the protons provides a determination of the instantaneous luminosity. The elastically scattered protons are measured by detectors which are 17 m, 140 m and 240 m away from the interaction point. The instantaneous luminosity has to be integrated over time to get the integrated luminosity of a certain period of the LHC run. The third way to calculate the integrated luminosity is done by analyzing pure QED or SM processes where the cross-section of the physics process (including branching ratio) is well known. One has to count the number

of measured events in a certain period of the LHC run of this chosen benchmark process and can then calculate the integrated luminosity of this period. For this calculation the reconstruction and trigger efficiency, the geometric acceptance of the detector, the dead-time of the data acquisition system, trigger pre-scales and failures and losses have to be taken into account.
In the beginning of the LHC run it is very difficult to measure the absolute value of the betatron emittance, i.e. the phase space volume occupied by the beam, which is part of the function to determine the instantaneous luminosity from beam parameters. Also the measurement of scattered protons will not be very precise because also the detectors for the scattered protons have to be calibrated and their properties have to be understood. The calculation via the cross-section of known processes will suffer from the uncertainties of the reconstruction and trigger efficiencies amongst others.
This systematic uncertainty has thus been assumed to be 20%, since in the early time of the LHC run, the time scale which this thesis focuses on, it will be quite large [35].

The effective systematic uncertainty on the leptoquark cross-section is between 13% and 25% for the tested leptoquark masses and the value for a second generation leptoquark with m_{LQ}= 400 GeV is given in the table. For details of the calculation see Section 2.5.

The systematic uncertainty on the cross-sections of $t\bar{t}$, decaying not fully hadronically, and Drell-Yan processes were estimated to be 12% [43] and 10% [35], respectively. For the calculation of the systematic uncertainty on $t\bar{t}$ two different PDFs (the updated CTEQ6.1 [21] and MRST2001E [44]) have been taken and the variables of the PDF have been varied. The largest error of the 2 different PDFs has been taken as PDF uncertainty. Also the renormalization and factorization scale has been varied. The largest part of this systematic uncertainty is due to the this scale variation. These two errors have been combined to get the total systematic uncertainty on the cross-section of $t\bar{t}$.

The muon identification, reconstruction and trigger uncertainty are assumed to be 5% altogether [45], so the systematic uncertainty sums up to 10% all together for second generation leptoquark pair events, since there are two muons in each event. The so-called Tag&Probe-method [46] normally used to test the identification, reconstruction and triggering cannot be used, since the method uses real Z-bosons decaying into two muons, so the resulting muons have a low energy compared to the muons used in this analysis. There are some gaps in the detector for cables etc. so some muons can escape the ATLAS detector without being detected. The uncertainty in the reconstruction arises mainly from the limited knowledge of the magnetic field in the muon spectrometer and the alignment of the muon chambers amongst others [45]. The trigger uncertainty arises from

the Resistive Plate Chambers (RPCs) and Thin Gap Chambers (TGC), which are used as a trigger in the barrel- and endcap-region respectively. The RPCs also provide the necessary timing information for the drift-time measurement of the MDT-chambers.

The systematic uncertainty of the muon energy scale is assumed to be 1% [45]. The reason for this systematic uncertainty is similar to the reason for the systematic uncertainty in the Jet Energy Scale (see below), only except not in respect to the hadronic calorimeter but the muon detectors. The energy of all muons has been increased and decreased by 1% and the number of signal and background events after all cuts have been studied. The largest difference between these two numbers and the number of events left after all cuts without any change to the muon energies has been taken as effective systematic uncertainty.

The uncertainty due to muon $1/p_T$ resolution was estimated using a Gaussian smearing of $1/p_T$ with a width of $0.011/p_T \oplus 0.00017$ [45], where p_T is in GeV. This smearing corresponds to roughly 100% of the p_T of the muons, since the p_T of the muons is quite high. Again the number of signal and background events after all cuts with and without the smearing has been calculated. This difference divided by the number of events after all cuts without muon smearing has been taken as effective systematic uncertainty. The muon $1/p_T$ resolution arises from several factors: the fact that the muon detectors are not aligned perfectly, the statistical fluctuations of the muon energy loss in material between the muon detectors and the interaction point, ambiguities fitting the track, single tube resolution and electrical noise of the detector components amongst others.

The Jet Energy Scale (JES) will affect the efficiency of selection criteria involving jet energies. Jet energies are measured in a sampling calorimeter. So one has to know which jet energy corresponds to which deposited energy in the detector material of the sampling calorimeter. In the beginning of the LHC run the calibration will be quite imprecise. Also unpredicted detector effects will most likely occur like at other detectors at large high energy physics experiments at the beginning of their physics runs and it will take some time to fully understand these effects. The uncertainty on the JES has been estimated by changing the energy of all jets simultaneously by $\pm 10\%$ and $\pm 20\%$, for $|\eta_{jet}| \leq 3.2$ and $|\eta_{jet}| > 3.2$ respectively [47]. The largest difference between the number of signal events and background events left after all cuts without change to the energy of the jets and 1. with increasing the energy of the jets and 2. with decreasing the energy of the jets has been calculated. This difference has been divided by the number of events of a sample left after all cuts without any change to the energy of the jets. This relative error has been assumed as the effective systematic uncertainty.

The systematic uncertainty due to jet energy resolution was estimated using a Gaussian smearing of jet energies in such a way that the relative jet energy resolution widens from $0.60/\sqrt{E} \oplus 0.05$ to $0.75/\sqrt{E} \oplus 0.07$ for $|\eta_{jet}| \leq 3.2$, and from $0.90/\sqrt{E} \oplus 0.07$ to $1.10/\sqrt{E} \oplus 0.10$ for $|\eta_{jet}| > 3.2$ [47], where E is in GeV. Again the number of events after all cuts with and without this jet smearing has been calculated. This difference divided by the number of events after all cuts has been taken as effective systematic uncertainty. The systematic uncertainty due to jet energy resolution comes from many sources which can be grouped in 2 categories: 1. physics effects like fluctuations of the deposition of energy outside of the jet clustering cone and 2. detector effects like the resolution of the calorimeter.

The systematic uncertainty of the Monte-Carlo modeling in Drell-Yan events was estimated by comparing a Monte-Carlo sample produced with PYTHIA and a Monte-Carlo sample produced with ALPGEN. Different MC sample generators have a different treatment of jets and initial and final state radiation amongst others. The available ALPGEN DY Monte-Carlo sample has $110 < m_Z^{MC} < 200$ GeV. So $110 < m_Z^{MC} < 200$ GeV was also required for the events coming from the PYTHIA DY sample. The number of events left after the basic selection cuts and $S_T \geq 600$ GeV was compared. This difference was divided by the number of events of the PYTHIA sample left after these cuts and this ratio was taken as systematic uncertainty.

Also the statistical uncertainties on the number of signal and background Monte-Carlo events have to be considered. These uncertainties were interpreted as systematic uncertainties on the number of events after all cuts. The size of the effective systematic uncertainty has been assumed to be $\sqrt{n}$ where n is the number of Monte-Carlo events of a sample left after all cuts.

The total systematic uncertainty is the quadratically added sum of all individual systematic uncertainties. For a second generation leptoquark $m_{LQ} = 400$ GeV the total systematic uncertainty of the signal is 30.6% and the total systematic uncertainty of the background is 51.7%.

Table 6.2 shows the total sum on the number of signal and backgrounds events for the tested second generation leptoquark masses.

As expected the total effective systematic uncertainty of the signal rises with increasing second generation leptoquark mass; as the mass increases the decay particles, i.e. the muons and the jets, have more energy and so the systematic uncertainties on them increase. Especially the systematic uncertainty from the JES increases dramatically; from having an effective systematic uncertainty of 5.8% on the signal for $m_{LQ} = 300$ GeV, over 12.0% on the signal for $m_{LQ} = 600$ GeV it reaches 23.1% on the signal for $m_{LQ} = 800$ GeV. This is because the cuts become harder for higher second generation leptoquark masses. At higher second generation leptoquark masses a larger percentage of signal events are close to the

source of systematic uncertainty	size of systematic uncertainty	effective systematic uncertainty on signal	effective systematic uncertainty on backgrounds
Integrated luminosity	20%	20%	20%
LQ cross-section	14.9%	14.9%	-
DY $m_Z^{MC} > 60$ GeV cross-section	10%	-	4%
$t\bar{t}$ cross-section	12%	-	7.2%
muon identification and trigger	5% per muon	10%	10%
muon resolution	100%	8.6%	11.3%
jet energy scale	10%-20%	11.3%	37.7%
jet resolution	dependent on E^{jet}	2.6%	3.8%
uncertainty of MC modeling	30%	-	18%
statistical uncertainty of MC	$\sqrt{n}$	2.4%	23.4%
quadratic sum of all uncertainties	-	30.6%	51.7%

Table 6.1: Systematic and statistical uncertainties for second generation leptoquark $m_{LQ} = 400$ GeV signal and background events with cuts for $m_{LQ} = 400$ GeV

tested leptoquark mass	300 GeV	400 GeV	600 GeV	800 GeV
total effective systematic uncertainty on signal	28.2%	30.6%	32.5%	43.0%
total effective systematic uncertainty on background	36.5%	51.7%	85.4%	> 100%

Table 6.2: Total sum of systematic uncertainties on the number of signal and background events for the tested second generation leptoquark masses

cut values, so a similar change in the JES suppresses (or let pass) many more signal events at higher second generation leptoquark masses than at lower second generation leptoquark masses.
Also the total effective systematic uncertainty of the background rises with increasing second generation leptoquark mass, because harder cuts are applied, so only particles with larger energy are left. Varying the JES has a larger effect on these high-energetic particles; the effective systematic uncertainty of the JES rises from 15.1% on the background for $m_{LQ} = 300$ GeV, over 53.9% on the background for $m_{LQ} = 600$ GeV to over 100% on the background for $m_{LQ} = 800$ GeV.
Also the statistical uncertainty increases with the tested second generation leptoquark mass, since there are fewer and fewer events of the Monte-Carlo background samples left after all cuts. For the tested second generation leptoquark $m_{LQ} = 800$ GeV there is only one event left of all background events in the MC samples.

Chapter 7

Discovery Reach of ATLAS with Early Data

The significance of the signal has been calculated with the significance calculator S_{cP} [40] (see also Appendix B). The significance is defined in units of Gaussian standard deviations σ. They correspond to the one-sided probability of observing a certain number of events exceeding the Monte-Carlo-predicted background Nb at a given luminosity. This probability is usually referred to as confidence level of the background CLb(N), where N is the number of observed events. The expected σ corresponds to CLb(Ns +Nb), where Ns is the expected number of signal events.
In other words: for a set integrated luminosity it is calculated how many events are expected if there are only background events and no signal events and how many events are expected if there are background and signal events. For very few background events left Poisson statistics has to be applied and the probability that the number, where one assumed only background events, fluctuates up to the number, where one assumed signal and background events, is calculated. A 5σ significance corresponds to a probability of $5 \cdot 10^{-7}$ for this fluctuation.
If both signal and background events were distributed Gaussian, the significance calculated this way would be equal to $\frac{S}{\sqrt{B}}$, where S is the number of signal events and B is the number of background events for a given integrated luminosity. The significance corresponds to the probability that the number of background events B fluctuates up to the sum of signal and background events S+B.
The systematic uncertainties of the number of background events and the trigger efficiencies of signal and background events have been included in the significance calculations. The dimuon mass-, S_T- and leptoquark mass window-cut were optimized to minimize the integrated luminosity needed to reach a 5σ discovery for a tested second generation leptoquark mass. It has been assumed that 100% of the second generation leptoquarks decay into a charged muon and a quark unless otherwise stated.

Table 7.1 shows the integrated luminosity needed for a 5σ discovery for different tested second generation leptoquark masses including the trigger efficiencies and systematic uncertainties; in the table also the numbers calculated without systematic uncertainties are given. Figure 7.1 shows the same data in a histogram. Second generation leptoquarks with masses up to around 400 GeV can be discovered with a 5σ significance in a very early phase of the LHC run, i.e. in the first few months. To discover second generation leptoquarks with masses around 600 GeV with a 5σ significance an integrated luminosity of around 100 pb^{-1} is needed which corresponds to about several months of the LHC run.
It has been calculated that an integrated luminosity of 663 pb^{-1} is needed to discover a second generation leptoquark with $m_{LQ} = 800$ GeV with a 5σ significance. The number of background events left using selection cuts for $m_{LQ} = 800$ GeV is very low. For the optimized cuts for a 5σ significance the absolute number of background events of the Monte Carlo samples after all cuts equals 1. So the calculated number is just an estimate; the main focus in this thesis is on lower second generation leptoquark masses.

Tested second generation leptoquark mass	Expected integrated luminosity needed for 5σ discovery	
	with sys. uncertainties	without sys. uncertainties
300 GeV	1.51 pb^{-1}	1.36 pb^{-1}
400 GeV	7.42 pb^{-1}	6.43 pb^{-1}
600 GeV	103.3 pb^{-1}	68.2 pb^{-1}
800 GeV	663 pb^{-1}	353 pb^{-1}

Table 7.1: Integrated luminosities needed for 5σ discovery of different tested second generation leptoquark masses

Table 7.2 shows the expected integrated luminosities needed for a 95% exclusion for second generation leptoquarks with different masses; the cuts optimized for a 5σ discovery have been used. To exclude the signal with a 95% confidence level the probabilty that the number of signal and background events fluctuates down to the number of measured events at the given integrated luminosity is 5% or less. The trigger efficiencies and systematic uncertainties of signal and background have been included in this calculation. The exclusion limits have been calculated with TLimit of the ROOT package [48]. TLimit computes limits using the likelihood ratio method [49].

So far is has been assumed that all second generation leptoquarks decay into a charged lepton and a quark, i.e. $\beta = 1$ has been assumed. Since there are 2 leptoquarks in each event β^2 corresponds to the fraction of leptoquark pair

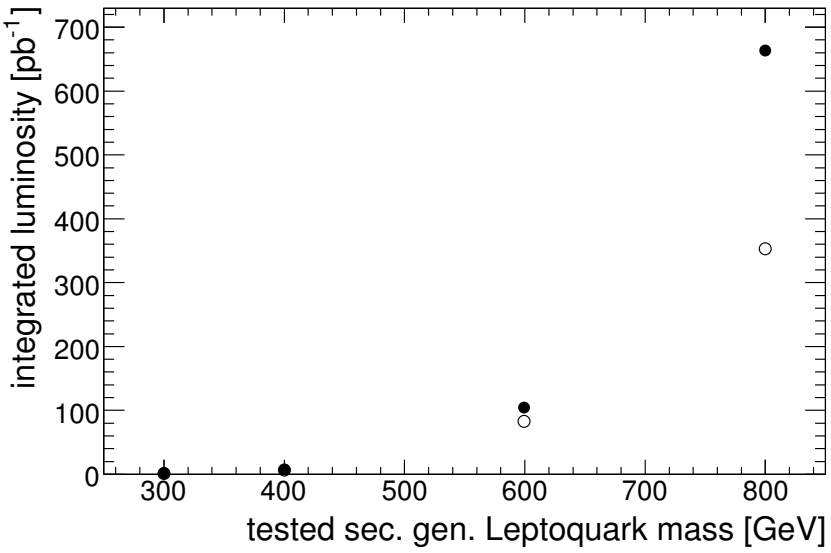

Figure 7.1: Integrated luminosities needed for 5σ discovery of different tested second generation leptoquark masses with systematic uncertainties (closed circles) and without systematic uncertainties (open circles); the open circles at 300 GeV and 400 GeV are not visible since they lie underneath the closed circles.

Tested second generation leptoquark mass	Expected integrated luminosity needed for 95% exclusion
300 GeV	0.76 pb^{-1}
400 GeV	4.1 pb^{-1}
600 GeV	61 pb^{-1}
800 GeV	261 pb^{-1}

Table 7.2: Integrated luminosities needed for 95% exclusion of different tested second generation leptoquark masses

events, where both leptoquarks decay into a charged lepton and a quark. Figure 7.2 shows β^2 for a second generation leptoquark $m_{LQ} = 400$ GeV which can be discovered with a significance of 5σ with and without systematic uncertainties. The optimized cuts for $\beta = 1$ have been used for this calculation. For $\beta^2 = 0.25$, i.e. $\beta = 0.5$, an integrated luminosity of 70.5 pb^{-1} is needed for a 5σ discovery of a second generation leptoquark with $m_{LQ} = 400$ GeV including the trigger efficiencies and the systematic uncertainties; without systematic uncertainties an integrated luminosity of 45.5 pb^{-1} is needed for a 5σ discovery of a second generation leptoquark with $m_{LQ} = 400$ GeV.

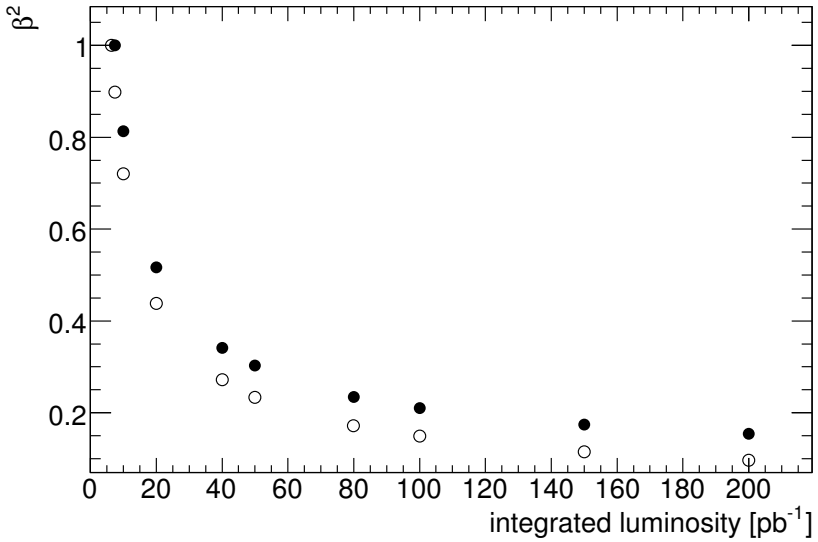

Figure 7.2: β^2 of second generation leptoquark $m_{LQ} = 400$ GeV which can be discovered with a significance of 5σ with systematic uncertainties (closed circles) and without systematic uncertainties (open circles)

The second generation leptoquark masses $m_{LQ} = 300$ GeV, $m_{LQ} = 400$ GeV and $m_{LQ} = 600$ GeV (and $m_{LQ} = 800$ GeV) have been studied individually. To estimate the sensitivity for masses between these tested masses an interpolation of signal and background has been carried out. The signal efficiency has been interpolated linearly between the 3 mass points. The cross-sections for the second generation leptoquark masses between the tested masses have been calculated in next-to-leading order and multiplied by the interpolated efficiency to get the remaining signal cross-section. The S_T-, dimuon mass- and leptoquark mass window-cuts have been interpolated linearly between these points and the number of background events left after all cuts has been analyzed for each cut combination. Then the smallest β^2 which can be discovered with an integrated luminosity of 100 pb^{-1} has been calculated. The results can be seen in Figure

7.3. Since the statistics of the background samples is not very large there are many ups and downs along the increasing second generation leptoquark mass. A few background events more or less make a huge impact on the resulting β^2; this is caused by events passing or failing the cuts as the cuts change with the tested second generation leptoquark mass. One can see a different size of the slope for the interpolation between $m_{LQ} = 300$ GeV and $m_{LQ} = 400$ GeV and the interpolation between $m_{LQ} = 400$ GeV and $m_{LQ} = 600$ GeV. The slope of β^2 is larger between $m_{LQ} = 400$ GeV and $m_{LQ} = 600$ GeV. This is because the leptoquark mass window-cut decreases, i.e. the window becomes smaller, more strongly than the other cuts are increased at the same time. The mass window changes from a size of 150 GeV at $m_{LQ} = 300$ GeV to a size of 75 GeV at $m_{LQ} = 400$ GeV, but it increases, i.e. the window becomes much larger, from a window size of 75 GeV at $m_{LQ} = 400$ GeV to a window size of 200 GeV at $m_{LQ} = 600$ GeV.

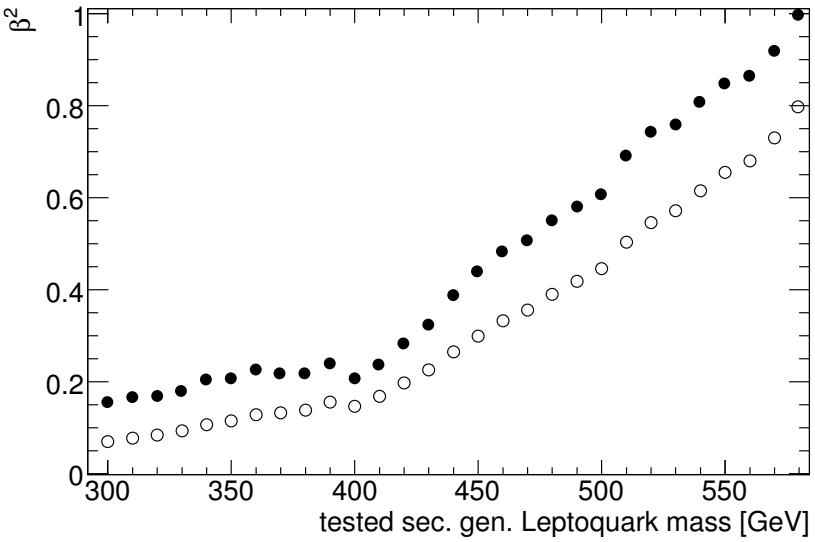

Figure 7.3: Interpolated β^2 of different second generation leptoquark masses which can be discovered with a significance of 5σ at an integrated luminosity of 100 pb^{-1} with systematic uncertainties (closed circles) and without systematic uncertainties (open circles)

Chapter 8

Conclusion and Outlook

Scalar second generation leptoquarks have a very distinct signal which distinguishes them from almost all Standard Model (SM) processes. Second generation leptoquarks decay into a lepton and a quark; it has been assumed in this thesis that 100% of all leptoquarks decay into a muon and a quark. Only pair production of scalar second generation leptoquark has been studied since the single production depends on the unknown Yukawa coupling between a quark, a lepton and a leptoquark. This thesis studied many different variables which could be used to distinguish second generation leptoquark events from SM processes. It was found that the best variables which can be used for this discrimination are the cuts on the transverse momenta of the muons, S_T (the scalar sum of the 2 selected muons and 2 selected jets), the mass of the dimuon system (of the 2 selected muons) and the reconstructed second generation leptoquark mass.
With cuts on these variables, where the cuts on the latter 3 variables are optimized for a discovery with 5σ significance, scalar second generation leptoquarks can be discovered in an early phase of the LHC run. Scalar second generation leptoquarks slightly above the current 95% exclusion limits with masses between 300 GeV and 400 GeV could be discovered with an integrated luminosity from 1.51 pb^{-1} up to 7.42 pb^{-1}. This corresponds to a few days up to several months of the LHC run. For higher second generation leptoquark masses of 600 GeV and 800 GeV an integrated luminosity of 103.3 pb^{-1} and 663 pb^{-1} is needed for a discovery with 5σ significance respectively (see Table 8.1). For the calculation of these integrated luminosities the trigger efficiencies and systematic uncertainties have been considered. Especially the systematic uncertainties were estimated conservatively and their impact has been studied carefully since the ATLAS detector will not be perfectly understood in the early phase of the LHC run.

For the highest second generation leptoquark mass which has been tested, $m_{LQ} = 800$ GeV, the statistics of simulated MC background samples is already very low. From all background samples the number of background events of the Monte Carlo samples left after the optimized selection cuts equals 1. So the given

Tested second generation leptoquark mass	Expected integrated luminosity needed for 5σ discovery	
	with sys. uncertainties	without sys. uncertainties
300 GeV	1.51 pb^{-1}	1.36 pb^{-1}
400 GeV	7.42 pb^{-1}	6.43 pb^{-1}
600 GeV	103.3 pb^{-1}	68.2 pb^{-1}
800 GeV	663 pb^{-1}	353 pb^{-1}

Table 8.1: Integrated luminosities needed for 5σ discovery of different tested second generation leptoquark masses

numbers are just an estimate.

The start of the LHC run in fall of 2008 will mark the start of a new era in high energy physics. The LHC will collide protons at much higher energies than any collider ever before. Probably and hopefully there will be many new physics phenomena which can be observed at center-of-mass energies of up to 14 TeV. One of the new particles which could be discovered with the ATLAS detector are leptoquarks. Scalar second generation leptoquarks could be the first new particles to be discovered with very early data from the ATLAS detector at the LHC. The first paper of the DØ experiment at Tevatron has also been on the search for leptoquarks. The discovery of scalar second generation leptoquarks would be an exciting indication for the existence of extended gauge symmetries like superstring-inspired E_6 models, grand-unified-theories etc. [50]. Their existence could explain the almost complete symmetry between the quark and the lepton sector.

Appendix A

Plots for Other Tested Leptoquark Masses

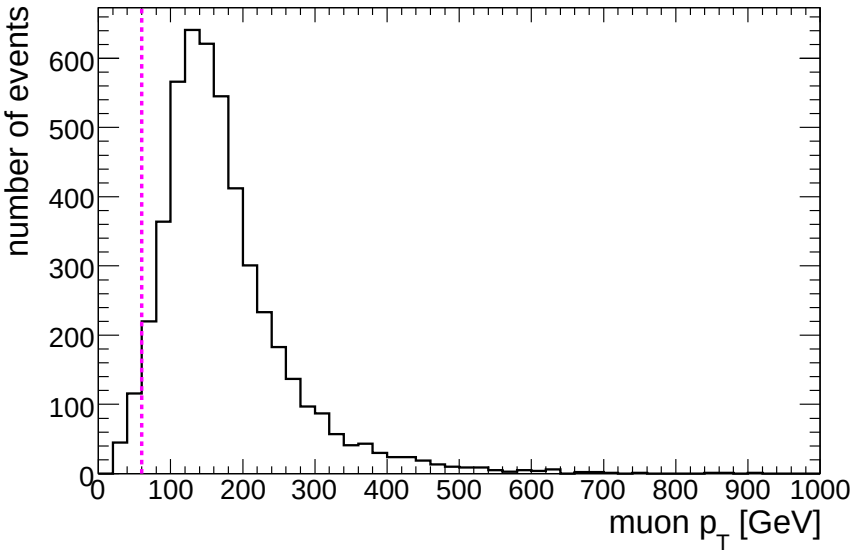

Figure A.1: p_T distribution of second generation leptoquark m_{LQ}=300 GeV of the muon of the selected two muons, which has the highest p_T, after preselection cuts, not normalized. The vertical lines indicate the $p_T^{muon} \geq 60$ GeV requirement.

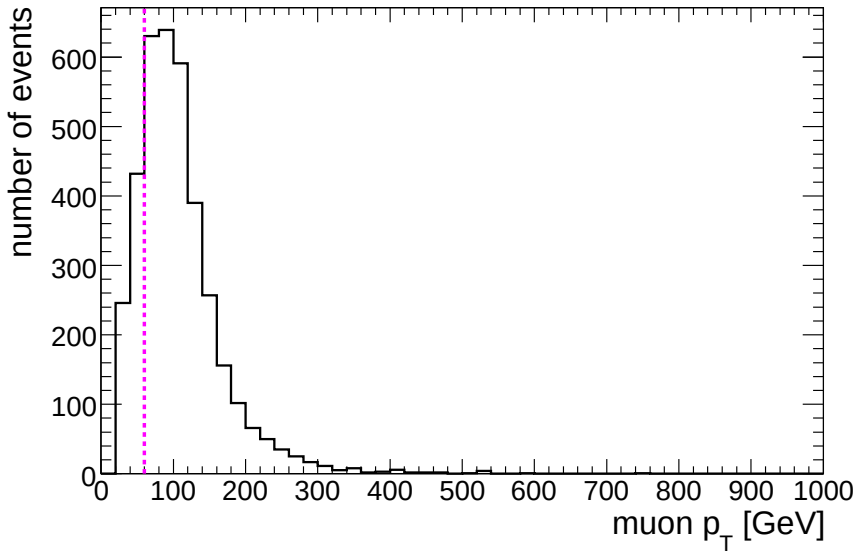

Figure A.2: p_T distribution of second generation leptoquark m_{LQ}=300 GeV of the muon of the selected two muons, which has the lowest p_T, after preselection cuts, not normalized. The vertical lines indicate the $p_T^{muon} \geq 60$ GeV requirement.

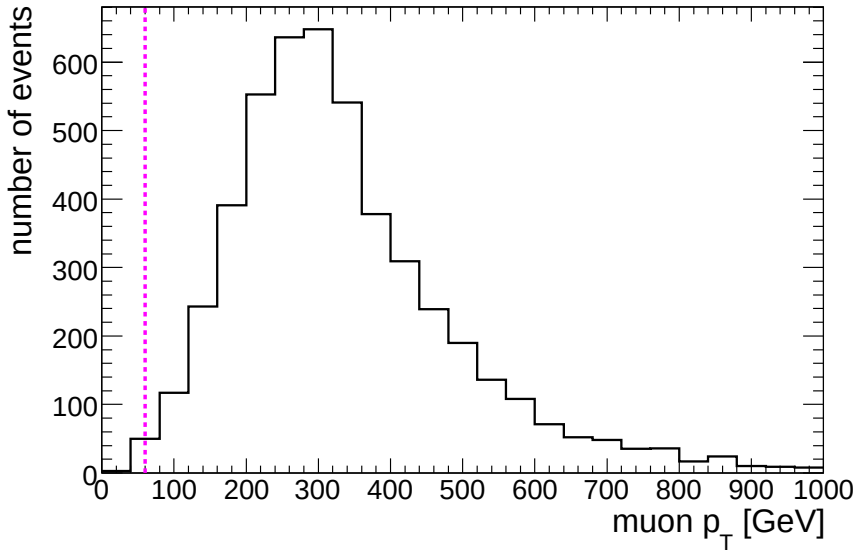

Figure A.3: p_T distribution of second generation leptoquark m_{LQ}=600 GeV of the muon of the selected two muons, which has the highest p_T, after preselection cuts, not normalized. The vertical lines indicate the $p_T^{muon} \geq 60$ GeV requirement.

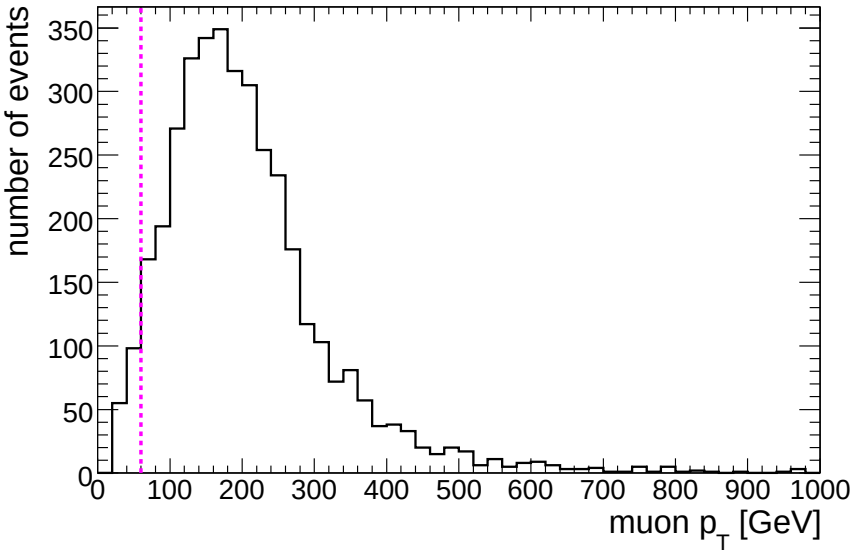

Figure A.4: p_T distribution of second generation leptoquark m_{LQ}=600 GeV of the muon of the selected two muons, which has the lowest p_T, after preselection cuts, not normalized. The vertical lines indicate the $p_T^{muon} \geq 60$ GeV requirement.

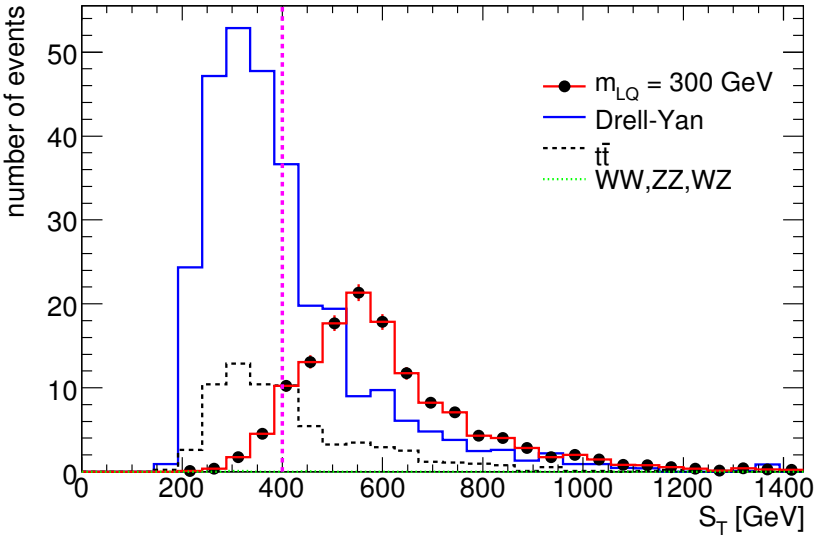

Figure A.5: S_T distributions for second generation leptoquark (m_{LQ}=300 GeV) signal, and DY and $t\bar{t}$, decaying not fully hadronically, backgrounds after baseline selection and the requirements $p_T^{\mu} > 60$ GeV and $E_T^{jet} > 25$ GeV normalized to 100 pb^{-1} of integrated pp luminosity. The vertical line indicates the $S_T \geq 400$ GeV requirement.

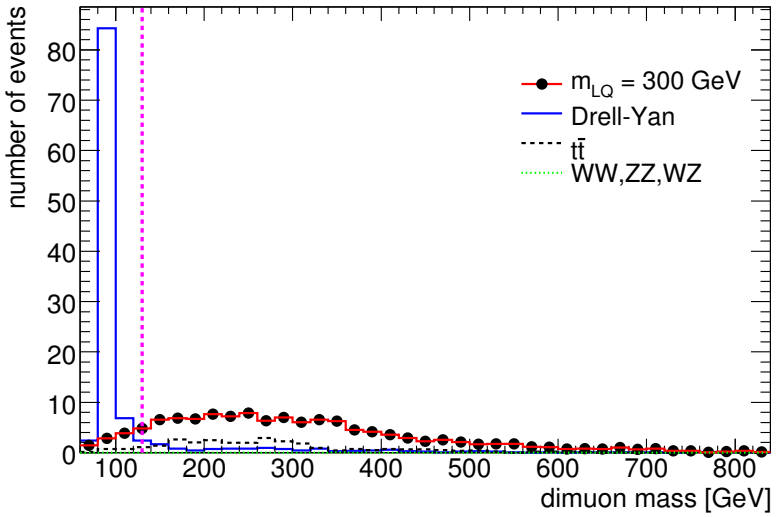

Figure A.6: Dimuon reconstructed invariant mass distributions for second generation leptoquark ($m_{LQ} = 300$ GeV) signal, and DY and $t\bar{t}$ backgrounds after the S_T selection normalized to 100 pb^{-1} of integrated pp luminosity. The vertical line indicates the $M(\mu\mu) \geq 130$ GeV requirement.

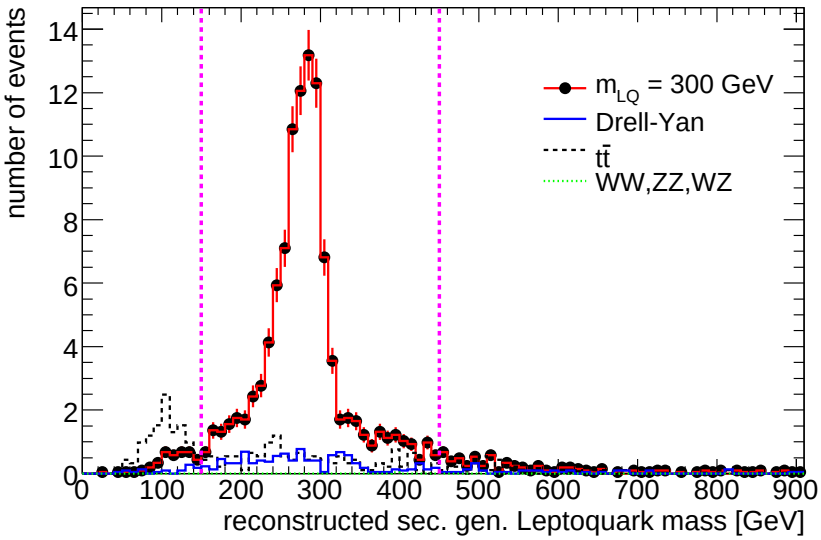

Figure A.7: Reconstructed second generation leptoquark mass distributions for second generation leptoquark (m_{LQ} = 300 GeV) signal, and DY and $t\bar{t}$ backgrounds after applying all but leptoquark mass window selection criteria normalized to 100 pb^{-1} of integrated pp luminosity. The vertical lines indicate the leptoquark signal invariant mass window.

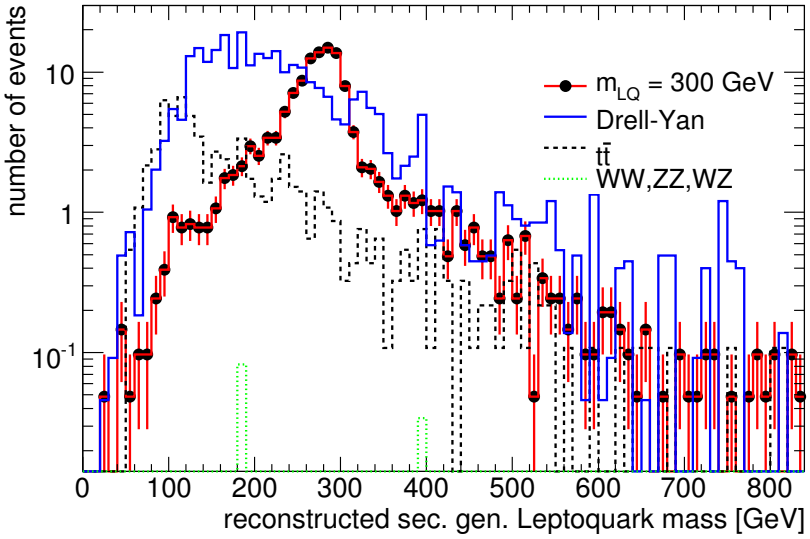

Figure A.8: Reconstructed second generation leptoquark mass distributions for second generation leptoquark (m_{LQ} = 300 GeV) signal, and DY and $t\bar{t}$ backgrounds after basic selection cuts normalized to 100 pb^{-1} of integrated pp luminosity

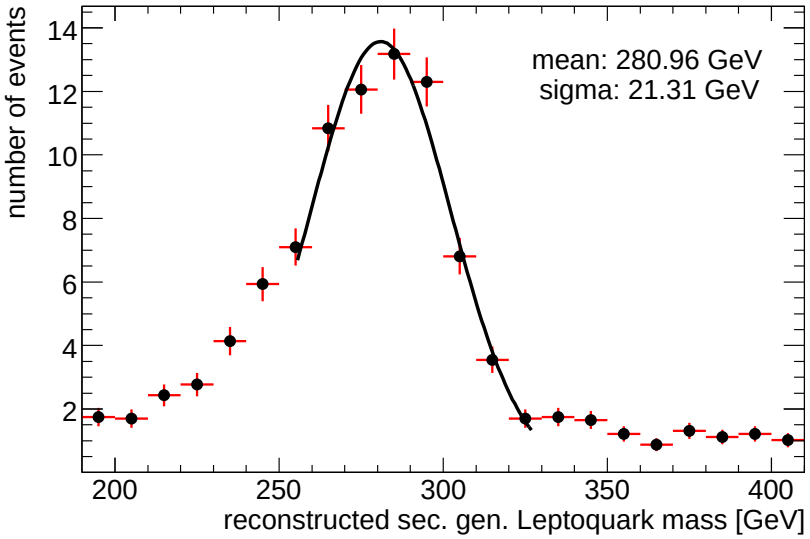

Figure A.9: Reconstructed second generation leptoquark mass distribution for m_{LQ} = 300 GeV with a Gaussian fit after all cuts normalized to 100 pb^{-1} of integrated pp luminosity

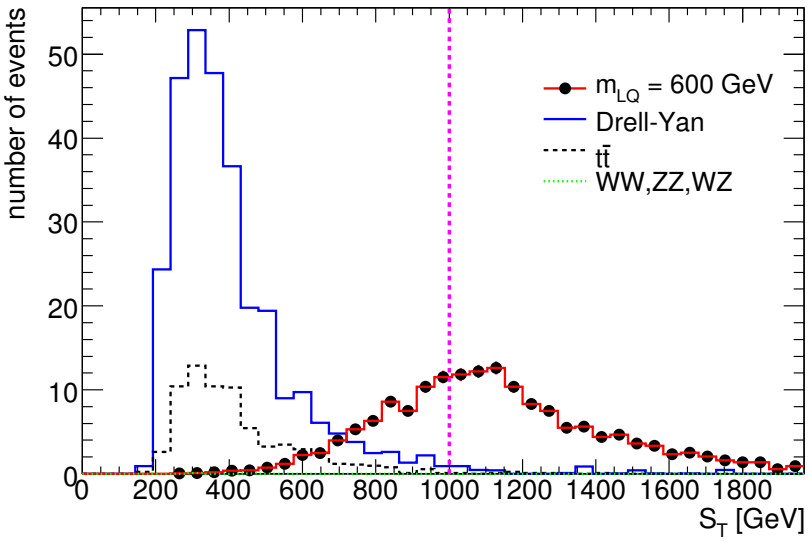

Figure A.10: S_T distributions for second generation leptoquark (m_{LQ}=600 GeV) signal, and DY and $t\bar{t}$ backgrounds after baseline selection and the requirements $p_T^{\mu} > 60$ GeV and $E_T^{jet} > 25$ GeV normalized to 100 pb^{-1} of integrated pp luminosity. The vertical line indicates the $S_T \geq 1000$ GeV requirement.

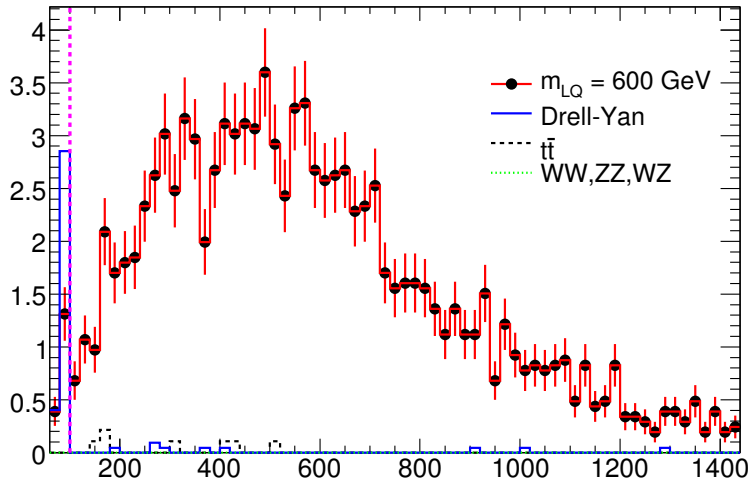

Figure A.11: Dimuon reconstructed invariant mass distributions for second generation leptoquark (m_{LQ} = 600 GeV) signal, and DY and $t\bar{t}$ backgrounds after the S_T selection normalized to 100 pb^{-1} of integrated pp luminosity. The vertical line indicates the $M(\mu\mu) \geq 130$ GeV requirement.

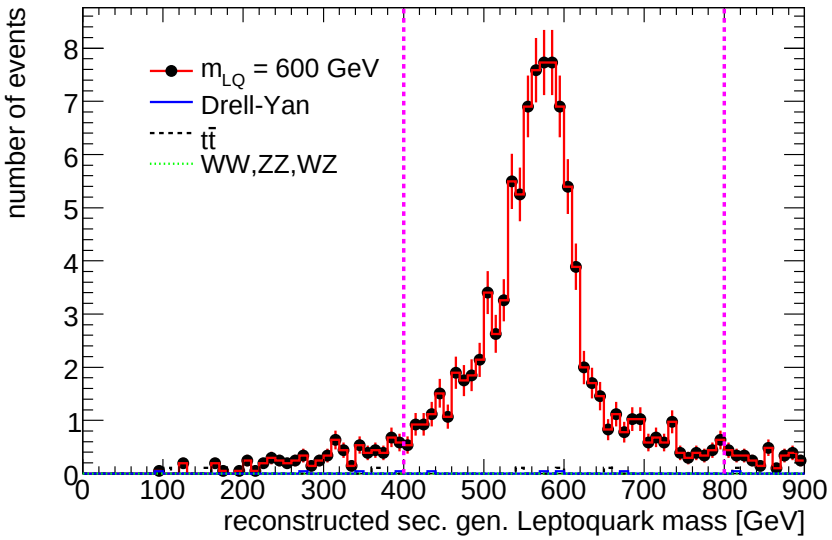

Figure A.12: Reconstructed second generation leptoquark mass distributions for second generation leptoquark (m_{LQ} = 600 GeV) signal, and DY and $t\bar{t}$ backgrounds after applying all but leptoquark mass window selection criteria normalized to 100 pb^{-1} of integrated pp luminosity. The vertical lines indicate the leptoquark signal invariant mass window.

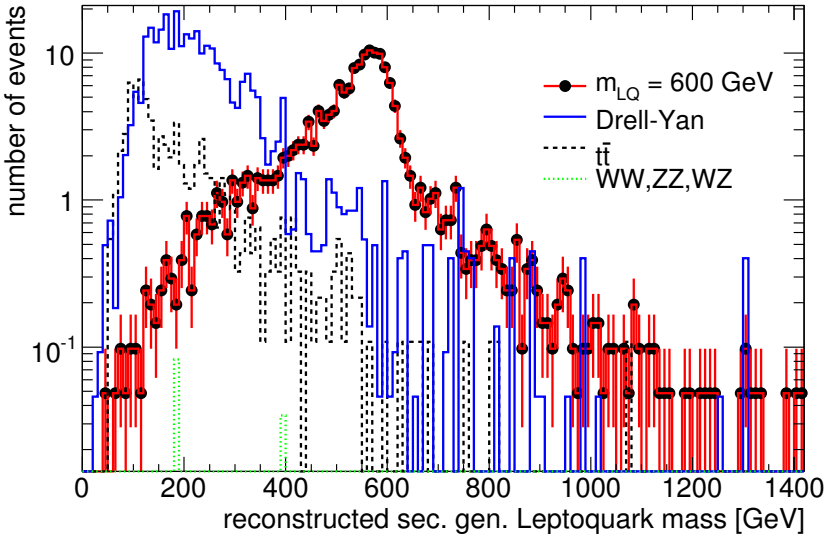

Figure A.13: Reconstructed second generation leptoquark mass distributions for second generation leptoquark ($m_{LQ} = 600$ GeV) signal, and DY and $t\bar{t}$ backgrounds after baseline selection normalized to 100 pb^{-1} of integrated pp luminosity

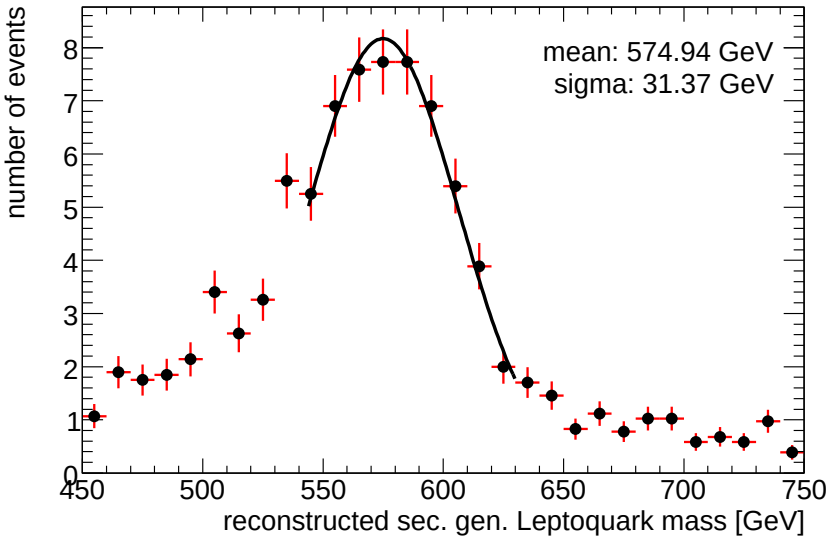

Figure A.14: Reconstructed second generation leptoquark mass distribution for $m_{LQ} = 600$ GeV with a Gaussian fit after all cuts normalized to 100 pb^{-1} of integrated pp luminosity

Appendix B

Calculation of the 5σ Discovery Level

This appendix describes the calculation of the 5σ discovery levels with the program S_{cP}. A more detailed description can be found in [40].
One of the simplest definitions of significance is $S_1 = \frac{s}{\sqrt{b}}$. This definition assumes a symmetrical Gaussian distribution of signal and background. For asymmetrical distribution these definitions of significance can be used only as approximations [51]. For Poisson distributions a better and analog definition of significance is S_{cP} [52]. The significance S_{cP} is the probability from Poisson distribution with a mean b to observe b+s or more events, converted to the equivalent number of sigmas of a Gaussian distribution:

$$\beta = \frac{1}{\sqrt{2\pi}} \int_{S_{cP}}^{\infty} e^{-\frac{x^2}{2}} dx \text{ where } \beta = \sum_{i=s+b}^{\infty} \frac{b^i e^{-b}}{i!}$$

The systematic uncertainty on the number of background events with statistical properties (the normal distribution with mean which equals 0 and the variance σ_b^2) of the background can be included in the calculation of the significance with the program S_{cP}; the parameter of the Poisson distribution is changed accordingly in the S_{cP} program when the systematic uncertainty is given. For the calculation of a discovery with a 5σ significance S_{cP} has been used in this thesis.

Appendix C

Datasets Used

The following ATLAS datasets have been used in this analysis:

- scalar second generation leptoquark m_{LQ} = 300 GeV:
  trig1_misal1_mc12.006678.Pythia_LQ_muc_300.merge.AOD.v12000604
- scalar second generation leptoquark m_{LQ} = 400 GeV:
  trig1_misal1_mc12.006679.Pythia_LQ_muc_400.merge.AOD.v12000604
- scalar second generation leptoquark m_{LQ} = 600 GeV:
  trig1_misal1_mc12.006680.Pythia_LQ_muc_600.merge.AOD.v12000604
- scalar second generation leptoquark m_{LQ} = 800 GeV:
  trig1_misal1_mc12.006681.Pythia_LQ_muc_800.merge.AOD.v12000604
- no-all hadronic $t\bar{t}$:
  trig1_misal1_mc12.005200.T1_McAtNlo_Jimmy.recon.AOD.v12000604
- $Z/\gamma^* \rightarrow \mu\mu$ $m_Z^{MC} > 60$ GeV:
  trig1_misal1_csc11_V2.005145.PythiaZmumu.recon.AOD.v12000601
- $Z/\gamma^* \rightarrow \mu\mu$ $m_Z^{MC} > 150$ GeV:
  trig1_misal1_csc11.005115.JimmyZmumuM150.merge.AOD.v12000604
- WW:
  trig1_misal1_csc11.005985.WW_Herwig.recon.AOD.v12000601
- ZZ:
  trig1_misal1_csc11.005986.ZZ_Herwig.merge.AOD.v12000605
- WZ:
  trig1_misal1_csc11.005987.WZ_Herwig.merge.AOD.v12000605

- QCD di-jet:
  trig1_misal1_csc11.005010.J1_pythia_jetjet.recon.AOD.v12000601
  trig1_misal1_csc11_V1.005011.J2_pythia_jetjet.recon.AOD.v12000604
  trig1_misal1_csc11.005012.J3_pythia_jetjet.recon.AOD.v12000604
  trig1_misal1_csc11.005013.J4_pythia_jetjet.recon.AOD.v12000605
  trig1_misal1_csc11_V2.005014.J5_pythia_jetjet.recon.AOD.v12000601
  trig1_misal1_csc11_V2.005015.J6_pythia_jetjet.recon.AOD.v12000604
  trig1_misal1_csc11.005016.J7_pythia_jetjet.recon.AOD.v12000604
  misal1_csc11.005017.J8_pythia_jetjet.recon.AOD.v12000601_tid006737

- Z with set additional number of partons:
  trig1_misal1_mc12.008142.AlpgenJimmyZmumuNp0LooseCut.recon.AOD.v12000604
  trig1_misal1_mc12.008143.AlpgenJimmyZmumuNp1LooseCut.recon.AOD.v12000604
  trig1_misal1_mc12.008144.AlpgenJimmyZmumuNp2LooseCut.recon.AOD.v12000604
  trig1_misal1_mc12.008145.AlpgenJimmyZmumuNp3LooseCut.recon.AOD.v12000604
  trig1_misal1_mc12.008146.AlpgenJimmyZmumuNp4LooseCut.recon.AOD.v12000604
  trig1_misal1_mc12.008147.AlpgenJimmyZmumuNp5LooseCut.recon.AOD.v12000604

- $Z/\gamma^* \rightarrow \tau\tau$ $m_{ll} > 60$ GeV:
  trig1_misal1_csc11.005142.JimmyZtautau.recon.AOD.v12000601

- single t-quark:
  trig1_misal1_mc12.005500.AcerMC_Wt.merge.AOD.v12000605

- W + b-jets
  trig1_misal1_csc11.005281.AcerMCbbW.recon.AOD.v12000601

The scalar second generation leptoquark samples have been generated with PYTHIA v6.403 [30]. Both single and pair production has been generated in the same MC sample(s). Only pair production leptoquark events have been selected on MC level. The PYTHIA parameters for $m_{LQ} = 300$ GeV were (jobOptions.py):

```
theApp.Dlls   += [ "Pythia_i" ]
theApp.TopAlg = ["Pythia"]
#
#--------------------------------------------------------------
#
Pythia = Algorithm( "Pythia" )
#
```

```
#  Full user control
#
Pythia.PythiaCommand += ["pysubs msel 0"]
#
#  LQ production
#
#++
#
#     qg -> lLQ
#
Pythia.PythiaCommand += ["pysubs msub 162 1"]
#
#     gg -> LQLQ
#
Pythia.PythiaCommand += ["pysubs msub 163 1"]
#
#     qqbar -> LQLQ
#
Pythia.PythiaCommand += ["pysubs msub 164 1"]
#
#  LQ mass
#
Pythia.PythiaCommand += ["pydat2 pmas 42 1 300."]
#
#  To avoid problems in MC generation
#
Pythia.PythiaCommand += ["pysubs ckin 41 200.0"]
Pythia.PythiaCommand += ["pysubs ckin 42 400.0"]
Pythia.PythiaCommand += ["pysubs ckin 43 200.0"]
Pythia.PythiaCommand += ["pysubs ckin 44 400.0"]
#
#  Branching fraction for the decay described below
#
Pythia.PythiaCommand += ["pydat3 brat 539 1."]
#
#  This is relevant to both the decay AND
#  production mechanism for single LQ
#
Pythia.PythiaCommand += ["pydat3 kfdp 539 1 4"]
Pythia.PythiaCommand += ["pydat3 kfdp 539 2 13"]
#
#  Coupling: lamda=sqrt(4 pi*alpha_em)
#
```

```
#  the choice was made to make single LQ production
#  to have approx. same cross section as pair production
#
Pythia.PythiaCommand += ["pydat1 paru 151 .8"]
#
#--------------------------------------------------------------------
#
#  According to
#  https://uimon.cern.ch/twiki/bin/view/Atlas/GeneratorValidation
#  (10/08/05)
#
Pythia.PythiaCommand += ["pypars mstp 68 1"]
Pythia.PythiaCommand += ["pypars mstp 70 2"]
Pythia.PythiaCommand += ["pypars mstp 82 4"]
Pythia.PythiaCommand += ["pypars parp 82 2.6"]
Pythia.PythiaCommand += ["pypars parp 84 0.3"]
Pythia.PythiaCommand += ["pypars parp 90 0.24"]
Pythia.PythiaCommand += ["pydat1 mstj 11 3"]
Pythia.PythiaCommand += ["pydat1 mstj 22 2"]
Pythia.PythiaCommand += ["pydat1 parj 54 -0.07"]
Pythia.PythiaCommand += ["pydat1 parj 55 -0.006"]
#
#  In order to prevent double counting in Pythia when PHOTOS is used
#
Pythia.PythiaCommand += ["pydat1 parj 90 20000"]
#
# 12/20/05 Pythia.PythiaCommand += ["pypars mstp 128 0"]
#
Pythia.PythiaCommand += ["pypars mstp 128 1"]
#
Pythia.PythiaCommand += ["pypars mstp 51 10042", "pypars mstp 52 2",
                         "pypars mstp 53 10042", "pypars mstp 54 2",
                         "pypars mstp 55 10042", "pypars mstp 56 2"]
#
#--------------------------------------------------------------------
#
Pythia.PythiaCommand += ["pyinit pylisti 12"]
#
Pythia.PythiaCommand += ["pyinit pylistf 1"]
#
Pythia.PythiaCommand += ["pystat 1 3 4 5"]
#
#  Print the event listing for events x though y:
```

```
#
Pythia.PythiaCommand += ["pyinit dumpr 1 20"]
#
#--------------------------------------------------------------
#
# ... Tauola
include ( "DC3_joboptions/DC3_Tauola_Fragment.py" )

# ... Photos
include ( "DC3_joboptions/DC3_Photos_Fragment.py" )
#
#--------------------------------------------------------------
```

And similarly for the other second generation leptoquark masses; just changing the generated mass and the mass window (lines just below "To avoid problems in MC generation").

Appendix D

ATLAS Software Installation in the GRID

D.1 The GRID

ATLAS will produce a large amount of data; about 1 PetaByte of data will be recorded per year. The physicists of the ATLAS experiment need to access and analyze this huge amount of data from institutes all over the world. For this purpose a computing GRID has been developed. The GRID allows integrated and common usage of the available resources which are distributed all over the world. The GRID as implemented in ATLAS is divided in so-called Tiers. The Tier structure can be seen in Figure D.1. All data will be recorded at the Tier-0 center which is the CERN computing facility. One full copy of all raw data will be distributed over the Tier-1 centers; these are large computing centers in the various regions. Each region or cloud as they are called consists of one Tier-1 center and several Tier-2 centers linked to this Tier-1 center. For example the German cloud consists of GridKA as a Tier-1 center and many Tier-2 centers in Germany, Switzerland, Poland and the Czech Republic. Each Tier-2 center stores only part of the data; its computing resources are mainly intended for group or individual analysis and centralized simulation. At the very bottom there are the computer clusters at some universities and the individual PCs of the physicists which are the Tier-3. The AODs of the simulated and recorded data have to be distributed to the Tier-2 centers in the world. There has to be an adequate bandwidth between the Tier-1 and the Tier-2 centers and between the different Tier-2 centers in order to allow this.

D.2 The ATLAS Software Installation

The ATHENA software package is in constant development. New versions of ATHENA come out every 2-4 weeks. The new versions of ATHENA have to

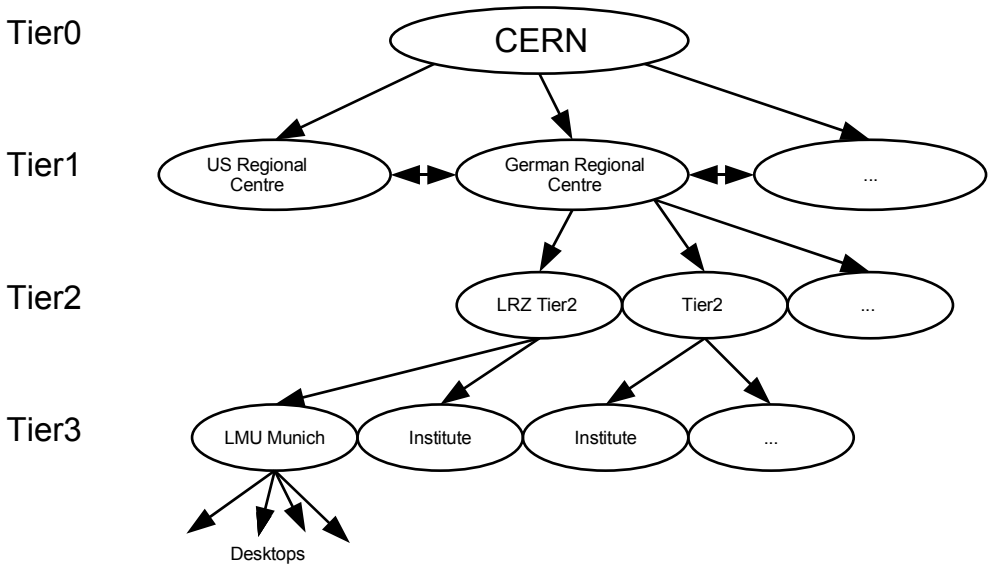

Figure D.1: The Tier structure of the LCG grid

be installed at all Tier-1 and Tier-2 centers worldwide as fast as possible. An installation team of 4-6 persons is responsible for this; each person is the main responsible person for a so-called cloud in the grid. A cloud consists of all Tier-2 sites which are associated with a specific Tier-1 site. The tool for the installation of new ATHENA versions over the grid is called Light Job Submission Framework for Installations (LJSFi) [53]. LJSFi is able to automatically discover, check, test and tag the full set of resources available in the LCG/EGEE to the ATLAS Virtual Organization in a few hours, depending on the site availability. The LJSFi automatically defines the job description file and configures it for the specific computing element and required task.
When a new version is released an automatic installation at all LCG [54] sites is triggered. Also users can request installations of specific releases and view the logging information via a web page. The access to the information of the installation is restricted to users with a valid certificate.
The software installation is performed in 3 steps:

- Site checks
- Installation task
- Output validation

The site checks consist of a pilot job which checks the basic setup and environment of a computing element. The installation jobs are run on the worker nodes at the

sites. After the installation task the LJSFi retrieves the job output and the exit codes from the grid middleware. The exit code is used to update a database of all installation requests.
The number of successful and failed jobs can be seen in Figure D.2; the check-site jobs are not included. The installation efficiency can be seen in Figure D.3; the efficiency is mostly between 60%-70%.

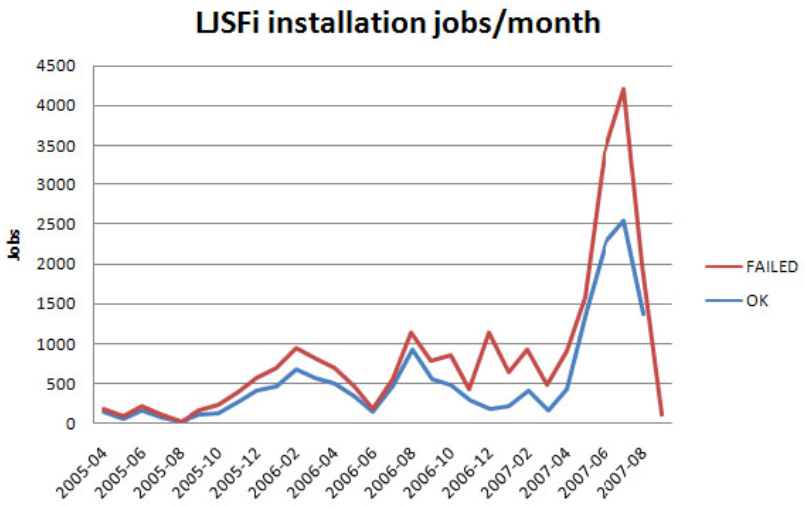

Figure D.2: LJSFi installation jobs per month. The plot does not include the pilot jobs used for the site checks. [53]

If the automatically configured installation jobs are not successful, the ATHENA installation has to be done manually. One person of the installation team has to take over the installation request and has to try a manual installation. Then the person has to view the logging information to get an idea which part of the ATHENA installation or validation process failed. The person then has to contact the local site administrator to discuss the problem.

One of the most common problems was wrongly set permissions of the directories where the software should be installed to, i.e. no right to write in the corresponding directories. After several installation periods the rights of the directories have been set accordingly and if problems arise at a site they are more complex. There are many different operating systems installed at the LCG sites, because the operating system support is often provided by existing computing centers, which don't want to support one more operating system just for the LCG grid. So the problems which occur are often quite diverse depending on the installed operating system and change with every software release. Sometimes it takes weeks or even months until a problem at a site is solved or until a hack is done to circumvent the problem until a permanent solution is available.

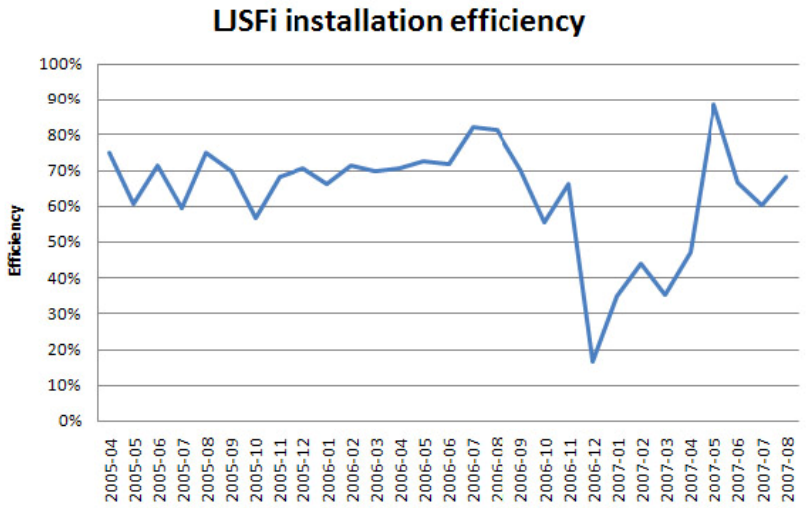

Figure D.3: LJSFi installation efficiency. The efficiency is dominated by the site status. The drop in the efficiency is due to the activation of the automatic installation module in late 2006, requesting the installation of several new sites, not yet ready for the ATLAS software deployment. The situation has become stable from May 2007. [53]

List of Figures

List of Tables

Bibliography

[1] W.-M.Yao et al. (Particle Data Group). The Review of Particle Physics. *J. Phys. G*, 33:1, 2006. 1, 2.1

[2] W. Buchmüller, R. Rückl and D. Wyler. Leptoquarks in Lepton-Quark Collisions. *Phys. Lett. B*, 448:442 (1987) and erratum in Phys. Lett. B. 448 (1999) 320, 1987. 1, 2.4

[3] The H1 Collaboration, C. Adloff et al. Observation of events at very high Q^2 in ep collisions at HERA. *Z. Phys. C*, 74:191, 1997. 1

[4] The ZEUS Collaboration, J.Breitweg et al. Comparison of ZEUS data with standard model predictions for e^+p $\rightarrow$ e+X scattering at high x and Q^2. *Z. Phys. C*, 74:207, 1997. 1

[5] The H1 Collaboration, C. Adloff et al. A Search for Leptoquark Bosons and Lepton Flavor Violation in positron-proton collisions at HERA. *Eur. Phys. Journal C*, 11:447, 1999. 1

[6] The H1 Collaboration, C. Adloff et al. Search for compositeness, leptoquarks and large extra dimensions in e q contact interactions at HERA. *Phys. Lett. B*, 479:358–370, 2000. 1

[7] The H1 Collaboration, C. Adloff et al. A search for leptoquark bosons in e^- p collisions at HERA. *Phys. Lett. B*, 523:234–242, 2001. 1

[8] Jogesh C. Pati and Abdus Salam. Lepton Number as the Fourth Color. *Phys. Rev.*, D10:275–289, 1974. Erratum-ibid.D11:703-703,1975. 2.2

[9] JoAnne L. Hewett and Thomas G. Rizzo. Low-Energy Phenomenology of Superstring Inspired E(6) Models. *Phys. Rept.*, 183:193, 1989. 2.2

[10] Stephen P. Martin. A supersymmetry primer. in G.L. Kane (editor): Perspectives on supersymmetry (1997) or arXiv:hep-ph/9709356. 2.3

[11] M. Kuze and Y. Sirois. Search for Particles and Forces Beyond the Standard Model at HERA ep and TeVatron $p\bar{p}$ Colliders. *Progress in Particle*

and Nuclear Physics, 50:1–62, 2003. http://arxiv.org/pdf/hep-ex/0211048; erratum:ibid.53:583-677,2004. 2.3, 2.4, 2.6

[12] T. Christiansen. *Search for Second-Generation Leptoquarks in $p\bar{p}$ Collisions.* PhD thesis, Luwig-Maximilians-Universität München, 2003. http://www.etp.physik.uni-muenchen.de/dokumente/thesis/phd_tchrist.pdf. 2.4

[13] H. Murayama and T. Yanagida. A viable SU(5) GUT with light Leptoquark Bosons. *Mod. Phys. Let. A*, 7:147, 1992. 2.4

[14] T. Rizzo. Desert GUTs and New Light Degrees of Freedom. *Phys. Rev. D*, 45:3903, 1992. 2.4

[15] J.C. Pati and A. Salam. Unified Lepton-Hadron Symmetry and a Gauge Theory of the Basic Interactions. *Phys. Rev. D*, 8:1240, 1973. 2.4

[16] P.H. Frampton and B.-H. Lee. SU(15) Grand Unification. *Phys. Rev. Lett.*, 64:619, 1990. 2.4

[17] P.H. Frampton and T.W. Kephart. Higgs Sector and Proton Decay in SU(15) Grand Unification. *Phys. Rev. D.*, 37:3892, 1990. 2.4

[18] P.H. Frampton. Light Leptoquarks as possible Signature of Strong Electroweak Unification. *Mod. Phys. Lett. A*, 7:559, 1992. 2.4

[19] J.L. Hewett andd S. Pakvasa. Leptoquark Production in Hadron Colliders. *Phys. Rev. D*, 37:3165, 1988. 2.5

[20] M. Krämer, T. Plehn, M. Spira and P.M. Zerwas. Pair production of scalar leptoquarks at the LHC. *Phys. Rev. D*, 71:57503, 2005. http://arxiv.org/pdf/hep-ph/0411038. 2.5, 2.2, 8

[21] J. Pumplin, D.R. Stump, J. Huston, H.L. Lai, P. Nadolsky, W.K. Tung. New generation of parton distributions with uncertainties from global QCD analysis. *Journal of High Energy Physics*, 207:12, 2002. see also http://www.phys.psu.edu/ cteq/. 2.5, 6

[22] P. Calfayan. Search for 2^{nd} generation Leptoquarks at DØ . PhD Thesis, LMU München. 2.6

[23] A. Abulencia et al. Search for second-generation scalar leptoquarks in $p\bar{p}$ collisions at $\sqrt{s} = 1.96$ TeV. *Phys. Rev. D*, 73:051102, 2006. 2.6

[24] P. Abreu et al. Limits on the production of scalar leptoquarks from Z0 decays at LEP. *Phys. Lett.*, B316:620–630, 1993. 2.6

[25] CERN ATLAS homepage. http://atlas.web.cern.ch/. 3.1, 3.2, 3.3, 3.4, 3.5, 3.6, 3.8, 8

[26] The ATLAS Collaboration. ATLAS Detector And Physics Performance. Technical Design Report, CERN, 1999. 3.2, 5

[27] M. Schott, G. Duckeck et al. Study of the Sagitta Resolution of MDT Chambers with Cosmic Muons. ATLAS Note. 3.2.3

[28] The ATLAS Collaboration. ATLAS Computing TDR. Technical Design Report, CERN, 2005. 3.3.3

[29] The Gaudi Project. http://proj-gaudi.web.cern.ch. 3.4

[30] Torbjörn Sjöstrand, Stephen Mrenna and Peter Skands. PYTHIA 6.4 physics and manual. *JHEP*, 05:026, 2006. 3.4, 4.1, C

[31] The Herwig++ Event Generator. http://projects.hepforge.org/herwig/. 3.4, 4.1

[32] GEANT 4. http://geant4.cern.ch/. 3.4

[33] The ATLAS software workbook. https://twiki.cern.ch/twiki/bin/view/Atlas/WorkBookFullChain. 3.4, 3.9, 8

[34] Johannes Blumlein, Edward Boos, and Alexander Kryukov. Leptoquark pair production in hadronic interactions. *Z. Phys.*, C76:137–153, 1997. see also arXiv:hep-ph/9610408. 4

[35] The ATLAS Collaboration. Homepage of the ATLAS CSC notes. https://twiki.cern.ch/twiki/bin/view/Atlas/CSCNotesList. 4.1, 6, 8

[36] Combined Muon Track Reconstruction with STACO. http://atlas-samusog.web.cern.ch/atlas-samusog/muonboy/DocPublishedTexts/phytdr.staco.pdf, 2007. 4.2

[37] The ATLAS Collaboration. Muon Reconstruction and Identification Performance in ATLAS: Studies with Simulated Monte Carlo Samples. CERN Yellow book. 4.2

[38] Gerald C. Blazey et al. Run II jet physics. *arxiv: hep-ex/0005012*, 2000. 4.2

[39] The ATLAS Collaboration. Reconstruction and identification of electrons in ATLAS. CERN Yellow book. 4.2

[40] S.I. Bityukov, S.E. Erofeeva, N.V. Krasnikov and A.N. Nikitenko. Program for evaluation of the significance, confidence intervals and limits by direct probabilities calculations. Proceedings of conference PHYSTAT 05, Statistical problems in Particle Physics, 12th-15th September 2005. Oxford. 4.3, 7, B

[41] Thilo Pauly. Luminosity Determination Based on Beam Parameters. https://twiki.cern.ch/twiki/pub/Atlas/FrequentlyAskedQuestions/MachineParameters.pdf. 6

[42] Maarten Boonekamp. Luminosity measurement in ATLAS. Prepared for 12th International Workshop on Deep Inelastic Scattering (DIS 2004), Strbske Pleso, Slovakia, 14-18 April 2004. 6

[43] E.E. van der Kraaij. Uncertainties on the $t\bar{t}$ cross-section and its ratio on the W cross-section at the LHC. http://doc.cern.ch//archive/electronic/cern/others/atlnot/Communication/phys/com-phys-2006-040.pdf. 6

[44] A.D. Martin, R.G. Roberts, W.J. Stirling and R.S. Thorne. Uncertainties of predictions from parton distributions, I. Experimental errors. *Eur. Phys. Journal C*, 28:455, 2003. arXiv:hep-ph/0211080. 6

[45] The ATLAS Collaboration. In-Situ Determination of the Performance of the ATLAS Muon Spectrometer. CERN Yellow book. 6

[46] M. Schott. Study of the Z Boson Production at the ATLAS Experiment with First Data. PhD Thesis, LMU München. 6

[47] The ATLAS Collaboration. Jet Energy Scale: In-Situ Calibration strategies in ATLAS. CERN Yellow book. 6

[48] Rene Brun and Fons Rademakers. ROOT - An Object Oriented Data Analysis Framework. *Nucl. Inst. & Meth. in Phys. Res. A*, 389:81–86, September 1997. Proceedings AIHENP'96 Workshop, Lausanne, Sep. 1996, see also http://root.cern.ch/. 7

[49] Thomas Junk. Confidence level computation for combining searches with small statistics. *Nucl. Instrum. Meth.*, A434:435–443, 1999. see also arXiv:hep-ex/9902006. 7

[50] Gernot Krobath. Discovery potential of the LHC for extended gauge symmetries. *arXiv: 0710.4708*, 2007. 8

[51] S.I. Bityukov and N.V. Krasnikov. On the observability of a signal above background. *Nucl. Instrum. Meth.*, A452:518–524, 2000. B

[52] Ilya V. Narsky. Estimation of upper limits using a Poisson statistic. *Nucl. Instrum. Meth.*, A450:444–455, 2000. B

[53] Alessandro De Salvo, Gernot Krobath et al. The ATLAS Software Installation system for LCG/EGEE. To be published in the Proceedings of the conference CHEP'07, Victoria, Canada. http://www.chep2007.com. D.2, D.2, D.3, 8

[54] LCG grid. http://lcg.web.cern.ch/LCG/. D.2

Danksagungen

Als erstes möchte ich Prof. Dorothee Schaile herzlich danken, daß sie mir die Möglichkeit gegeben hat, meine Doktorarbeit an ihrem Lehrstuhl durchzuführen.

Desweiteren danke ich Herrn PD Raimund Ströhmer für die sehr gute Unterstützung und die vielen Ideen und Ratschläge für meine Arbeit.

Mein Dank geht an Herrn Prof. Wolfgang Dünnweber für die Erstellung des Zweitgutachtens.

Herr Prof. Otmar Biebel hat mir durch sein Detailwissen des LHC und des ATLAS Detektors und seiner Hilfsbereitschaft oft viel weiter geholfen, dafür vielen Dank.

Ich möchte Cedric Serfon, John Kennedy und Günter Duckeck für die Hilfe bei zahlreichen Computer- und GRID-Problemen danken.

Ich bedanke mich sehr für das Korrekturlesen der Arbeit und zahlreiche Verbesserungsvorschläge bei Michael Stöver, Thomas Müller, Christian Kummer, Raphael Mameghani und PD Raimund Ströhmer.

Für die vielen netten und informativen Gespräche möchte ich mich herzlich bei Matthias Schott, Thomas Müller, Julien de Graat und Markus Lichtnecker bedanken.

Benjamin Ruckert, Felix Rauscher und Johannes Ebke möchte ich für die gute und nette Büroatmosphäre danken.

Ganz herzlich möchte ich mich bei meinen Eltern für die Unterstützung bedanken.